

# UNIVERSITY OF TWENTE.

## Modelling breach erosion of coversand ridges in the IJssel floodplain induced by water overflow in early medieval times



Roy Dierx  
M.Sc. Thesis  
November 2020

*Cover picture:*

High water in the river IJssel and its floodplain at Gorssel on 08/02/2020  
(Van Lottum, 2020)

# Modelling breach erosion of coversand ridges in the IJssel floodplain induced by water overflow in early medieval times

*Master thesis Civil Engineering and Management  
University of Twente  
Faculty of Engineering Technology  
Department of Water Engineering and Management*

*Author:* Roy Dierx

*Supervisors:* Anouk Bomers University of Twente  
Kim Cohen Utrecht University  
Suzanne Hulscher University of Twente

---

## Preface

This report presents the thesis that forms the finishing of my Master in Civil Engineering and Management. This graduation research was carried out at the Department of Water Engineering and Management at the University of Twente in collaboration with the Department of Physical Geography at Utrecht University. Hopefully, the findings of this thesis provide a valuable contribution to the research regarding the erosion of coversand ridges in the IJssel floodplain and the formation of the river IJssel as a river Rhine distributary in medieval times.

I would like to thank the members of my graduation committee for their supervision and support throughout this research. First of all, I want to express my gratitude to Anouk Bomers for her suggestions on the modelling aspects and her critical reflections which improved my academic writing skills. Secondly, I would like to thank Kim Cohen for his creative suggestions regarding the geographical and historical aspects in this research and his critical reflections which improved the scientific value of this research. Furthermore, I want to thank Suzanne Hulscher for her critical view to increase the scientific value and academic level of this research.

Finally, I want to thank my family, friends and fellow students who supported me during my life as a student and during this research.

*Roy Dierx*

---

## Abstract

Coversand ridges are natural higher elevated areas (relative to the surrounding land), which consist of coversand. Coversand ridges formed in the last part of the glacial period due to wind transport and some coversand ridges created a watershed between the Rhine and IJssel floodplain. Research found that the river IJssel came into existence between 300 and 750 AD and it is hypothesised that a large-magnitude flooding was the trigger for the erosion of the coversand ridges in the IJssel floodplain. Due to this large-magnitude flooding, earlier research found that two initial breaches formed in the coversand ridges. Where one breach eventually expanded and became part of the river IJssel (referred as the 'easterly breach'), the second breach partly silted and stopped being used as a flood path (referred as the 'westerly breach'). A case study is done on the formation of the river IJssel, a distributary of the river Rhine in the Netherlands. In this case study a static coupled hydrodynamic-erosion model is set up to simulate potential coversand ridge breach scenarios in the IJssel floodplain.

Understanding the annexation process of the IJssel floodplain by the river Rhine is of archeological-historical interest and can offer an opportunity to quantify major historical floods of the river Rhine. Besides this, the quantification of these major historic floods is of interest for designing projects and safety assessments in the future. The objective of this research is therefore to obtain insight in the erosion processes of two developing breaches in a coversand ridge during flood induced overflows in the IJssel floodplain.

It is chosen to use a static modelling approach, because a dynamic model of a developing breach and the interaction of two developing breaches is very sensitive due to the complex hydrodynamics in a developing breach. Besides this, the breach process took place between 300 and 750 AD, which brings the uncertainty that the process cannot be validated. In the static modelling approach, several stages within a breach process were developed. To obtain insight in the erosion processes during a flood induced overflow at two breach locations, these breach stages imply variations in the width and depth. The different breach stages were implemented in a Digital Elevation Model and were used as input for a hydrodynamic model. The hydrodynamic properties, like the flow velocity and water depth in the breach and discharge through the breach, were extracted from the hydrodynamic model and used as input for the erosion model. The differences between the quantitative results of the various scenarios were analysed qualitatively, with a focus on differences between the easterly and the westerly breach during a flood induced overflow.

The different scenarios developed in this research give a unanimous result, in which the hydrodynamics in the easterly breach are more favourable to induce erosion of the coversand ridge than the westerly breach. This also causes the easterly breach to have better conditions to expand and eventually become part of the river IJssel. Taking the present situation of the river IJssel into consideration, which is also located at the easterly breach, this result can be validated. In former research it is hypothesized that the easterly breach eroded and expanded that much, during a flood induced overflow, that subsequent floods could flow through the easterly breach and did not reach the westerly breach as a flood path anymore. This hypothesis is in line with the results as presented in this research.

For future research, it is recommended to develop a morphological model of a simple breach or small channel with the same dimensions as used in this research. The results of the morphological model, consisting of the sediment transport in the channel and thus the erosion and sedimentation rates, can be linked to the results of this research. This detailed morphodynamic model, creates more insight into the breach development in a coversand ridge.

---

## List of Symbols

Variable	Meaning	Unit
$\beta$	Slope angle	$^{\circ}$
$D_*$	Dimensionless grain size parameter	–
$D_{50}$	Median grain size	$m$
$E$	Pick-up rate	$kg/m^2/s$
$f_D$	Damping factor	–
$F_s$	Force due to the flowing water	$N$
$g$	Gravitational acceleration	$m/s^2$
$G$	Force of Gravity	$N$
$h$	Water depth	$m$
$k_s$	Nikuradse roughness height	$m$
$\mu$	Ripple factor	–
$n$	Manning's coefficient	$m/s^{1/3}$
$n_0$	In-situ porosity	–
$\phi$	Angle of internal friction	$^{\circ}$
$\Phi$	Transport parameter	–
$\Psi$	Flow parameter	–
$\nu$	Kinematic viscosity coefficient of the fluid	$m^2/s$
$q_s$	Sediment transport per meter width	$m^3/s/m$
$\rho_s$	Sediment density	$kg/m^3$
$\rho_w$	Water density	$kg/m^3$
$s$	Sediment transport per meter width	$m^3/s/m$
$S$	Cross-sectional sediment transport	$m^3/s$
$s_d$	Relative density	–
$t$	Breach stage	–
$T$	Time	$s$
$\tau$	Grain-related bed shear stress	$N/m^2$
$\theta$	Grain-related Shields parameter	–
$\theta_{cr}$	Shields critical value at the initiation of motion	–
$U$	Depth-averaged flow velocity	$m/s$
$u_*$	Bed shear velocity	$m/s$
$v_e$	Erosion velocity perpendicular to the bed	$m/s$
$v_{wall}$	Erosion velocity of the sides of the breach	$m/s$
$V$	Volume	$m^3$
$w_s$	Fall velocity of a sediment particle	$m/s$

### Important terms

Breach depth	The depth of the breach in the coversand ridges; One of the main variables in this research
Breach stage	A static moment in time in the process of a developing breach during a flood wave
Breach width	The width of the breach in the coversand ridges; One of the main variables in this research
Coversand ridge	A natural elevated area that formed in the last part of the glacial period due to wind transport
Easterly breach	The breach in the coversand ridge that eventually expanded and became part of the river IJssel
Westerly breach	The breach in the coversand ridge that eventually partly silted and was abandoned as a flood path

# Contents

Preface . . . . .	i
Abstract . . . . .	ii
List of Symbols . . . . .	iii
<b>1 Introduction</b>	<b>1</b>
1.1 River branch formation . . . . .	1
1.2 Case study . . . . .	2
1.3 Problem definition and research objective . . . . .	4
1.4 Research approach & Thesis outline . . . . .	5
<b>2 Research inputs, constraints and assumptions</b>	<b>7</b>
2.1 Reconstruction coversand ridge . . . . .	7
2.2 Defining breach stages . . . . .	8
2.3 Topographic schematisation and model forcing . . . . .	9
2.3.1 Breach dimensions . . . . .	9
2.3.2 Flood wave propagation and return period . . . . .	12
<b>3 Method</b>	<b>13</b>
3.1 Hydrodynamic model . . . . .	13
3.1.1 Model set-up . . . . .	13
3.1.2 Data extraction from hydrodynamic model . . . . .	16
3.2 Erosion model . . . . .	17
3.2.1 Erosion equation . . . . .	17
3.2.2 Sediment transport capacity . . . . .	19
<b>4 Results</b>	<b>21</b>
4.1 Hydrodynamic model . . . . .	21
4.1.1 Validation model . . . . .	21
4.1.2 Hydrodynamic conditions . . . . .	22
4.1.3 Translation to the breach stages . . . . .	27
4.2 Erosion model . . . . .	27
4.2.1 Bed shear stress . . . . .	27
4.2.2 Erosion velocity . . . . .	28
4.2.3 Sediment transport capacity . . . . .	30
<b>5 Discussion &amp; Recommendations</b>	<b>34</b>
5.1 Discussion . . . . .	34
5.1.1 Research set-up . . . . .	34
5.1.2 Sensitivity model . . . . .	35
5.1.3 Comparison with the chute cut-off in the river Wabash . . . . .	37
5.2 Recommendations . . . . .	37
<b>6 Conclusion</b>	<b>39</b>

<b>References</b>		<b>40</b>
<b>Appendix</b>		<b>44</b>
<b>A Study area</b>		<b>44</b>
<b>B Hydrodynamic model equations</b>		<b>45</b>
B.1 1D Unsteady flow equations . . . . .		45
B.2 2D Full momentum equations . . . . .		46
B.3 Weir flow coefficient . . . . .		46
<b>C Overview of results</b>		<b>47</b>
<b>D Manning Coefficient determination</b>		<b>49</b>
<b>E Figures</b>		<b>51</b>
E.1 Erosion velocity . . . . .		51
E.2 Sediment transport capacity . . . . .		52

# Chapter 1

## Introduction

In this research, a modelling study is done on developing breaches in coversand ridges, which have contributed to the formation of the river IJssel branch as a river Rhine distributary in early medieval times (300-750 AD) during a rare extreme flood wave. Understanding the annexation process of the IJssel floodplain by the river Rhine is of archeological-historical interest and can offer an opportunity for future safety assessments of embankments by adding additional historical data. A static modelling approach is used for gaining insight into the breach process from a small breach to a developed breach, because a dynamic modelling approach on the scale required for this research is not feasible. The process of a developing breach happens quickly and to gain insight in the development several static situations (moments in time) during a breach process are developed. These situations are called stages. The dimensions of the breaches are the main variables in this research and are based on LiDAR (Light Detection And Ranging) data of the current situation of a similar preserved breach in the coversand ridges. A coupled hydrodynamic-erosion model with the various stages is set up using a reconstructed Digital Elevation Model (DEM) of the Rhine and IJssel floodplain of the early medieval time period. The output of this static coupled hydrodynamic-erosion model is analysed qualitatively. The separate stages during a breach process are used to set up a timeline of what happened during the full breach process of the coversand ridges and how this could have contributed to the formation of the river IJssel as a river Rhine distributary.

### 1.1 River branch formation

For the uniform observer it may appear that rivers flow through their floodplains like they have been there all the time. A floodplain is the whole area that can flood during a flood wave in this context. The course of a river through its floodplain is on the other hand not as simple as that: rivers form, change their course in the floodplain due to channel diversion and river branches can eventually run dry due to another river branch with a more favourable path in the floodplain.

A diversion of a main channel is typically initiated by flows that overtop the channel banks and is maintained by the erosion of a new distributary channel through the main channel bank or levee (Yuill et al., 2016). A crevasse splay (Figure 1.1) is a depositional land form created by the diversion of river water and sediment from its channel into a floodplain (North & Davidson, 2012). Despite being a primarily depositional land form at its upstream begin, a crevasse splay experiences an initial evolutionary phase that is primarily erosional. During this phase, sediment-laden river water spills from a main river channel and incises a new course through the river banks into a floodplain (Yuill et al., 2016).

In some cases crevasse splays can evolve into a new river, causing a river to abandon its old river channel, because of a greater crevasse slope than the main channel slope. This process is known as avulsion (Allen, 1965; Boggs, 2014). Avulsion is a threshold process inherent to channelized depositional systems where channels aggrade or prograde faster than the surrounding non-channelized regions (Hajek & Wolinsky, 2012). The process of a river changing course on a floodplain or in a delta, may take 100–1,000 years

(Stouthamer, 2001) and a successful avulsion requires both reach-scale cross-channel flow potential energy exceeding a threshold, and availability of a more favorable path at landscape-scale (Mohrig et al., 2000; Hajek and Wolinsky, 2012). During this changing course, more channels can develop. The process of an avulsion can be seen as a bifurcation of the main channel into two channels (Mohrig et al., 2000; Kleinhans et al., 2013). A bifurcation can persist if it is stable, in which case we call the avulsion a 'partial avulsion' (the avulsion process ends with the new channel taking over a part of the discharge, the old channel loses a part of its original discharge, but does not get abandoned (Stouthamer, 2001)). A bifurcation is considered to have stabilised if the division of flow and sediment between the two downstream branches no longer changes majorly over time, although it may fluctuate as the discharge entering the bifurcation rises and falls (Kleinhans et al., 2013).

In the above mentioned stages in the formation of a river, the river only changes course in the floodplain that was already annexed by the river. Rarer is the course change of a river that annexes a new floodplain by breaching through an elevation that forms the edge of the floodplain. This annexation of a new floodplain is called avulsion-by-annexation (Smith et al., 1989). This research studies the formation of the river IJssel, which is a special case, since it caused for the annexation of a new floodplain and not a local shift of a river on the same floodplain (Cohen & Lodder, 2007).

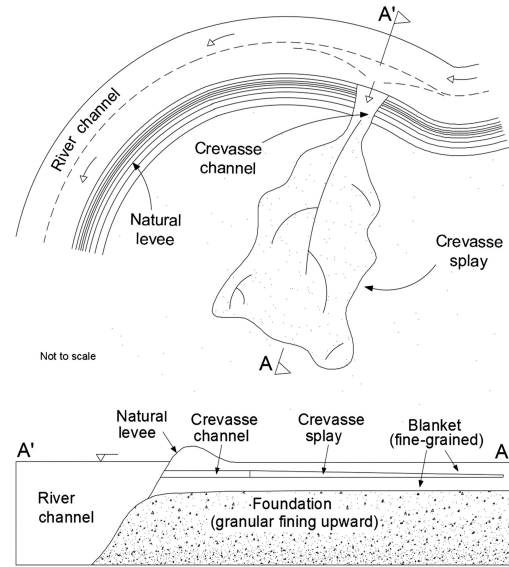


**Figure 1.1:** A crevasse splay in a floodplain (Polanco-Boulware & Rice, 2016)

## 1.2 Case study

Today, the river Rhine enters the Netherlands near Lobith, as is shown in Figure 1.2 and Appendix A. Downstream of Lobith, the river Rhine bifurcates into the river Waal and the Pannerdensch Canal; the Pannerdensch Canal then bifurcates into the rivers IJssel and Nederrijn. The river Rhine and its distributaries have not always flown in the same way. For example, 2,000 years ago, in Roman times, the bifurcation of the river Rhine into the rivers Nederrijn and Waal existed, but the IJssel branch had not yet formed. Around 800 AD (1,200 years ago), the river IJssel did exist, but it was a very young river (Makaske et al., 2008; Cohen, 2010). The river IJssel came into existence between 300 and 750 AD. During this time period a large scale flood event or multiple flood events must have occurred which triggered the river Nederrijn to bifurcate into the river IJssel (Cohen, 2010), as an avulsion-by-annexation.

Before the river IJssel initiated, the part of the IJssel valley downstream of Deventer was a separate river floodplain that was not part of the Rhine floodplain (Figure 1.3). The upstream part of the IJssel branch (the part South of Zutphen), at that time was probably drained by a small river (Makaske et al., 2008), draining toward the river Rhine (Figure 1.3). A natural elevated area separated the IJssel and Rhine floodplains. This natural elevated area consisted of coversand. These so-called coversand ridges have formed during the last part of the last glacial period between 30,000 to 11,700 years ago (Cohen et al., 2009). During the last glacial period the floodplain was not vegetated, so the wind could easily blow sand particles over the floodplain. In the IJssel floodplain, the dominant wind transport direction was from North - North-West. Due to the direction of the wind, the coversand ridges have a parabolic shape as shown in Figure 1.3. After the glacial period, the floodplain and the developed coversand ridges became vegetated, the plants were able to keep the sand in place, which partly resulted in the elevated areas as they are present in the IJssel floodplain nowadays (Cohen, 2010).

The coversand ridges caused for a higher elevated area in the floodplain. Before the river Rhine was embanked, peak discharges from the river Rhine have led to floods that reached the South side of the coversand ridges (e.g. archeologically observed at the Berkel valley just South of Zutphen; Groothedde (2010)), but these floods

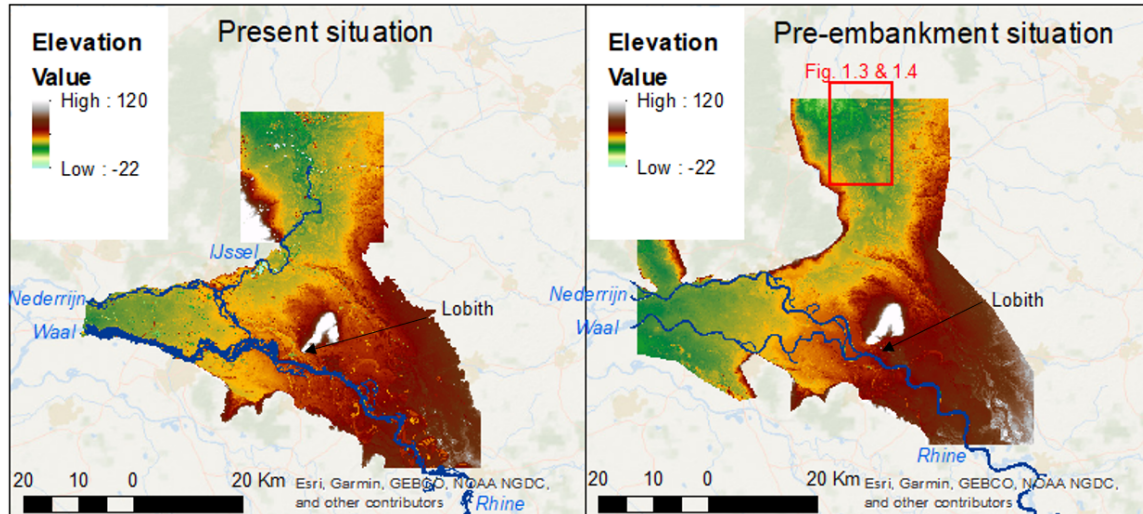


**Figure 1.2:** Study area of the river Rhine and its distributaries in the Netherlands. Left: the present situation of the river Rhine and its distributaries; Right: the pre-embankment situation (< 800 AD) of the river Rhine and its distributaries (Using a paleo Digital Elevation Model by Van der Meulen et al. (2020))

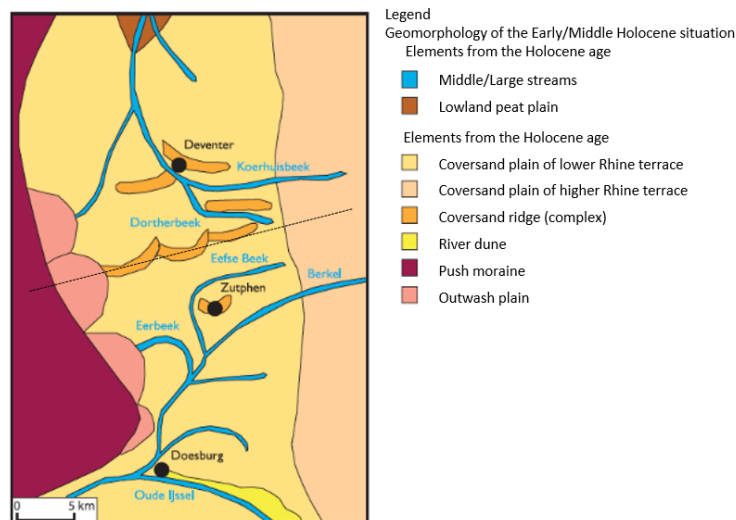


**Figure 1.3:** Schematic overview of the streams in that drained the IJssel valley before the IJssel avulsion (Vermeulen & Haveman, 2008). The dotted line represents the separation of the IJssel floodplain (North of the dotted line) from the Rhine floodplain (South of the dotted line).

would drain back to the river Rhine via the old streams that were present in the pre-embanked situation. To make it possible for the river Rhine to discharge North of the coversand ridges (near Deventer and further North in Figure 1.3), the coversand ridges that created the natural barrier must have eroded and breached to eventually cause for a more favourable course of the river Rhine resulting in the formation of the river IJssel.

The formation of the first initiation of the breach of the coversand ridges that separated the Rhine floodplain from the IJssel floodplain must have formed due to an extreme flood event. This extreme flood event caused high water levels on the Rhine floodplain (and thus also near Zutphen in Figure 1.3). This then caused overflow of the coversand ridge, induced erosion and eventually a breach of the coversand ridges North of Zutphen (Makaske et al., 2008; Cohen et al., 2016). Indications of such a breach are found at two locations along the coversand ridges (Cohen et al., 2009). These locations are shown in the middle and right figure of Figure 1.4. At the location where the river IJssel eventually formed, and still flows as it does nowadays,

the initial breach characteristics are partially preserved. In this report this breach will be referred to as the easterly breach or the breach near Gorssel. The other breach is located West of where the IJssel flows (at the question mark in the middle and right figure of Figure 1.4). Its initial breach characteristics induced by the overflow are completely preserved. This will be referred to as the westerly breach or the breach near Voorst. After the initial breach of both locations, both breach locations have been active and have discharged water, but where the easterly breach expanded and became part of the river IJssel, the westerly breach eventually silted and has not been active since (Cohen, 2010). The differences, as can be currently observed, between the two initial breaches are caused by subsequent floods. Where the IJssel branch continued to form meanders in later times (Figure 1.4), only fragments of the initial breach that formed the river IJssel are preserved. At the westerly location, features like the splay and breach dimensions are more completely preserved, because no floods have caused floods at that part of the floodplain (Cohen et al., 2009; Cohen and Stouthamer, 2012).

Understanding the annexation process of the IJssel floodplain by the river Rhine is of archeological-historical interest and can offer an opportunity to quantify major historical floods of the river Rhine (Cohen, 2010). Besides this, the quantification of these major historic floods is of interest for designing projects and safety assessments in the future. Now, only 100 years of measurement data is available. This data is currently extrapolated for i.e. safety assessments of embankments (Cohen & Lodder, 2007). Adding historical floods outside of this measurement data can decrease the uncertainty of these extrapolations and can give more certainty to current and future safety assessments of embankments (Bomers et al., 2019b).

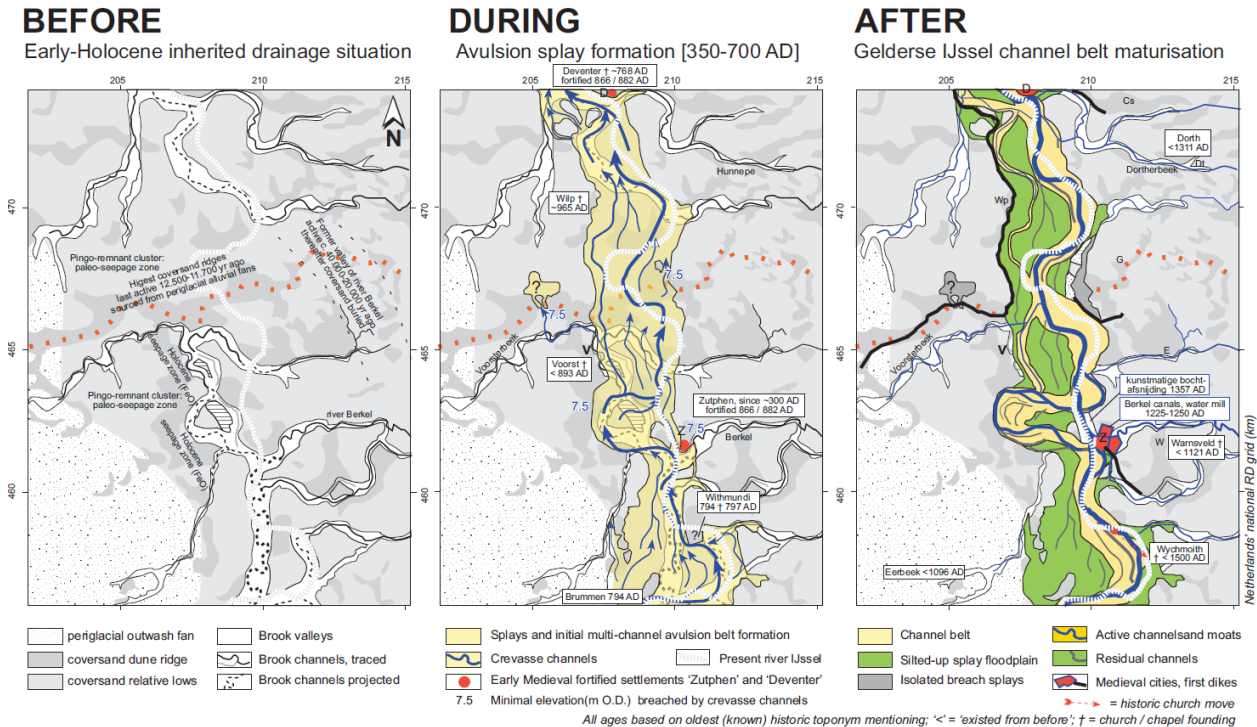


**Figure 1.4:** Stages of IJssel formation (Cohen et al., 2009; Cohen, 2010). **Before situation:** The water from the floodplains of the IJssel and the Rhine are drained separately; **During situation:** The coversand ridge breached at two location during a peak discharge of the river Rhine, the formed avulsion splay discharges from the river Rhine, the river IJssel is not a fully meandering river. During this stage the easterly breach expanded during subsequent high discharges and the westerly breach eventually silted; **After situation:** The river IJssel matured and is a fully meandering river.

### 1.3 Problem definition and research objective

The river IJssel came into existence between approximately 300 and 750 AD and is the youngest natural distributary of the Rhine delta (Makaske et al., 2008). Extreme flood waves are the most probable trigger

to erode the coversand ridges and trigger the formation of the IJssel branch. During this erosion and the formation of the first stages that became the river IJssel, two initial breaches formed in the coversand ridges. Both breaches can be traced back to approximately 1300-1700 years ago (350 and 750 AD) from geological mapping and dating (Cohen et al., 2009). Where one breach eventually partly silted (westerly breach), the other breach expanded and became part of the river IJssel (easterly breach; Cohen, 2010). The reason why the westerly breach partly silted and was abandoned as a flood path, and the easterly breach expanded and became part of the river IJssel is not known.

A next step in the reconstruction of the formation of the river IJssel and the annexation processes of the IJssel floodplain by the river Rhine is to gain insight in the erosion processes in the formed breaches in the coversand ridges and the development of these breaches. To obtain this insight flood waves with different peak discharges and return periods are selected that could have contributed to the erosion in the breaches of the coversand ridges. With the insight into the hydrodynamic and erosional properties of both breaches during various flood waves, the differences between the two breaches can lead to understanding why the easterly breach expanded and the westerly breach silted up. This leads to the main objective of this study:

*Obtain quantitative insight in the erosion processes of two developing breaches in a coversand ridge during flood induced overflows in the IJssel floodplain.*

To meet this research objective, the following research questions will be addressed:

1. *What are the relevant parameters in the breach development process that are used as input of a hydrodynamic model?*
2. *What are the hydrodynamic properties in the breaches under different flood waves, breach depths and breach widths?*
3. *How does the erosion differ in both breaches for the different parameter settings?*

## 1.4 Research approach & Thesis outline

The IJssel floodplain is annexed by the river Rhine approximately 1300-1700 years ago. No real time data is known about that time period, but from geological mapping and dating a best guess can be made of the initial breach dimensions in the coversand ridge. In Chapter 2, first, a reconstruction of the Rhine and IJssel floodplain is done for the time period before the annexation of the IJssel floodplain by the river Rhine (Figure 1.4). This reconstruction includes a connected coversand ridge that functions as a barrier for the river Rhine to discharge North.

The processes in breach development are complex. Because of the complexity in the different stages of breach development from the initial erosion of the crest of the coversand ridge to a discharging breach in the coversand ridge, and the dynamic modelling of this, a static modelling approach is used. This static modelling approach consists of different stages of the breach development process, from a small to a larger breach in depth and width. These different stages are constructed and implemented in the reconstructed coversand ridge (Chapter 2). With the implementation of the different breach stages in the connected coversand ridges a passage is created from the Rhine floodplain to the IJssel floodplain, so an extreme flood wave on the Rhine floodplain can discharge to the IJssel floodplain.

With these different stages of the breach development in the coversand ridge a hydrodynamic-erosion model is set up (Chapter 3). In the hydrodynamic model several flood waves, with different peak discharges, are simulated over a Digital Elevation Model (DEM) of the reconstructed floodplain. The output of the hydrodynamic model consists of the water depth and flow velocity in the breaches and discharge through the breaches. This output is then used for the quantification of the erosion locally in both breaches using an erosion equation and sediment transport capacity through both breaches during a flood wave in Chapter 4.

The determination of the erosion in a developing breach and the sediment transport capacity through it are uncertain, because (e.g.) a developing breach is not in equilibrium, the reconstructed breaches are a best guess using geological mapping and dating and little validation data is available. For this reason, a qualitative

analysis is done on the quantified erosion and sediment transport capacity differences between the two initial breaches, the different stages of the breaches and the various flood waves (Chapter 4).

In Chapter 5 the results and the research method are discussed and the recommendations that follow from the discussion are presented. In Chapter 6 the conclusion is presented.

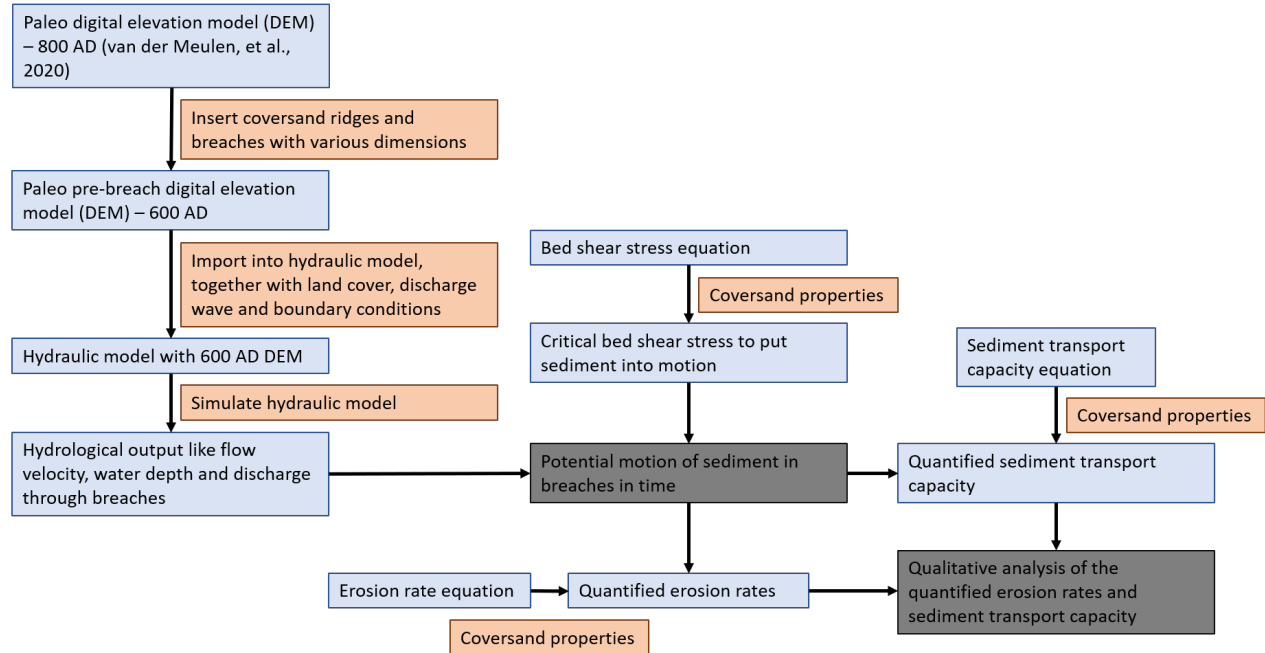


Figure 1.5: Flow chart of the modelling steps in this research

## Chapter 2

# Research inputs, constraints and assumptions

This section first describes the preliminary modifications that are required for this research, then the assumptions that are made in this research and at last defines the research boundaries.

### 2.1 Reconstruction coversand ridge

Van der Meulen et al. (2020) constructed a Digital Elevation Model (DEM) of the best guess of the early medieval times around 800 AD of the Rhine and IJssel floodplains. Major human influences such as roads and buildings, land subsidence due to mining (near the Ruhr confluence in Germany), river embankments and normalisation of rivers are restored in this DEM. With this reconstruction a flood wave can be simulated that represents the pre-embanked flood pattern and inundation extent of the Rhine and IJssel floodplains. In this situation the IJssel and Rhine floodplains are connected. This implies that the coversand ridge that split the Rhine from the IJssel floodplain already breached. For this reason, a DEM is reconstructed which includes a best guess of the connected coversand ridges prior to the initial breach (Figure 2.1). The reconstruction of the coversand ridges is done using the knowledge about the dimensions and shape of coversand ridges still present East and West of the breach, from the literature (i.e. Cohen et al. (2009), Makaske et al. (2008), Vermeulen and Haveman (2008)) and expertise judgement (Cohen, pers. comm.).

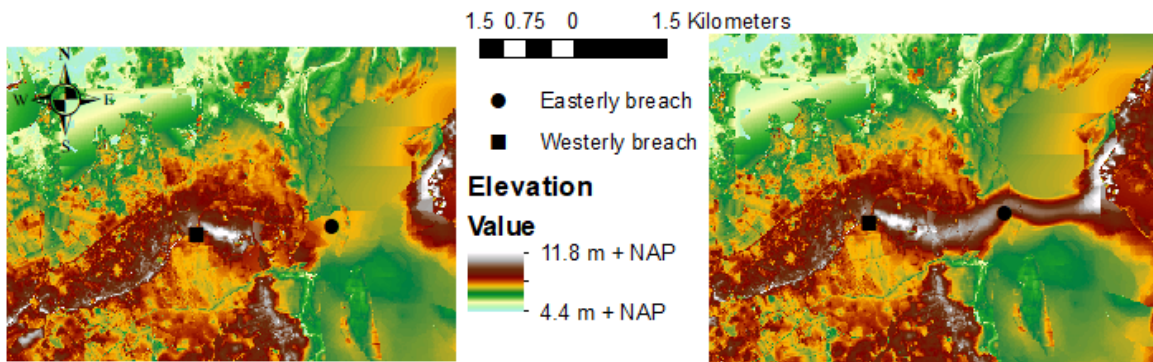


**Figure 2.1:** *Reconstructed connection coversand ridges. Left figure: After the breach of the coversand ridge; Right figure: Prior to the breach of the coversand ridge*

The left of Figure 2.1 represents the situation after the breach in which the IJssel is not a fully meandering river, but a passage for discharging North to the IJssel floodplain and eventually into the Zuiderzee (now

IJssel Lake) is already carved in the floodplain. The right figure represents the situation prior to the initiation of the breach with the parabolic shaped connected coversand ridge (Figure 1.3).

## 2.2 Defining breach stages

Defining various stages in time of a developing breach is required for the static modelling approach performed in this research. Various hydrological, hydrodynamic and geological factors affect the development of a breach (Wu et al., 2012). Every breach, whether in embankments, like dams and levees, or in naturally formed barriers, is different and the prediction of flow and sediment transport through a breach is challenging (Wu et al., 2012). The prediction of dynamic basic geometric and temporal parameters of a breach are widely recognised to have large uncertainties. Because of the scale of the study area and the breaches in this research (and the interaction between two breaches) and the fast process of a breach formation it is chosen to use a static modelling approach. In this static modelling approach several static situations in time within the breach development process are constructed to eventually analyse the process of a developing breach. Before these situations are constructed, the different stages within the breach process considered in this research are explained.

As stated above, the prediction of a breach process has large uncertainties. Especially the parameters in the initiation phase of a breach have great uncertainty. In the initiation phase, a breach is formed due to a failure mechanism. This can be, for example, an overflowing failure, a piping failure or a sliding failure. In this research, only an overflowing failure is considered, because this is the most likely failure to have happened (Cohen & Lodder, 2007). During this phase it is assumed that the initial damage is so large that it completely erodes the vegetated layer of a barrier and uncovers the sand core of this barrier (Visser, 1998). The type of vegetation in the top layer of the barrier, in this case a coversand ridge, has a major influence on the amount of damage the overflowing water must cause before an initial breach is even formed (Wahl, 2004). Besides the aforementioned uncertainties, the initial breaches in the coversand ridges have formed approximately 1300-1700 years ago (Cohen, 2010), which brings the uncertainty that the breach process is not monitored and no real-time data is available for calibration and validation of the breach development simulations.

The development of a breach from the initial erosion of the crest to an expanded discharging breach during a flood wave can be divided in several stages (Visser, 1998). In this research, four different stages of the breach process are defined (partly based on Visser (1998)) and shown in Figure 2.2:

1. Stage 1: This is the initial phase, the water level is rising and overflows the coversand ridge. During this phase the water flows over the part of the coversand ridge at which the threshold water level is reached. The top layer of the coversand ridge is vegetated and at a local point the hydrodynamic conditions become large enough to initiate erosion of the vegetated layer on the crest. The location of this initial erosion along the crest of the coversand ridge is uncertain.
2. Stage 2: The water level rises to its maximum, the vegetated layer is fully eroded locally at the breach location; the sand core is uncovered. With the sand core uncovered, the breach deepens and widens rapidly due to the small resistance of the non-cohesive sand during the high water level.
3. Stage 3: The water level stabilises at its maximum and the sand core is washed out rapidly to the base of the coversand ridge at the downstream side. During this stage the breach mainly grows laterally until the water level starts to drop and the flow velocity starts to decrease.
4. Stage 4: The water level and the flow velocities in the breach decrease. The water level will decrease to the base level of the coversand ridge. Due to the decrease in flow velocities, the sediment transport through the breach, upstream and downstream of the breach decreases. The sediment partly settles in the breach and the breach silts up to a certain degree.

The initial erosion of the coversand ridges is highly uncertain and the initial breach stage is difficult to model. With the little knowledge on a detailed scale of that time period on top of that, the initial breach stage is not of interest for this research and is thus outside of the research scope. What is known about that time period is that two breaches have formed (Cohen et al., 2009). From geological mapping and dating, it can be

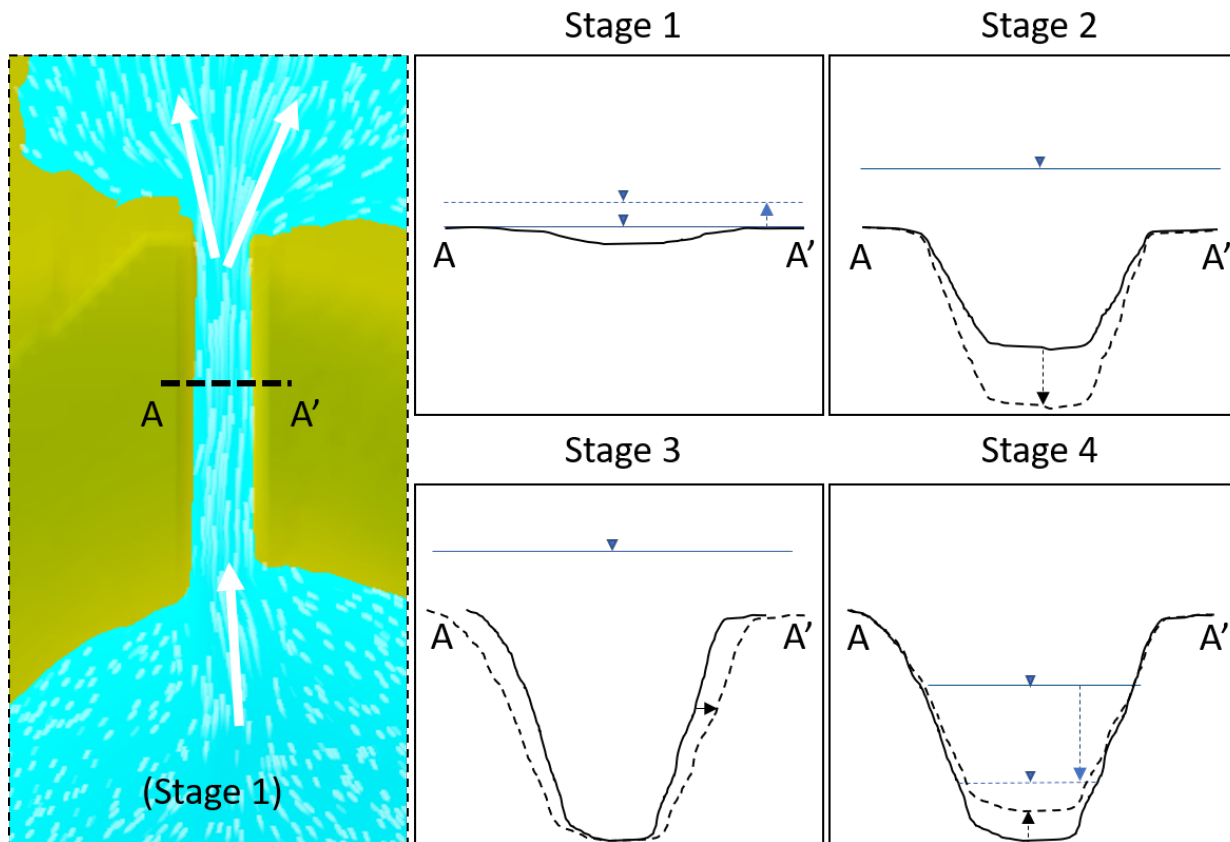


**Figure 2.2:** Cross-sectional view of the stages of a breach in a coversand ridge distinguished in this research

concluded that erosion of the coversand ridge has taken place at those two breach locations and thus must have had the best hydrodynamic conditions to initiate erosion. This knowledge gives the opportunity to skip the initial erosion phase with all its uncertainties in advance and focus on the stages where the vegetated layer is eroded and only non-cohesive sediment is left in the breach. Modelling the erosion of non-cohesive sediment is less uncertain and for this reason, it is chosen to focus on the breach development of two breaches in the coversand ridge during the Stages 2, 3 and partly 4 for various flood waves.

## 2.3 Topographic schematisation and model forcing

The initial breaches of the coversand ridge formed during a major flood event at some moment between 350-700 AD (Cohen, 2010). It is not known how these two breaches interact with each other and why one breach silted, while the other expanded to eventually trigger the Nederrijn to permanently bifurcate into a fully meandering river IJssel and discharge to the Zuiderzee. As stated in the previous section, various hydrological, hydrodynamic and geological factors affect the development of a breach (Wu et al., 2012). By varying various geological breach variables, such as width and depth and the hydrodynamic properties of the flood wave, a sensitivity analysis is performed to obtain insight into the interaction between both breaches under various circumstances. This section elaborates on the model variables that are used for the various parameter settings in this research.

### 2.3.1 Breach dimensions

The westerly breach is relatively well preserved. From geological mapping and dating at this breach location it is found that the westerly breach was around 4 meters deep from the crest to the deepest point in the breach, but eventually silted to a depth of 2 meters as it is preserved today (Cohen et al., 2009). From

the DEM of the present situation of the westerly breach it can be measured that the widest cross-section is around 100 meters.

No prior research is known on the development of a breach in a coversand ridge. Therefore, to gain insight in the development of a breach during a discharge wave, dam breach studies are used (Oumeraci et al., 2005). Within these studies empirical relations are found between the breach width to breach depth ratio and the breach width to discharge ratio. From these case studies can, on the other hand, be concluded that each case gives different results. The differences in and on dams itself (cohesion of sediment, phreatic line, vegetated layer) and differences in measurements during the breach development give different outcomes for each case. The various dam breach studies result in a maximum width-depth ratio of around 5 (Coleman et al., 2002; D. L. Fread, 1988; Singh, 1996). This means that 1 meter depth gives a 5 meters width. With the current knowledge about the maximum depth and width that has occurred in the westerly breach (4 meters x 100 meters), these empirical relations from the dam breach studies cannot be used.

In the static modelling approach, various breach dimensions with different depths and widths are implemented in the pre-breach DEM with the reconstructed coversand ridge. By simulating various flood waves over the pre-breach DEM and analysing the hydrodynamic and erosional properties of the flow in the breaches, insight is obtained in the development of the breach during various stages of the breach. The dimensions of the constructed breaches in the coversand ridges are based on the current knowledge about this case study. The best guess for maximum width and depth of the easterly breach are respectively 100 and 4 meters. For this reason, it is chosen to use these dimensions as the maximum dimensions of both breaches in the coversand ridge. To get insight in the hydrodynamics and sediment transport capacity of the stage of an expanding breach (Stage 2 & 3) it is decided to implement breaches with a width of 50 and 100 meters and three different depths (1, 2 and 4 meters). The cross-section profiles of these breach widths and the longitudinal profiles through the center of the breach are shown in Figure 2.3.

Next to the aforementioned breach dimensions, a case with a breach with shallow shoulders is also implemented in the DEM. This case represents the moment just after the collapse of the sidewalls, something which can happen in reality. This development can occur due to the following events: The breach will first expand in depth until the breach is at bed level (relative to the surrounding ground) or somewhat below it (between Stage 2 and Stage 3). At that moment, the sidewalls can already collapse, because it is too steep, or they will expand in width (Stage 3). In the latter scenario, a vegetated top layer is present left and right of the breach. Because of the larger cohesion that is caused by the vegetation of this layer, this layer will erode less easily than the non-cohesive sediment layer underneath it. The erosion starts at the bottom of the 'wall' of the breach, because this consists of non-cohesive sediment. When certain amounts of sand are eroded from underneath the vegetated layer, the vegetated layer will collapse. At this moment (Figure 2.3; 50 m - 4 m (Shoulders)), the centre of the breach is still the deepest part of the breach, but the collapsed wall causes for a situation in which the breach has shallow shoulders. Just after the collapse, the flow velocities on the shallow shoulders are thought to be significantly larger than the flow velocities on the floodplain. In combination with a small water depth, the breach will continue to erode rapidly to the base of the coversand ridge and the 'cut and collapse' cycle continues (Wang et al., 2016).

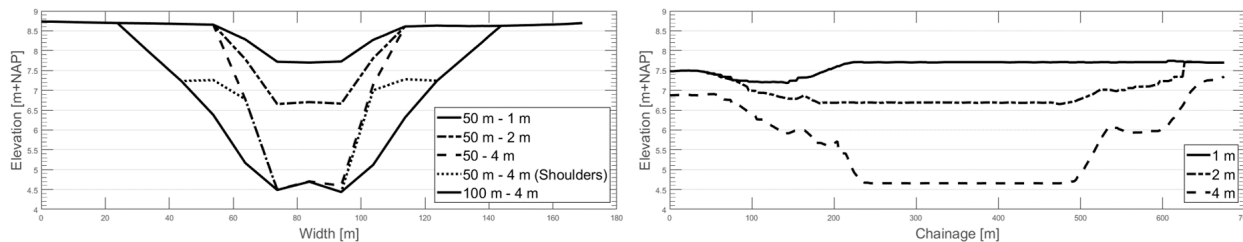


**Figure 2.3:** Left: Cross-sectional view of the various breach dimensions used in this research; Right: Longitudinal view of the various breach depths used in this research

From the historical data it is known that the easterly breach kept expanding and the westerly breach eventually silted. At one point in time the easterly breach must have been greater in width than the westerly

breach. To gain insight in the interaction of the breaches during the erosion phase, a scenario is constructed, that consists of a 50 meters wide westerly breach and a 100 meters wide easterly breach. In this scenario both breaches have a depth of 4 meters.

Lastly a scenario is constructed in which the westerly breach is larger than the easterly breach (100 and 50 meters respectively). This scenario could have occurred if the westerly breach initiated first. If during this scenario the easterly breach is subject to significantly larger erosion velocities than the westerly breach, it can be concluded that although the westerly breach was initially larger, the easterly breach would still expand faster and the river IJssel would form there.

In short, the following dimensions are used for the implementation of the breaches in the coversand ridge in the pre-breach DEM (Table 2.1):

**Table 2.1:** Various dimensions of the breaches in the coversand ridges for the static modelling approach

Westerly breach		Easterly breach	
Width [m]	Depth [m]	Width [m]	Depth [m]
<i>Equal dimensions</i>			
50	1	50	1
50	2	50	2
50	4	50	4
100	4	100	4
<i>Shallow shoulders</i>			
100	4	100	4
<i>Different widths</i>			
50	4	100	4
100	4	50	4

### Bathymetry breach

Next to the breach itself, the bathymetry of the incoming flow funnel and the outgoing flow splay is constructed and implemented in the DEM. At the incoming flow funnel, the flow velocities will increase and will gradually erode the entrance of the breach. At the exit, when there is a very high concentration of sediment in the water during stage 2 and 3, the mixture forms a debris flow. If this flow spreads out, the flow quickly loses energy and deposits the sediment, creating a outgoing flow splay (Figure 2.4; Gary Nichols, 2009). The entrance is cup shaped and the exit has a trumpet like shape.

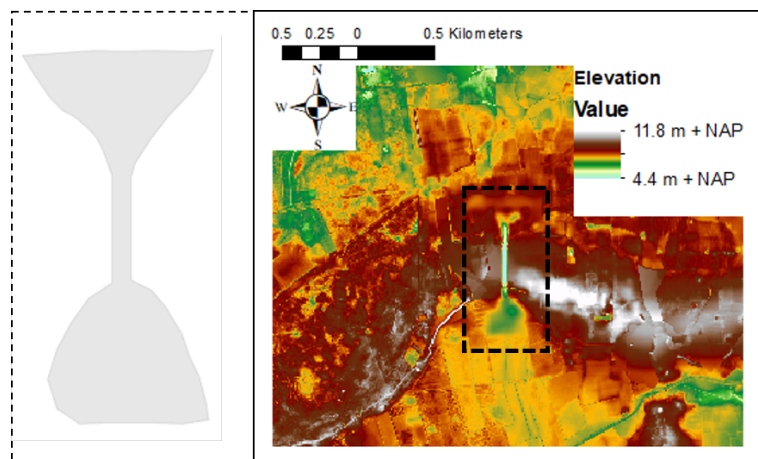


**Figure 2.4:** Breach in coversand ridge, with the flood wave flowing from South to North. Right: The contour of the constructed breaches in the coversand ridge; Left: An example of the constructed breach in the coversand ridge (Example: 50 meters width and 4 meters depth)

### 2.3.2 Flood wave propagation and return period

The process of a river changing course on a floodplain or in a delta, may take 100-1,000 years (Stouthamer, 2001). The development of the river IJssel as a bifurcation of the river Nederrijn also took time. During this period, various flood waves with different peak discharges have flood the floodplain, which could have contributed to the development of the river IJssel.

As first hypothesized in Cohen and Lodder (2007) on geological grounds and supported by hydrodynamic modelling by van der Meulen et al. (In Prep) a flood wave with a peak discharge of  $14,000 \text{ m}^3/\text{s}$  is the most probable trigger to overtop and erode the coversand ridges. To put this into perspective, the mean discharge of the river Rhine is around  $2,200 \text{ m}^3/\text{s}$ . Smaller events than  $14,000 \text{ m}^3/\text{s}$  are reckoned not have the potential energy and water level to overtop and trigger the erosion of the coversand ridge. A flood wave with a peak of  $14,000 \text{ m}^3/\text{s}$  at Andernach (Figure 3.1) results in a discharge of approximately  $4,500 \text{ m}^3/\text{s}$  on the IJssel floodplain and  $8,500 \text{ m}^3/\text{s}$  via the rest of the Rhine delta. Due to the dissipation of the flood wave over the floodplain the peak of  $14,000 \text{ m}^3/\text{s}$  at Andernach spreads out resulting in a peak discharge of approximately  $13,000 \text{ m}^3/\text{s}$  downstream. In the simulation over the paleo-DEM, the discharge partitioning results in a discharge of 35% of the total discharge via the IJssel floodplain and 65% on the rest of the floodplain (van der Meulen et al., In Prep). At Andernach, a flood wave with a peak discharge of  $14,000 \text{ m}^3/\text{s}$  in the present situation has a statistical return period of 200 years (Hegnauer, 2017). In a pre-embanked situation this return period would be larger due to the greater retention in large floodplain areas further upstream in the Rhine catchment relative to the present situation, which dissipated the flood wave more in the past. In the paleo situation, greater areas of the floodplain, with denser vegetation, decelerated the delivery of water from hill slopes and propagation of flood waves. Besides this the drainage of precipitation to the river system accelerated due to the present urbanisation.

After the peak discharge of  $14,000 \text{ m}^3/\text{s}$ , smaller subsequent floods could have contributed to the breach development and eventually on the formation of the meandering river IJssel. This can be assumed, because the paleo-DEM of 800 AD of Van der Meulen et al. (2020) already shows a lower elevated course of the river Rhine to the coversand ridges, which can be used for the drainage of the river Rhine. Flood waves with peak discharges of  $10,000 \text{ m}^3/\text{s}$  and  $6,000 \text{ m}^3/\text{s}$  are used for obtaining insight in the impact that smaller floods can have on the existing breaches (Figure 2.5). At Andernach, these peak discharges have a return period of 20 and 3 years respectively in the present situation. The various discharge waves are scaled on the discharge wave of 1925/1926 (Bomers et al., 2019a). The shape of this discharge wave closely resembles the average of modelled extreme flood waves of the Rhine near Andernach, using the GRADE (Generator of Rainfall and Discharge Extremes) approach of Hegnauer et al. (2014), and is thus the most representative discharge wave.

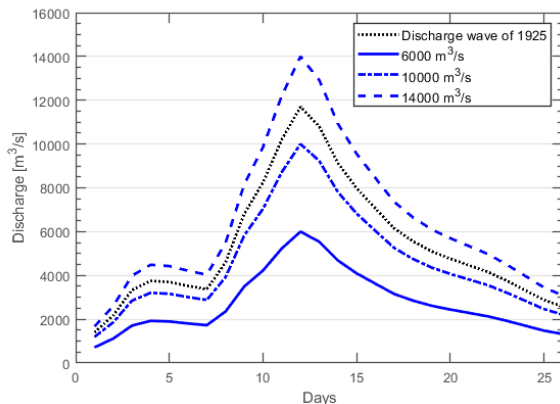


**Figure 2.5:** Discharge waves with various peak discharges scaled from the 1925/1926 discharge wave (Bomers et al., 2019a)

# Chapter 3

## Method

This chapter elaborates on the coupled hydrodynamic-erosion model that is used in this research. The hydrodynamic is set up analogously to Bomers et al. (2019a) and van der Meulen et al. (In Prep). The first section elaborates on the model set up of the hydrodynamic model. The second part of this chapter elaborates on the erosion model that is developed for this research and the link between the hydrodynamic and erosion model.

### 3.1 Hydrodynamic model

#### 3.1.1 Model set-up

A hydrodynamic model is set up for the simulations of the various flood waves over the pre-breach DEM with the different breach dimensions (Table 2.1) analogously to Bomers et al. (2019a) and van der Meulen et al. (In Prep). Hydrodynamic models provide insight in the flow patterns and inundation extents of historic events (Bomers et al., 2019a). The hydrodynamic model requires a reconstruction of the historical geometry before the IJssel avulsion with the reconstructed coversand ridges and the roughness of the floodplain as input data. In addition, it requires proper boundary conditions to determine the flood wave propagation along the model domain. The hydrodynamic model computes among others the water depth, depth-averaged flow velocity and the discharge through the breaches.

A one-dimensional - two-dimensional (1D-2D) coupled hydrodynamic model is set up for the simulation of various flood waves (Figure 3.1). HEC-RAS (v. 5.0.3), developed by the Hydrologic Engineering Centre (HEC) of the US Army Corps of Engineers, is used as modelling software (Brunner, 2016). Bomers et al. (2019a) compared the 1D-2D coupled hydrodynamic model with a full 2D hydrodynamic model and concluded a coupled 1D-2D hydrodynamic model of the present situation of the Rhine and IJssel floodplain is capable of simulating maximum discharges with high accuracy. Input of the 1D-2D hydrodynamic model is the bathymetry and the roughness based on the land cover of the floodplain and its channels. The boundary conditions are a discharge wave that represents a flood upstream (Figure 2.5). These discharge waves are scaled on the extreme flood wave of 1925/1926 (van der Meulen et al., In Prep). Normal depths computed with the Manning's equation are used as downstream boundary conditions (Brunner, 2016). In the model, the main channels of the river Rhine and its branches (from before the IJssel avulsion) are schematized with 1D profiles (Figure 3.1). The 1D unsteady flow hydrodynamics are solved using the principle of conservation of mass (continuity), and the principle of conservation of momentum (Appendix B). To avoid a dry main channel bed at the start of the simulations an initial discharge of  $1,000 \text{ m}^3/\text{s}$  is used in the Lower Rhine (van der Meulen et al., In Prep).

The floodplains are discretized on a 2D grid with a resolution of 200x200 meters rectangular grid cells and flexible grid shapes along the model domain boundaries since 1D profiles are not capable of simulating the complex overland flow patterns in the floodplains (van der Meulen et al., In Prep). The coversand ridge are located on the floodplain and are thus in the 2D grid. The resolution at the breach locations in the coversand

ridges is increased, since a 200x200 meters grid covers the whole breach and not the differences within the breach. This resolution increase will be elaborated on in paragraph 3.1.1. The 1D profiles are coupled with the 2D grid using the weir-equation (Appendix B). The weir coefficient is set to a value corresponding to overland flow to enable correct prediction of the flow transfer and to keep the model stable. The 2D grid is solved using the Full Momentum equations (Appendix B).

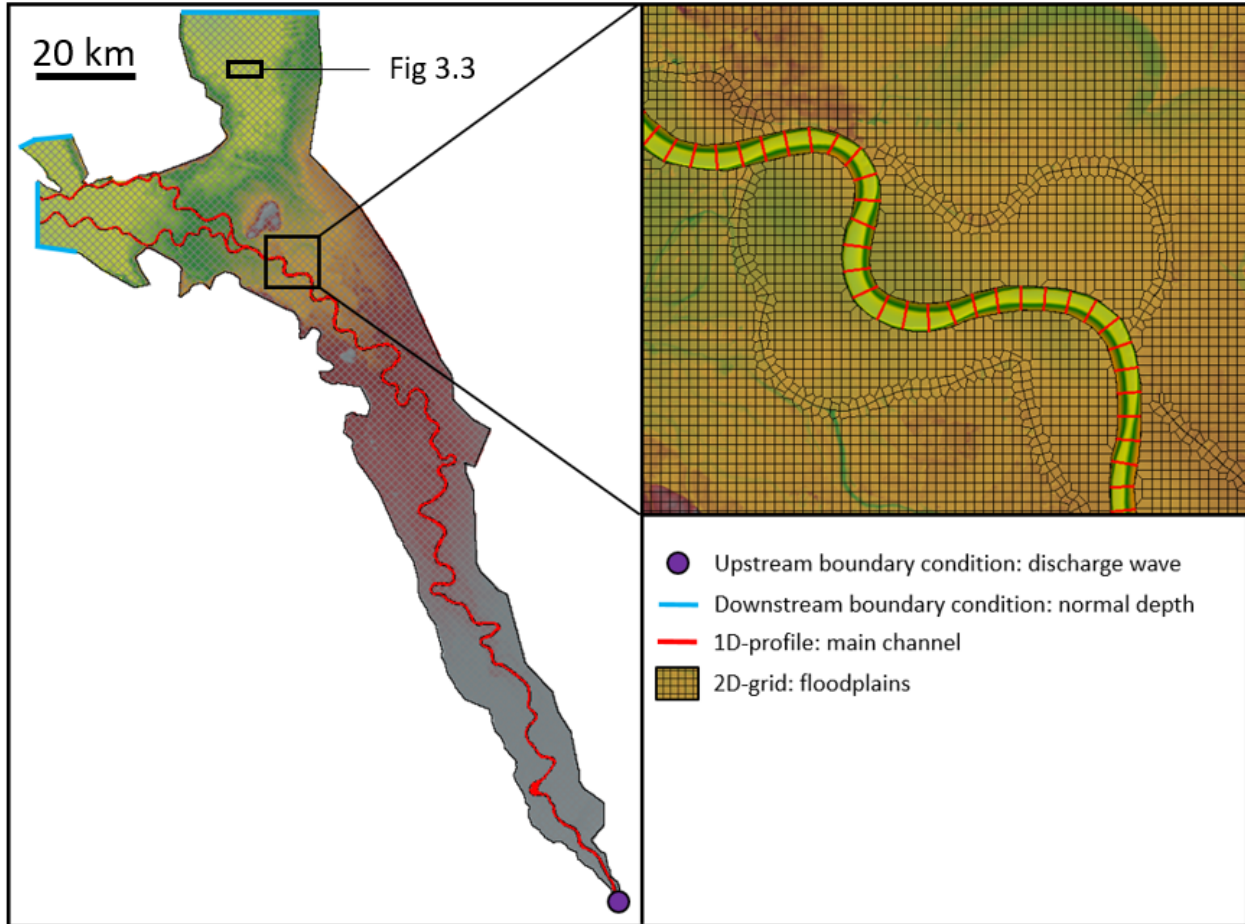


**Figure 3.1:** 1D-2D coupled grid of the full model domain set up by Bomers et al. (2019a). The 1D profiles are coupled to the 2D grid using the weir equation.

### Roughness coefficient

Water flow is subject to resistance and energy dissipation in open channels, on floodplains and also in breaches. hydrodynamic calculations of the flow in channels and overbank areas of floodplains require an evaluation of roughness characteristics. Most commonly, the Manning roughness coefficient ( $n$ ) is used to describe the flow resistance or relative roughness of a channel, overbank areas and floodplains (Robert & Jarrett, 1985). The Manning roughness coefficient is required as input for the simulations that are done in this research. The roughness on the floodplain and the river bed and banks are set up analogously to van der Meulen et al. (In Prep). The research of van der Meulen et al. (In Prep) converted land cover classes into roughness coefficients using the tables of Chow (1959). A distribution of the roughness classes is shown in Figure 3.2 and additional information of those classes is represented in Table 3.1. Next to the land cover classes of van der Meulen et al. (In Prep), one additional roughness coefficient is required for the representation of the roughness of the non-cohesive sediment in the breaches of the coversand ridges in this research. Due to the smaller sediment size of the coversand relative to the sediment in the rivers and different hydrodynamic properties, the roughness characteristics in a breach are not equal to the roughness characteristics of river

beds and banks.

An equation for the approximation of the Manning coefficient is:

$$n = 0.04k_s^{\frac{1}{6}} \quad (3.1)$$

In this equation  $k_s$  is the Nikuradse roughness height in  $m$ . For  $k_s$  often the grain diameter is used. Normally, one  $n$  value is selected for the entire range of depth of flow. Most relations between roughness and depth of flow are too technical for general use and often involve variables that are not usually measured onsite (Robert & Jarrett, 1985). The roughness coefficient in this study cannot be determined using measurements onsite. For this reason the roughness coefficient must be estimated.

The roughness can be estimated using Equation 3.1 or from the table of the base values of the Manning coefficient from Arcement and Schneider (1989). Equation 3.1 gives a Manning coefficient of  $0.001 \text{ m/s}^{\frac{1}{3}}$  using the grain diameter of the coversand of  $210 \mu\text{m}$  as the roughness height  $k_s$ . From the table of Arcement and Schneider (1989), shown in Figure D.1 in Appendix D, it is stated that sediment with a median grain size of around  $0.2 \text{ mm}$  has a Manning coefficient of  $0.012 \text{ m/s}^{1/3}$  in a sand channel if the flow is in upper regime. A flow is in upper regime if the power of stream flow washes out ripples and dunes, replacing it with a plane bed plus antidunes, and erosional chutes and pools. The upper regime is characterised with a Froude number larger than 1. From Figure D.2 can be found that the flow is in the upper regime above approximately  $1.8 \text{ m/s}$ . Bisschop et al. (2010) and van Rhee (2010) state that flow velocities in breaches can increase up to  $10 \text{ m/s}$  and are thus well over the threshold of  $1.8 \text{ m/s}$ . It is chosen to use a Manning's coefficient of 0.012 in the breaches, because it best represents the flow in upper regime, as present during stages 2 and 3 of the breach development.

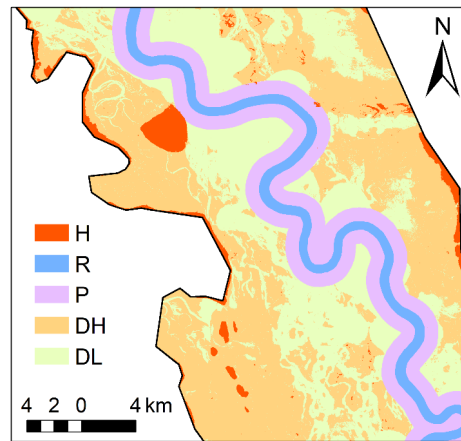


**Figure 3.2:** Distribution of roughness classes (van der Meulen et al., In Prep). The abbreviations and Manning's  $n$  values attributed to the different classes are given in Table 3.1

**Table 3.1:** Roughness classes and Manning's  $n$  values determined by van der Meulen et al. (In Prep). Land cover classes were converted into roughness coefficients using tables of Chow (1959)

Class	Definition	Manning's coefficient 'n'
H	High ground area > trend + 5 m vertical	0.1
R	River bed and banks River polygons + 100 m lateral	0.03
P	Proximal floodplain Border of R + 1000 m lateral	0.07
DH	Distal floodplain, high Remaining area > trend	0.05
DL	Distal floodplain, low Remaining area < trend	0.04
B	Breach Non-cohesive sediment in breach	0.012

### Grid size

A grid size with a resolution of 200x200 meters is used on the floodplain (Figure 3.1). For the simulation of the effects of various flood waves on the inundation extent, this resolution is sufficient. At the breach locations, a higher resolution is required. From historical mapping and dating at the breach locations, it is found that the width of the westerly breach location has a maximum of approximately 100 meters (Cohen et al., 2009). Using a 200x200 meters resolution grid, one cell covers the entire breach. This results in inaccurate results for the hydrodynamic simulation of the flood waves. In the hydrodynamic simulation the elevation of the center of the cell is used for the computation of the flow properties (i.e. flow velocity and water depth) for a grid cell for every time step. With this flow properties in the 200x200 grid cell, local flow properties are obtained at a 5x5 meters DEM resolution in the grid cell itself using a high resolution subgrid model (Casulli, 2008). For the inundation extent of a flood wave, this resolution does not lose much information according to Bomers et al. (2019a), but for the computation of the local flow velocities in a breach, a grid of 200x200 meters is not detailed enough. The grid is aligned to the crest of the coversand ridges and manually refined at the breach locations. By using a local refinement, the computational time does not increase significantly and the stability of the hydrodynamic model set-up by Bomers et al. (2019a) was maintained. This resulted in an unstructured grid with a mean grid size of 10x20 meters at the breach locations and a 200x200 meters grid at the remainder of the floodplain (Figure 3.3).

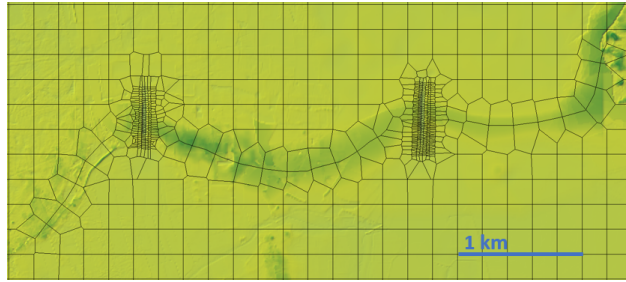


**Figure 3.3:** *Locally refined grid resolution in breaches at the coversand ridges*

### 3.1.2 Data extraction from hydrodynamic model

The breaches in the coversand ridges are located in the floodplain and thus in the 2D grid of the model. The flow properties, like flow velocity, water depth and discharge in the breaches, are extracted from the hydrodynamic model using 14 lateral and 5 longitudinal profile lines (Figure 3.4). The hydrodynamic software, HEC-RAS, computes directly usable hydrodynamic output at the cross-sectional profiles. These 1D profiles are generally present in the rivers, but not on the floodplain. At these cross-sectional profiles, the software post-processes the hydrodynamic simulation to results that are ready to be used for further calculations and can easily be extracted. On the 2D grid, this is not the case, so post-processing steps for processing the hydrodynamic output in the breaches were required, before it could be used for the erosion and sediment transport capacity model.

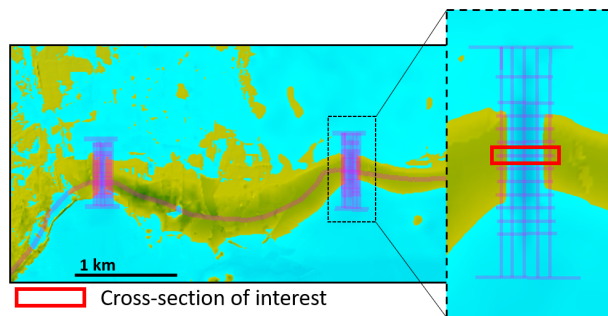


**Figure 3.4:** *Profile lines in the breaches for the data extraction from the hydrodynamic model*

## 3.2 Erosion model

### 3.2.1 Erosion equation

Several erosion equations from different backgrounds are suggested in the literature. Some erosion equations are established from historical dam breach data. These erosion equations are derived from the historical dam breach characteristics of different dam breaches. Parameters like eventual breach width, reservoir volume and crest height are mostly the base of these fully empirical erosion equations. Other erosion equations that are suggested in the literature have a physical background and thus take the physical characteristics of the soil and the flow into consideration (Oumeraci et al., 2005). Singh and Scarlatos (1988) states that the erosion rate at the breach is assumed to be a power function of the flow velocity. An example of such an equation is the pick-up rate equation developed by van Rijn (1984a) and adjusted for high flow velocities by van Rhee (2010). The equation is empirical, but is based and calibrated on the soil and flow characteristics. With the equation of van Rhee (2010), the erosion in the breaches can be computed using the flow velocity and water depth in the breaches, which is output of the hydrodynamic model. Based on experimental data, the following empirical pick-up function (Equation 3.2) is proposed for the erosion of a sand bed per unit area and time by van Rhee (2010):

$$E = 0.00033\rho_s[(s_d - 1)gD_{50}]^{0.5}(D_*)^{0.3}f_D \left( \frac{\theta - \theta_{cr}}{\theta_{cr}} \right)^{1.5} \quad (3.2)$$

With the equation for the pick-up rates for low and high flow velocities, the erosion rate (velocity)  $v_e$  in  $m/s$  perpendicular to the bed can be computed using Equation 3.3. In the pick-up rate equation, the direct horizontal erosion and thus pick-up rate of the sandy walls is neglected, because the breach width is much larger than the breach depth. The erosion of the sandy walls is elaborated on using Equation 3.5 further on in this section.

$$v_e = \frac{E}{\rho_s(1 - n_0)} \quad (3.3)$$

Table 3.2 documents the variables used in Equations 3.2 and 3.3:

**Table 3.2:** Variables of pick-up equation of sand particles of van Rhee (2010)

Variable	Meaning	Unit	Value
$v_e$	Erosion velocity perpendicular to the bed	$m/s$	Output
$E$	Pick-up rate	$kg/m^2/s$	Variable
$D_* = D_{50}[(s - 1)g/\nu^2]^{1/3}$	Dimensionless grain size parameter	-	5.3
$D_{50}$	Median grain size	$m$	$2.1 * 10^{-4}$
$\nu$	Kinematic viscosity coefficient of the fluid	$m^2/s$	$1 * 10^{-6}$
$s_d = \rho_s/\rho_w$	Relative density	-	2.65
$\rho_s$	Sediment density	$kg/m^3$	2650
$\rho_w$	Fluid density	$kg/m^3$	1000
$\theta = \tau/[(\rho_s - \rho_w)gD_{50}]$	Grain-related Shields parameter	-	Variable
$\tau = \rho_w g[U/C]^2$	Grain-related bed-shear stress	$N/m^2$	Variable
$U$	Depth-averaged flow velocity ( <b>Output of HEC-RAS</b> )	$m/s$	Variable
$C = h^{1/6}/n$	Chézy-coefficient	$m^{0.5}/s$	Variable
$h$	Water depth ( <b>Output of HEC-RAS</b> )	$m$	Variable
$n$	Manning coefficient	$s/m^{1/3}$	0.01
$\theta_{cr}$	Shields critical value at initiation of motion (obtained from the Shields curve (Shields, 1936)) or in terms of the grain size parameter ( $D_*$ ) as shown in Equation 3.4 (van Rijn, 1993)	-	0.048
$g$	Gravity acceleration	$m/s^2$	9.81
$f_D = 1/\theta$ for $\theta > 1$	Damping factor	-	Variable
$n_0$	In-situ porosity	-	0.4

The critical Shields parameter ( $\theta_{cr}$ ) is the critical condition for sediment to be put into motion and is expressed by the following relations:

$$\theta_{cr} = \begin{cases} \frac{0.24}{D_*} & \text{if } 1 < D_* \leq 4 \\ \frac{0.14}{D_*^{0.64}} & \text{if } 4 < D_* \leq 10 \\ \frac{0.04}{D_*^{0.1}} & \text{if } 10 < D_* \leq 20 \\ 0.013D_*^{0.29} & \text{if } 20 < D_* \leq 150 \\ 0.055 & \text{if } D_* > 150 \end{cases} \quad (3.4)$$

In the equation of van Rhee (2010) the erosion rates are computed perpendicular to the bed. With this equation only erosion rates at the centre of the breach, where the bed is horizontal, can be computed and not at the sides of the breach (the walls). A translation of the erosion rates in the centre to the erosion of the walls is required to gain insight into the lateral breach development. From the soil mechanics, considering non-cohesive sediment, is known that a slope can only be stable in the long term when the slope angle ( $\beta$ ) is less than the angle of internal friction ( $\phi$ ) (Figure 3.5). In this figure,  $G$  is the force of gravity,  $F_s$  the force due to the flowing water, which act on the sediment particles and  $F_i$  is the inwardly directed hydraulic gradient van Rhee (2010) suggests a straight-forward equation for the computation of the stability of these walls:

$$v_{wall} = \frac{v_e}{\sin \beta} \quad \text{if } \beta > \phi \quad (3.5)$$

This equation can be explained as follows, using two breaches with equal soil properties as an example: If a breach is subject to high flow velocities it will erode perpendicular to the bed and thus become deeper. When the breach deepens, the walls steepen until the slope angle becomes larger than the angle of internal friction. At this moment, the walls start to erode due to the instability and the breach will expand. If one of the two breaches is subject to higher erosion rates than the other breach, this breach will expand faster than the other.

This research is not focused on the detailed physics and dynamic computation of a developing breach, but only on gaining insight in the hydrodynamic and erosional properties of different breaches under various circumstances. For this reason, the horizontal erosion velocities are not computed, because these do not give more insight in the breach development than the vertical erosion velocities.

The erosion rate equation of van Rhee (2010) is dependent on the actual bed shear stress on site and the critical bed shear stress that is required for the soil to be put into motion. The equation shows that erosion only takes place if and only if the actual Shields parameter exceeds the critical Shields parameter. This can be translated to: erosion takes place if the actual bed shear stress on site exceeds the threshold value of the critical bed shear stress. Translating the critical Shields parameter to a critical bed shear stress using the equation for the grain-related Shields parameter in Table 3.2, gives a critical bed shear stress of  $0.16 \text{ N/m}^2$ . The actual bed shear stress that occurs on site gives a first impression on where sediment can be put into motion and thus erosion can occur in the breach. The determination of the actual bed shear stress in the breach versus the critical bed shear stress is less uncertain than the determination of actual erosion rates, as stated by Oumeraci et al. (2005). For this reason, the results first elaborate on the determination of the actual bed shear stresses that occur on the floodplain versus the critical bed shear stresses, before elaborating on the estimated erosion rates of the coversand ridges.

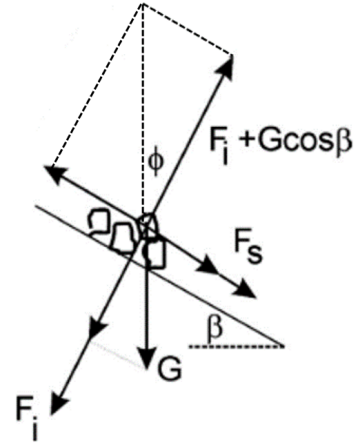


**Figure 3.5:** Stability of particles on a slope (van Rhee, 2010)

### 3.2.2 Sediment transport capacity

In the literature is stated that the prediction of erosion has strong uncertainties (Oumeraci et al., 2005), because each equation has a different empirical background. For this reason, the potential breach development is also computed using sediment transport capacity equations. For the dynamic simulation of the breach development and erosion, sediment transport capacity equations are used (i.e. D. L. Fread (1988)). For obtaining insight in the breach development in a static modelling approach, these equations can also be used. Three different sediment transport equations are considered. These are the sediment transport equations of Meyer-Peter and Müller (1948), Engelund and Hansen (1967) and van Rijn (1984b). The sediment transport equation of Engelund and Hansen (1967) is most applicable in this case. This equation proves to be especially applicable for the total load of relatively fine material, in which the suspended load plays a vital role. Besides this, the sediment transport equation of Meyer-Peter and Müller (1948) is only tested on sediment larger than 0.4 mm. The coversand has a mean diameter ( $D_{50}$ ) of 0.21 mm, so the equation of Meyer-Peter and Müller (1948) is less applicable then the equation of Engelund and Hansen (1967). The equation of van Rijn (1984b) requires the vertical flow velocity and sediment concentration profile in the water column. These vertical profiles are not the output of HEC-RAS and the computation of these profiles do not give additional certainty in the sediment transport capacity computations in the breaches. Therefore, it is chosen to not use the sediment transport equation of van Rijn (1984b). It should be noted that all three sediment transport capacity equations can be used for the computation of the sediment transport in the breaches, because each equation gives insight in the sediment transport processes in the breaches. The equation of Engelund and Hansen (1967) is best applicable in this case study, because it requires little input parameters and is especially applicable for the total load of relative fine material.

The equation of Engelund and Hansen (1967) for the sediment transport capacity is only valid under the following constraints (the parameters are explained in Table 3.2):

•

$$\mathbf{w_s / u_* < 1}$$

The fall velocity ( $w_s$ ) and bed shear velocity ( $u_*$ ) are calculated as follows:

$$w_s = \frac{10\nu}{D_{50}} \left( \sqrt{1 + \frac{0.01\Delta g D_{50}^3}{\nu^2}} - 1 \right) = 0.03 \text{ m/s} \quad (3.6)$$

$$u_* = \sqrt{\frac{\tau}{\rho}} = U \frac{\sqrt{g}}{C} \quad (3.7)$$

Substitution of equation 3.7 into this constraint and rewriting it for a minimal  $\tau$  at which the equation of Engelund and Hansen is valid gives:

$$\tau_{min} > w_s^2 \rho = 0.77 \text{ N/m}^2 \quad (3.8)$$

•

$$\mathbf{0.07 < \theta < 6.0}$$

The grain related Shields parameter can also be written as a minimum and maximum bed shear stress in which the equation of Engelund and Hansen is valid. Substitution of the equation for the grain related Shields parameter (Table 3.2) into this constraint and rewriting it gives:

$$0.07 * (\rho_s - \rho_w)gD_{50} < \tau < 6.0 * (\rho_s - \rho_w)gD_{50} \quad (3.9)$$

$$0.24 \text{ N/m}^2 < \tau < 20.4 \text{ N/m}^2$$

•

$$0.19 \text{ mm} < D_{50} < 0.93 \text{ mm}$$

This constraint is always true, because a grain size of 0.21 mm is assumed in the whole breach.

Combining the first two constraints of the equation of Engelund and Hansen gives that the equation is valid if the bed shear stress is between  $0.77 \text{ N/m}^2$  and  $20.4 \text{ N/m}^2$ . It should be noted that the computation of the sediment transport capacity outside of these boundaries are not fully incorrect, but the equation is less applicable to compute the sediment transport capacity for these extreme situations.

When the above mentioned constraints are true the sediment transport capacity can be calculated using the following equations:

$$q_s = \Phi \sqrt{g\Delta D^3} \quad (3.10)$$

In which  $\Phi$  is the transport parameter:

$$\Phi = 0.05\Psi^{\frac{5}{2}} \quad (3.11)$$

and  $\Psi$  the flow parameter:

$$\Psi = \frac{\mu\tau}{\rho g\Delta D} = \mu\theta \quad (3.12)$$

$\mu$  can be computed using:

$$\mu = \left(\frac{C^2}{g}\right)^{\frac{2}{5}} \quad (3.13)$$

Substitution of equation 3.11 and 3.12 into equation 3.10 gives:

$$\frac{q_s}{\sqrt{g\Delta D^3}} = 0.05 \left(\frac{u_*}{\sqrt{g\Delta D}}\right)^3 \left(\frac{u}{\sqrt{g\Delta D}}\right)^2 \quad (3.14)$$

To obtain a quick insight into the morphological behavior (is a river eroding or does sedimentation occur) it is often convenient to use a simplified version of the sediment transport equation to ease analytical manipulations. In general, sediment transport equations are of the form:

$$s = mu^n \quad \text{with } m = \frac{0.05}{\sqrt{g}C^3\Delta^2 D_{50}} \quad (3.15)$$

In this equation  $s$  is the sediment transport in  $m^3/s/m$ ,  $u$  is the flow velocity in  $m/s$  and  $n$  is equal to 5 because the conditions of the equation of Engelund and Hansen apply.

# Chapter 4

## Results

### 4.1 Hydrodynamic model

After the different breach dimensions are implemented in the DEM, the hydrodynamic model is simulated for all the different parameter settings (different breach depths, widths and discharge waves). The maximal flood wave extent of a flood wave with a peak discharge of  $14,000 \text{ m}^3/\text{s}$  at Andernach is shown in Figure 4.1. Due to flood wave dissipation this results in a peak discharge of  $13,000 \text{ m}^3/\text{s}$  at Lobith and a discharge partitioning of 35% via the IJssel floodplain and 65% via the remainder of the Rhine floodplain. From these simulations the local water depth and depth averaged flow velocity in both breaches are extracted at the 14 cross-sectional and 5 longitudinal profile lines (Section 3.1.2). Next to this, the discharge through the breaches is of interest, so this is also extracted from the model.

#### 4.1.1 Validation model

The input paleo-DEM constructed in section 2.1 represents the best guess of the pre-breach situation of the Rhine and IJssel floodplain. A pre-embankment DEM was set-up by Van der Meulen et al. (2020), that was adjusted in this research to fully restore the pre-breach coversand ridge divide (using expert judgement; Cohen, pers. comm.). No real time or in-situ data is available for the validation of the model. This section elaborates on the validation of the hydrodynamic model using the literature about breach development and former research of Bomers et al. (2019a) about the hydrodynamics of a model with a comparable set-up (for the same study area/model domain, but the present situation of the river Rhine and IJssel).

#### Flood wave extent

The model in this research is a lower-fidelity 1D-2D hydrodynamic model and is set-up analogously to the 1D-2D hydrodynamic model of Bomers et al. (2019a). A lower-fidelity model can result in less accurate results compared to a higher-fidelity model, due to a different response pattern of the system (Razavi et al., 2012). A higher-fidelity hydrodynamic model is able to compute detailed and accurate results of a potential flood along a river. Bomers et al. (2019a) validated the output of a lower-fidelity with the output of a higher-fidelity model also set-up by Bomers et al. (2019a) of the current situation of the Rhine floodplain.

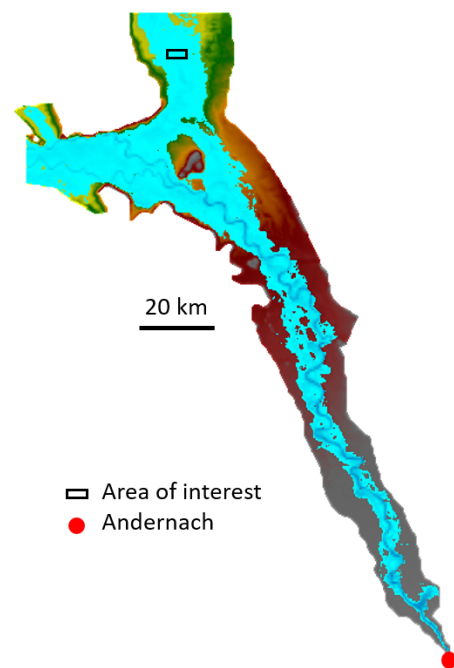


**Figure 4.1:** Flood wave extent using a flood wave with a peak discharge of  $14,000 \text{ m}^3/\text{s}$  at Andernach (Direct HEC-RAS output)

The higher-fidelity model of the current situation of the Rhine floodplain is calibrated on measured water levels. These calibrated input parameters of the higher-fidelity model were then used for the validation of the lower-fidelity model. This validation indicated that the maximum discharge deviation was 2.1 % compared to the higher-fidelity model and that the discharge partitioning along the Dutch Rhine river branches were accurately predicted. In this research it is assumed that the lower-fidelity 1D-2D hydrodynamic model of the pre-breach situation of the Rhine and IJssel floodplain also can be treated as a high-fidelity model, since the low-fidelity model accurately represents the discharge partitioning.

### **Hydrodynamic breach properties**

The validation of the computed flow velocities in the breaches are done using the literature about breach development. Van Rhee 2010, Bisschop et al. (2010) and Verheij (2002) describe that the flow velocities in breaches can be from 2  $m/s$  up to 10  $m/s$ . These velocities are also found in the models. The high flow velocities found in the breaches using the low-fidelity model are between 2  $m/s$  and 7  $m/s$  during stage 2 and 3 of the breach development process. It can be concluded that the lower-fidelity hydrodynamic model accurately represents the reality.

### **Roughness of the breach channel bed**

It is chosen to use a Manning's coefficient of 0.012  $m/s^{1/3}$  in the breaches (Arcement & Schneider, 1989), because van Rhee (2010) stated that the flow in a breach is in upper regime. From the results (Table 4.1) can be concluded that the flow is indeed in upper regime during the passage of the peak of the flood wave, with flow velocities ranging from 2  $m/s$  and 7  $m/s$ . In other words, it can be concluded that the correct Manning's coefficient for such localized extreme situations was selected.

## **4.1.2 Hydrodynamic conditions**

The flow velocities and water depths in the breaches are computed in the hydrodynamic model. An example of the flow velocities and water depth through the breaches at the peak of the discharge wave are shown in Figure 4.2 for the case of a 50 meters wide breach, 2 meters deep and a flood wave of 14,000  $m^3/s$ . At the peak of the discharge wave on the IJssel floodplain, the flow velocities and water depths through the breaches are the most extreme. From Figure 4.2 it can be concluded that the easterly breach is subject to larger flow velocities than the westerly breach and the water depth is also higher. Besides this, a larger portion of the discharge flows through the easterly breach than the westerly breach, which can be explained by the higher flow velocities and higher water depth in the easterly breach.

The above mentioned figures give a first insight into the differences in the hydrodynamic conditions in both breaches with equal conditions for both breaches during a flood wave. The main objective of this research is to obtain insight into the breach development, so understanding the hydrodynamic conditions during several stages of the breach development is also of importance. For this reason, the flow velocity and water depth in the centre of the breach are evaluated for the different parameter settings.

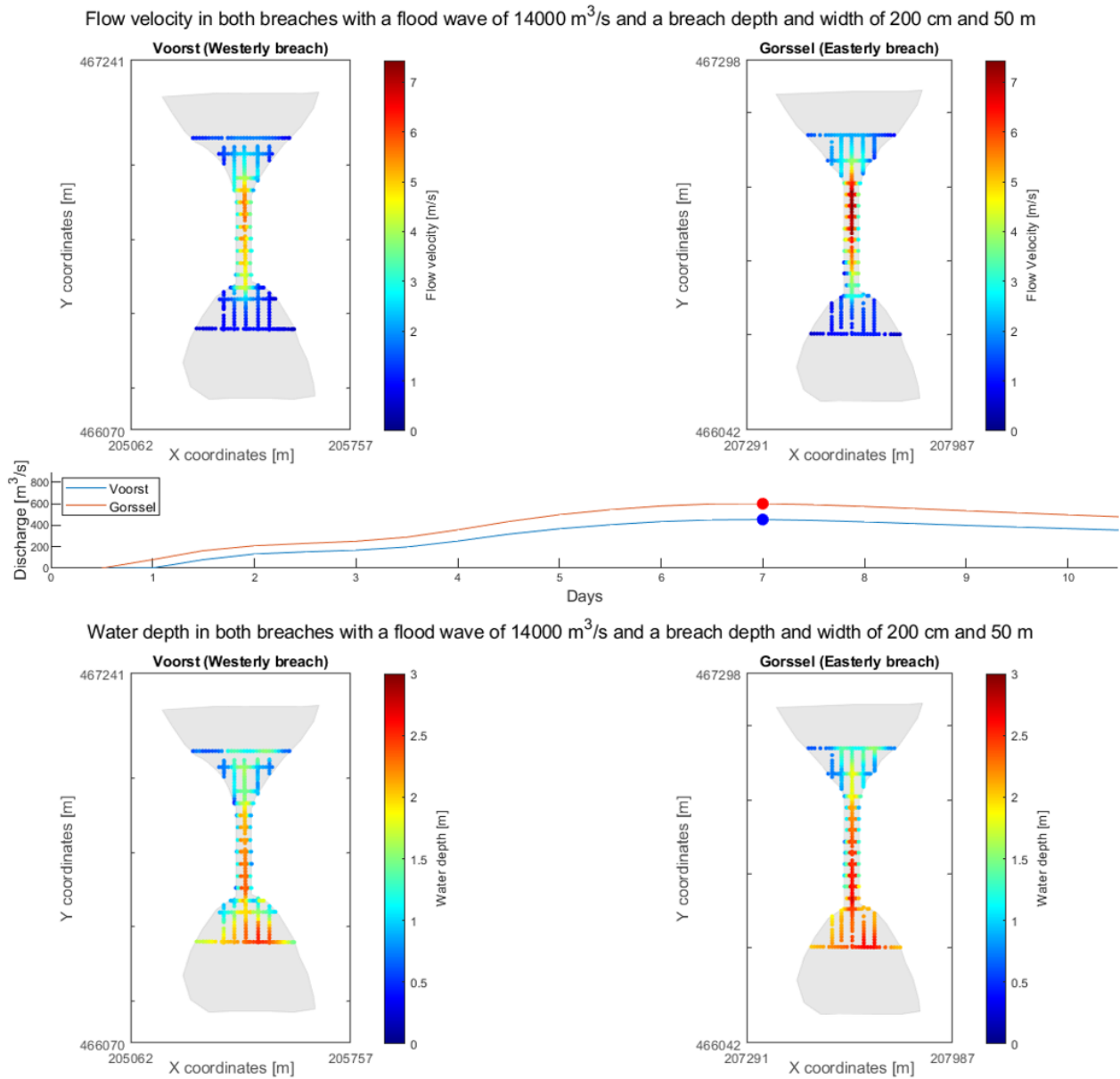


**Figure 4.2:** Example of the flow velocity and water depth through the breaches during a flood wave with a peak discharge of  $14,000 \text{ m}^3/\text{s}$  at Andernach (resulting in a discharge of  $3,500 \text{ m}^3/\text{s}$  on the IJssel floodplain). The discharge distribution through the breaches is shown in the middle graph (Post-processed HEC-RAS output).

**Cross-sectional flow velocity**

The output of the hydrodynamic model is analysed and the maximum flow velocities in the centre of the breach (cross-section of interest in Figure 3.4) are given in Table 4.1. The maximum cross-sectional flow velocities are shown in this table and not the distribution of the flow velocity over the cross-section of the breach, because the maximum flow velocity gives as much insight as the flow velocity distribution. If the maximum flow velocity is higher, the cross-sectional flow velocity distribution will also be higher.

Looking at the maximum flow velocities in Table 4.1 shows that the maximum flow velocity first increases from a depth of 1 meter to 2 meters, but decreases if the breach becomes deeper for all discharges. At a depth of 4 meters, the maximum flow velocity through the breach is less than at a depth of 2 meters. This is due to the bathymetry of the 4 meters deep breach. At this stage the breach is deeper than the surrounding floodplain, and this deeper area lead to deceleration of the flow.

**Table 4.1:** *The maximum flow velocities in the core of the breach for the different parameter settings*

Discharge [m <sup>3</sup> /s]	Westerly breach			Easterly breach		
	Width [m]	Depth [m]	Flow velocity [m/s]	Width [m]	Depth [m]	Flow velocity [m/s]
<i>Equal dimensions</i>						
10000	50	1	3.2	50	1	4.8
14000	50	1	3.8	50	1	5.5
10000	50	2	4.4	50	2	6.8
14000	50	2	5.0	50	2	7.3
10000	50	4	3.3	50	4	6.5
14000	50	4	4.1	50	4	7.1
10000	100	4	2.1	100	4	4.0
14000	100	4	2.7	100	4	4.7
<i>Shallow shoulders</i>						
10000	100	4	2.9	100	4	5.1
14000	100	4	3.5	100	4	5.9
<i>Different widths</i>						
6000	50	4	2.0	100	4	2.6
10000	50	4	3.3	100	4	4.0
14000	50	4	4.1	100	4	4.7
10000	100	4	2.5	50	4	6.3
14000	100	4	3.1	50	4	7.0

From Table 4.1 can be found that the maximum flow velocity is higher when the breach has shallow shoulders compared to the situation with a breach width of 100 meters. As stated in Section 2.3.1 the flow velocities on the shallow shoulders are thought to be larger than the flow velocities in a straight-forward trapezoidal breach with a width of 100 meters. For this reason, this section elaborates on these flow velocity differences. The flow velocities in the breaches are shown in Figure 4.3 for both situations and the cross-sectional differences in the flow velocity profile is shown in Figure 4.4. From these figures can be concluded that the flow velocity on the shallow shoulders is slightly higher compared to the situation with a breach width of 100 meters, but especially in the center of the breach the flow velocities increase significantly. This can be explained by the narrower breach width in the center. The discharge wave is almost equal for both situations, but the cross-sectional area decreases. A narrower breach then results in higher flow velocities than a wider breach.

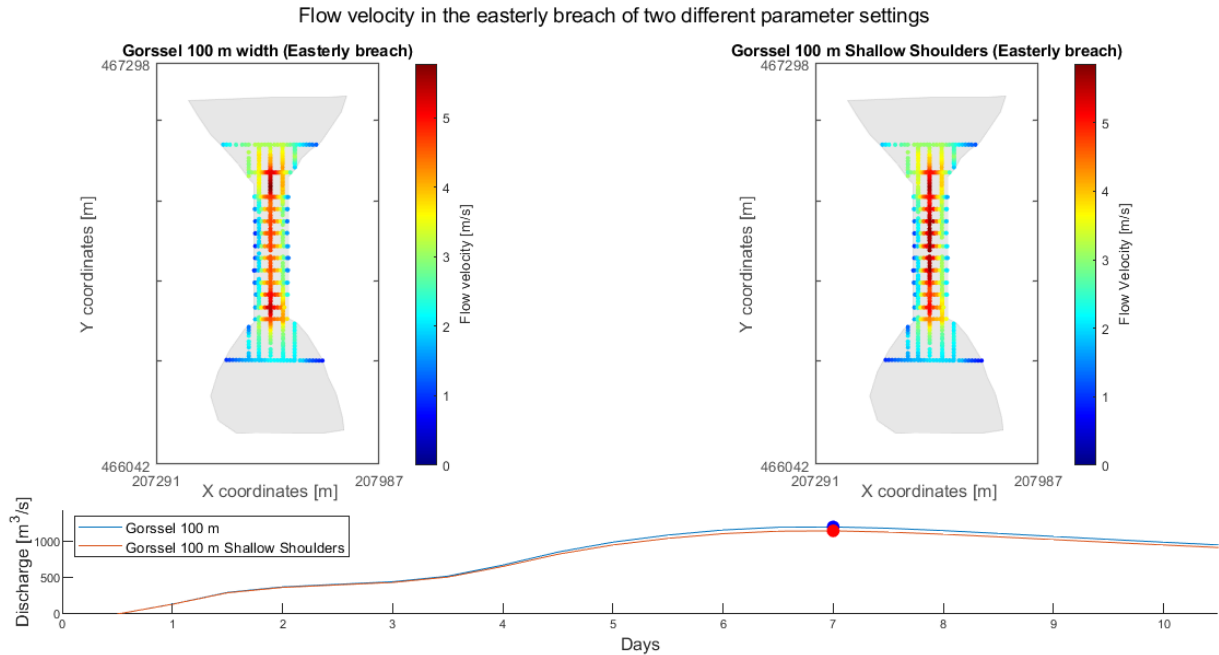


**Figure 4.3:** Flow velocity in the easterly breach for different parameter settings. Left: Breach with a width of 100 m; Right a breach width a width of 100 m and shallow shoulders (Post-processed HEC-RAS output)

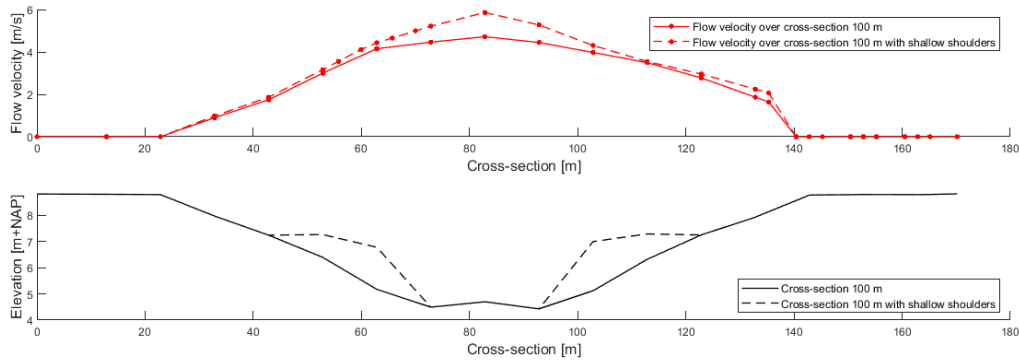


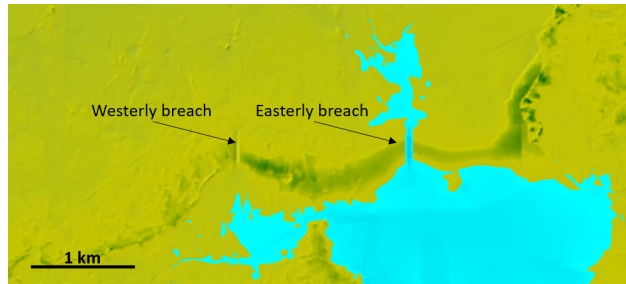
**Figure 4.4:** Velocity profile over cross-section in the easterly breach comparing a breach with 100 m width to a breach with 100 m width including shallow shoulders (Cross-section of interest in Figure 3.4)

### Water depth

The maximal cross-sectional water depth in the center of the breach is shown in Table 4.2. For the interpretation of these results it is important to note that the breach dimensions are exactly equal and the elevation relative to sea level (m+NAP) is equal for both breaches. From these results can be concluded that the water depth in the westerly breach is shallower for each parameter setting. This can be explained by the flood wave propagation (Figure 4.5). The flood wave reaches the coversand ridge at the easterly breach before it flows to the westerly breach. When the flood wave propagates to the westerly breach, the flood wave will dissipate more and the easterly breach discharges a portion of the flood wave, resulting in lower water levels and thus shallower water depths.

**Table 4.2:** *The maximum water depth in the core of the breach for the different parameter settings*

Westerly breach				Easterly breach		
Discharge	Width	Depth	Water depth	Width	Depth	Water depth
[ $m^3/s$ ]	[ $m$ ]	[ $m$ ]	[ $m$ ]	[ $m$ ]	[ $m$ ]	[ $m$ ]
<i>Equal dimensions</i>						
10000	50	1	1.2	50	1	1.3
14000	50	1	1.4	50	1	1.5
10000	50	2	2.1	50	2	2.2
14000	50	2	2.3	50	2	2.4
10000	50	4	4.2	50	4	4.3
14000	50	4	4.3	50	4	4.5
10000	100	4	4.3	100	4	4.4
14000	100	4	4.3	100	4	4.5
<i>Shallow shoulders</i>						
10000	100	4	4.3	100	4	4.4
14000	100	4	4.4	100	4	4.6
<i>Different widths</i>						
6000	50	4	3.8	100	4	3.9
10000	50	4	4.1	100	4	4.2
14000	50	4	4.3	100	4	4.4
10000	100	4	4.1	50	4	4.3
14000	100	4	4.3	50	4	4.5

**Figure 4.5:** *Flood wave propagation. During the flood wave, the easterly breach becomes active approximately 12 hours before the westerly breach (Direct HEC-RAS output).*

### Discharge distribution

Next to the water depth and depth averaged flow velocity locally in the breaches, the discharge distribution through the breaches and the total discharge over the floodplain is computed. This discharge distribution gives a first insight into the discharge capacity of the breaches during a flood event and when these breaches start to discharge water from the Rhine floodplain to the IJssel floodplain. As already shown in Figure 4.2 the easterly breach discharges water approximately 12 hours before the westerly breach becomes active. Next to this, the easterly breach discharges more than the westerly breach for all the parameter settings with equal circumstances. The percentages of the total discharge for the breaches under the different parameter settings are shown in Table 4.3. With a smaller discharge wave, the easterly breach takes a larger portion of the total discharge on the IJssel floodplain. During a small flood wave,  $6000 m^3/s$  with a present return period of 3 years, a breach with a width of 100 meters already takes approximately half of the total discharge. This indicates that during a flood wave of  $6000 m^3/s$  and an easterly breach of approximately 200 meters and equal depth, has the capacity to discharge all the water flowing over the IJssel floodplain and the westerly breach will stay dry. If this happens, the easterly breach will continue to expand and a young river IJssel will start to form meanders and carve a course through the floodplain to a matured branch of the Rhine delta.

**Table 4.3:** Discharge distribution in the breaches for the different parameter settings as a portion of the total discharge on the IJssel floodplain

Westerly breach			Easterly breach			
Discharge	Width	Depth	% of total discharge	Width	Depth	% of total discharge
[ $m^3/s$ ]	[ $m$ ]	[ $m$ ]	[%]	[ $m$ ]	[ $m$ ]	[%]
<i>Equal dimensions</i>						
10000	50	1	5	50	1	8
14000	50	1	5	50	1	7
10000	50	2	12	50	2	16
14000	50	2	10	50	2	13
10000	50	4	17	50	4	27
14000	50	4	14	50	4	21
10000	100	4	20	100	4	32
14000	100	4	17	100	4	26
<i>Shallow shoulders</i>						
10000	100	4	19	100	4	31
14000	100	4	16	100	4	25
<i>Different widths</i>						
6000	50	4	21	100	4	44
10000	50	4	17	100	4	32
14000	50	4	14	100	4	26
10000	100	4	20	50	4	28
14000	100	4	17	50	4	23

### 4.1.3 Translation to the breach stages

In this section, a qualitative analysis is done of the hydrodynamic results using the different breach stages set-up in Section 2.2. During the flood wave, the water level rises in the breaches (Stage 2). In the easterly breach, the water level rises at an earlier moment in time than the westerly breach. With the sand core uncovered, the easterly breach also deepens and widens at an earlier moment in time than the westerly breach. The water level stabilises around the seventh day for both breaches from the first moment the flood wave reaches the coversand ridges (Figure 4.2). At this stabilisation (Stage 3), the easterly breach was subject to the flood for approximately 6.5 days and the westerly breach for 6 days. Together with the higher flow velocities in the easterly breach relative to the westerly breach, the easterly breach expanded more than the westerly breach. At this moment, the situation with a 50 meters wide westerly breach and 100 meters wide easterly breach is considered. During the stabilisation the easterly breach is already wider and is still subject to higher flow velocities (Table 4.1). Singh and Scarlatos (1988) states that the erosion rate is a power function of the flow velocity. Considering this, the easterly breach will still expand faster in the lateral direction than the easterly breach during Stage 3.

## 4.2 Erosion model

### 4.2.1 Bed shear stress

This section elaborates on the actual bed shear stress versus the critical bed shear stress for the sediment particles to be put into motion. The sediment in the breach consists of coversand, which is very fine sand. It is transported by the wind, so if water flows over the coversand, it will be easily washed away. Figure 4.6 represents the first moment in time during a flood wave of 6,000  $m^3/s$  at which the threshold value for the critical bed shear stress is exceeded. This threshold value is exceeded just after the breach discharges water. At this moment the hydrodynamic conditions are the least favourable for erosion and sediment transport during a flood wave. At the peak of the flood wave, the flow velocity and water depth have increased significantly and the hydrodynamic conditions become even more favourable for erosion and

sediment transport. This indicates that when a somewhat larger flood wave, than a flood wave of  $6,000 \text{ m}^3/\text{s}$  occurs, the bed shear stresses in the breaches always exceed the threshold value to put the particles into motion, and erosion and sediment transport can occur.

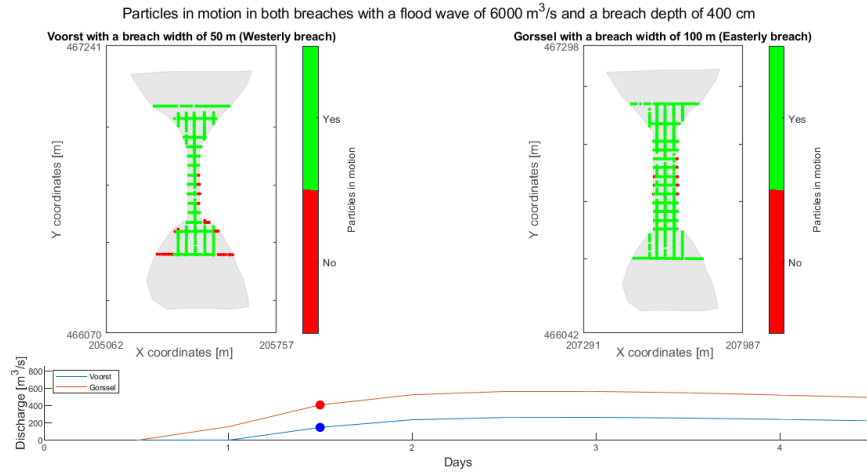


**Figure 4.6:** First moment during a flood wave with a peak discharge of  $6000 \text{ m}^3/\text{s}$  that the bed shear stress in the entire breach exceeds the critical bed shear stress of  $0.16 \text{ N/m}^2$

## 4.2.2 Erosion velocity

The erosion velocity locally in the breaches for the different parameter settings is computed using equations 3.2 and 3.3. This results in the erosion velocities perpendicular to the bed as shown in Figure 4.7 and Table 4.4. The erosion rates range to a maximum of  $17.6 \text{ mm/s}$  in a 2 meters deep breach. If we use this maximum erosion rate for a simple calculation of the erosion of a 2 meters deep breach, a breach only needs approximately 2 minutes to deepen from a 2 meters deep to a 4 meters deep breach. It should be noted that the sediment transport capacity of the flow in the breach also should be able to cope with these erosion rates. The aforementioned erosion rates seem to be extremely large, but they are in line with the literature:

- The Teton Dam, a 90 meters dam that failed due to a developed piping process. The outflow slowly increased during this piping failure, but once the dam collapsed and formed a remnant lower dam, it only took 12 minutes to erode to the base of the dam (according to Blanton (1977)). This gives a mean erosion rate of  $125 \text{ mm/s}$ .
- The Mantaro Landslide Dam, a landslide created a broad dam of approximately 170 meters high in the river Mantaro. It formed a lake that eventually overtopped the landslide dam. At the first 2 days it gradually eroded the downstream face, after this time the erosion started to increase and the 170 m high dam eroded to a trapezoidal-shaped breach with a depth of 120 meters and width of 250 meters in a time period of 6 to 10 hours (Lee & Duncan, 1975). This gives a mean erosion rate of  $5 \text{ mm/s}$ .

The results of the westerly breach in Figure 4.7 assume that the erosion velocities are the highest at the end of the flow funnel and the beginning of the flow splay. This is due to the bathymetry of the constructed breach with a depth of 4 meters (Figure 2.3). At these locations a large elevation difference is present, thus the water depth decreases, which accelerates the flow velocity and thus the erosion velocity. In a dynamic computation of the erosion in the breaches using this constructed schematized bathymetry, these location will initially erode faster than the surrounding bed until the transition is smoother. In reality this transition will also be smoother during the breach development than schematically reconstructed in this research. At a breach with a depth of 2 meters, this extreme erosion at the end of the flow funnel and the beginning of the flow splay are not present (Figure E.1). So, if the elevation transition is smoother, the erosion velocity decreases.

The erosion rates in the breaches differ significantly for both the parameter settings with equal breach widths

and the parameter settings with different breach widths. The erosion rates in the center of the breaches are shown in Table 4.4. In all the scenarios the easterly breach is subject to higher erosion velocities. In short, this means that with equal circumstances, the easterly breach will expand faster and even with double the width it will expand faster. This can be used for explaining the fact that the easterly breach became part of the river IJssel and the westerly breach eventually stopped being used.

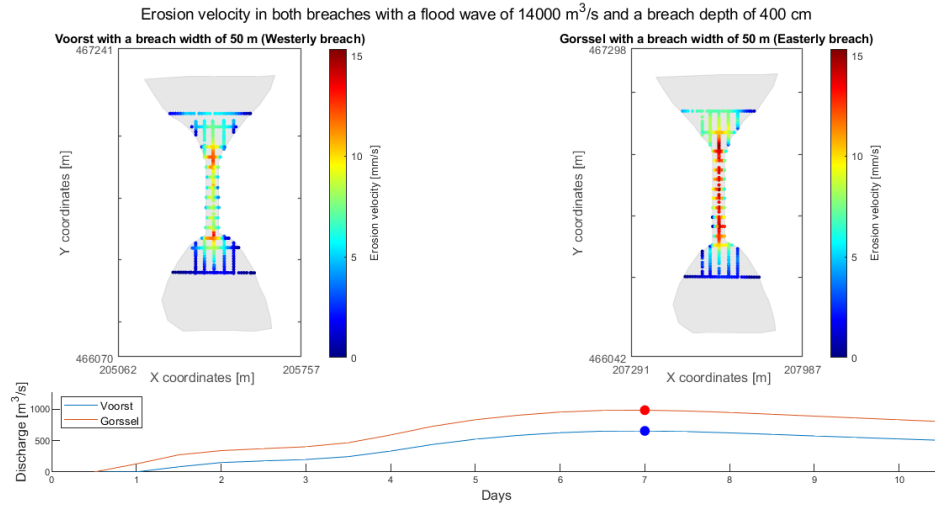


**Figure 4.7:** Erosion velocity in the breaches during the peak of a 14,000 m<sup>3</sup>/s discharge wave (resulting in a discharge of 3,500 m<sup>3</sup>/s on the IJssel floodplain; the same discharge wave and moment in time as shown in Figure 4.2)

**Table 4.4:** Maximum erosion velocity central in the breaches for the different parameter settings

		Westerly breach		Easterly breach		
Discharge	Width	Depth	Erosion velocity	Width	Depth	Erosion velocity
[m <sup>3</sup> /s]	[m]	[m]	[mm/s]	[m]	[m]	[mm/s]
<i>Equal dimensions</i>						
10000	50	1	8.2	50	1	12.4
14000	50	1	9.7	50	1	13.8
10000	50	2	10.3	50	2	16.0
14000	50	2	11.7	50	2	17.0
10000	50	4	6.7	50	4	13.7
14000	50	4	8.6	50	4	15.0
10000	100	4	3.6	100	4	8.4
14000	100	4	5.5	100	4	9.8
<i>Shallow shoulders</i>						
10000	100	4	5.8	100	4	10.8
14000	100	4	7.3	100	4	12.3
<i>Different widths</i>						
6000	50	4	3.0	100	4	5.5
10000	50	4	6.7	100	4	8.4
14000	50	4	8.5	100	4	9.7
10000	100	4	5.0	50	4	13.2
14000	100	4	6.4	50	4	14.7

### 4.2.3 Sediment transport capacity

The sediment transport capacity for both breaches under equal circumstances shows an advantage for the easterly breach (Table 4.5). Where the erosion rates in the previous section show around 30-50% lower rates for the westerly breach compared to the easterly breach, the sediment transport capacity of the westerly breach is at least 50% higher for all scenarios. This means that, assuming that the sediment transport capacity is the delaying factor and the same erosion rates would occur in both breaches, the easterly breach would be able to transport more than the westerly breach, because of the higher capacity. This results in a faster expanding easterly breach. Under equal circumstances the easterly breach always expands faster.

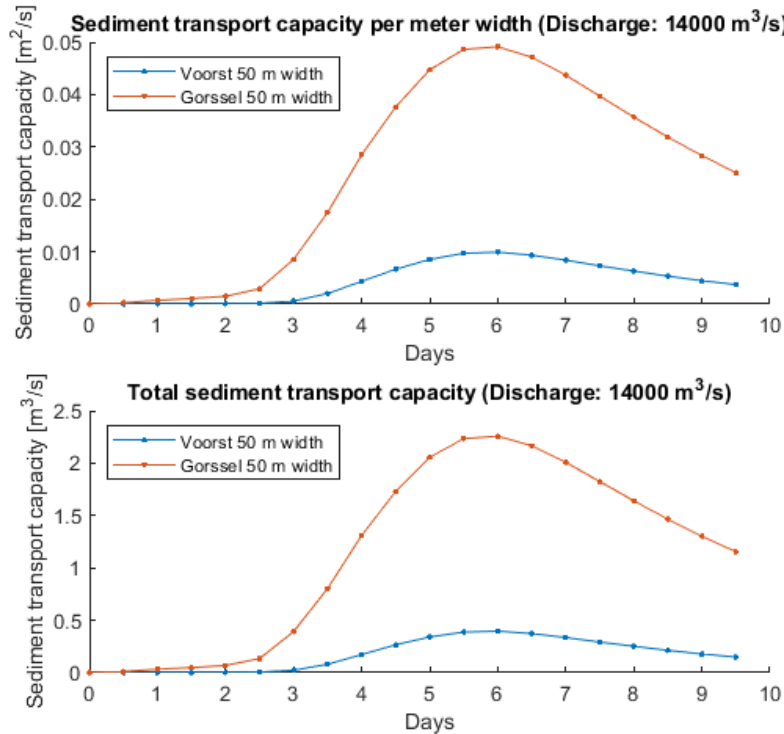


**Figure 4.8:** Sediment transport in time for a flood wave of 14,000 m<sup>3</sup>/s (resulting in a discharge of 3,500 m<sup>3</sup>/s on the IJssel floodplain) and a breach depth of 4 m of the cross-sectional profile central in the breach. Upper graph: Sediment transport capacity per meter width; Bottom graph: Total sediment transport capacity

Assuming that the erosion in both breaches initiated at the same time for simplification (see Figure 4.5 for further reasons of timing), the easterly breach will expand quicker, resulting in two breaches in which breach widths are different. For this reason, a scenario is constructed with different breach widths. The results of this scenario are shown in Table 4.5 and Figure 4.9. From these results can be concluded that with an extreme flood wave (14,000 m<sup>3</sup>/s), while the sediment transport capacity per meter width is larger for the westerly breach, the total sediment transport capacity in the wider easterly breach is higher and thus more sediment can be transported through this breach. The easterly breach, with its higher erosion rates, will therefor still expand faster than the narrower westerly breach.

With a less extreme flood wave (6,000 m<sup>3</sup>/s in Figure 4.9), the wider easterly breach discharges a large portion of the total discharge on the floodplain and the sediment transport capacity is for this reason also higher than the westerly breach. From this result can be concluded that with smaller flood waves, the easterly breach will expand faster and more than the westerly breach, eventually resulting in a breach that is wide enough to discharge all the water on the floodplain as in the present situation.

**Table 4.5:** Sediment transport capacity in the breaches for the different parameter settings

Westerly breach				Easterly breach			
Discharge	Width	Depth	Sediment transport capacity		Width	Depth	Sediment transport capacity
[ $m^3/s$ ]	[ $m$ ]	[ $m$ ]	[ $m^2/s$ ]	[ $m^3/s$ ]	[ $m$ ]	[ $m$ ]	[ $m^2/s$ ]
<i>Equal dimensions</i>							
10000	50	1	0.004	0.2	50	1	0.01
14000	50	1	0.01	0.4	50	1	0.02
10000	50	2	0.02	0.7	50	2	0.04
14000	50	2	0.03	1.3	50	2	0.07
10000	50	4	0.004	0.15	50	4	0.03
14000	50	4	0.01	0.4	50	4	0.05
10000	100	4	0.0002	0.02	100	4	0.003
14000	100	4	0.0007	0.07	100	4	0.006
<i>Shallow shoulders</i>							
10000	100	4	0.0008	0.08	100	4	0.006
14000	100	4	0.002	0.2	100	4	0.01
<i>Different widths</i>							
6000	50	4	0.002	0.01	100	4	0.003
10000	50	4	0.004	0.15	100	4	0.003
14000	50	4	0.01	0.43	100	4	0.006
10000	100	4	0.0003	0.03	50	4	0.04
14000	100	4	0.001	0.11	50	4	0.07

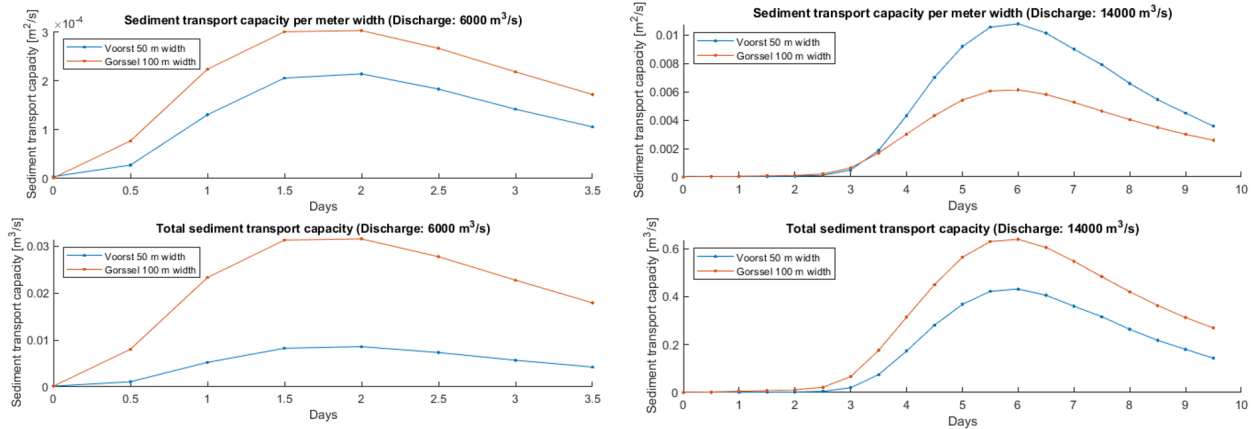


**Figure 4.9:** Sediment transport in time for a flood wave of  $6,000 m^3/s$  and  $14,000 m^3/s$  (resulting in a discharge of  $1,300$  and  $3,500 m^3/s$  respectively on the IJssel floodplain) with a breach width of  $50$  for the westerly (Voorst) and  $100$  meters for the easterly (Gorssel) breach and a breach depth of  $4$  m of the cross-sectional profile central in the breach. Upper graph: Sediment transport capacity per meter width; Bottom graph: Total sediment transport capacity

The scenarios described above assume a faster expanding easterly breach. A theoretical scenario in which the westerly breach initiated first and already expanded before the easterly breach initiated is also constructed. In this scenario the westerly breach is  $100$  meters wide and the easterly breach  $50$  meters. The results from this scenario are also shown in Table 4.5. From these results can be concluded that, although the erosion rates in the easterly breach are  $50\%$  higher (Table 4.4), the sediment transport capacity in the easterly breach is approximately  $30$  times higher than the westerly breach. The easterly breach will thus expand significantly

faster than the westerly breach, become equally large at some moment in time and eventually expand more than the westerly breach.

### Interpretation of the sediment transport capacity

This section gives a schematic overview of how the sediment transport capacity in both breaches under the various parameter settings can be interpreted.

The volume of the coversand ridge that washed away (cross-section of the coversand ridge is a 'trapezium' with crest 2 meters higher than surrounding local ground and a width of 300 meters, the length is around 2.2 kilometers), gives a roughly estimated volume of at least 880,000  $m^3$  (but probably more due to the surrounding floodplain that also eroded). This may have taken years and various repeated flood waves to wash away and is hard to predict. What can be roughly predicted is the time that is required for both breaches to expand from a breach with the smallest dimensions used in this research (50 meters width and 1 meter depth) to a breach with the greatest dimensions used in this research (100 meters width and 4 meters depth). In this situation it is assumed that the flood wave does not transport sediment before it reaches the breach, because the initial conditions are not known. The time for the erosion of a section of the coversand ridge with a certain sediment transport capacity can be written as:

$$T = \frac{V}{S} \quad (4.1)$$

With  $T$  the time in seconds that a total sediment transport capacity  $S$  in  $m^3/s$  requires to erode a certain volume ( $V$ ) in  $m^3$ .

With the sediment transport capacity as shown in Table 4.5 it takes around 4 hours for the easterly breach of 2 meters depth and 50 meters width to expand to a breach with a depth of 4 meters and a width of 100 meters if a discharge wave of 14,000  $m^3/s$  occurs. This is calculated with the volume loss of the coversand ridge divided by the mean sediment transport capacity of the parameter settings with a breach of 50x2 meters and 100x4 meters. For the westerly breach this would take 10 hours using the same calculation.

If the easterly breach expands, the flow velocity decreases and thus the sediment transport capacity per meter width decreases. After the maximum breach dimensions used in this research are reached, the erosion rate of the easterly breach will decrease. It is not known to what extent the easterly breach can expand during one flood wave and thus how much time it takes. The maximum breach width of the westerly breach is known on the other hand. The time that the maximum breach width (100 meters) and breach depth (4 meters) of the westerly breach is obtained, can be computed with more certainty. If we assume that both breaches initiated at the same time and this initiation uncovered the vegetated layer of the coversand ridge, leaving only non-cohesive sediment, the expansion of the first meter to the second meter of the westerly breach takes around 1 hour and the rest of the eventual expansion approximately 10 hours (as calculated above).

At the peak of the discharge wave, which lasts around a day, the westerly breach only requires half a day to erode to the dimensions as preserved nowadays. If the westerly breach was able to discharge for a much longer time period, this would imply that the breach would be larger than currently preserved. Assuming this to be true, this can be translated to a maximum time of half a day in which the easterly breach must expand to certain dimensions to withheld the westerly breach from eroding more than the maximum breach dimensions as currently preserved. From this can be concluded that the eventual breach was probably triggered due to one large discharge wave and not several discharge waves, because the westerly breach would have been wider.

### Stage 4: Sedimentation

Some longer simulations were done to get insight in the sedimentation of the breaches after the peak of the flood wave. At stage 4 of a breach development process, the water level and flow velocities decrease, which causes the sediment to settle and partly silt up the breach. This process is shown in Figure 4.10. This figure shows that after the peak of a flood wave of 10,000  $m^3/s$  and 14,000  $m^3/s$  the westerly breach (Voorst) almost has no sediment transport capacity, while the sediment transport capacity rates at the easterly breach

(Gorssel) still show significant quantities. The westerly breach will partly silt up and stops being used, while the easterly breach is still able to transport sediment and will expand further.

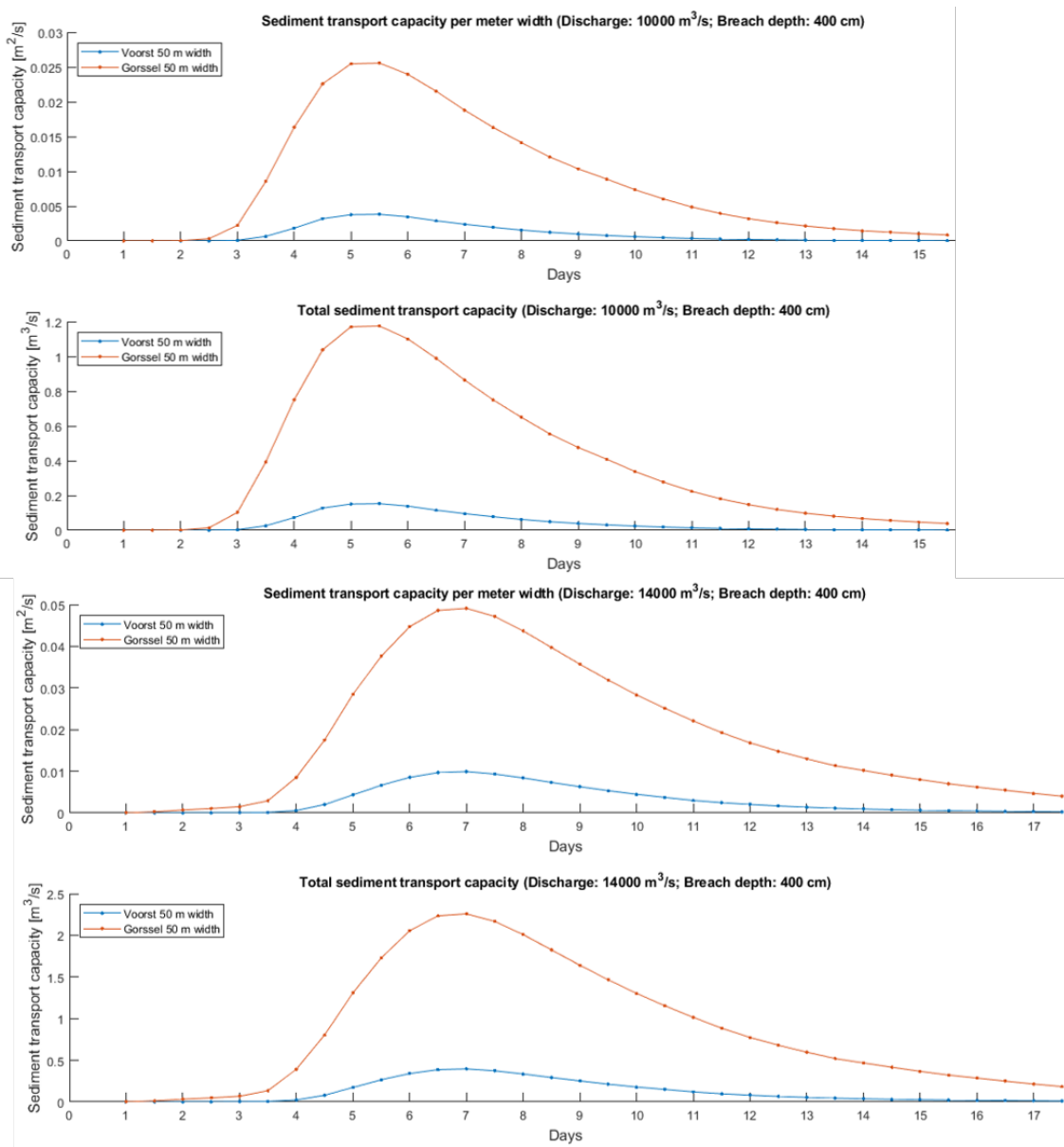


**Figure 4.10:** Sediment transport capacity in the breaches during the total flood wave (Voorst = easterly breach; Gorssel = westerly breach). Left: Transport capacity of a flood wave of 10,000 m<sup>3</sup>/s; Right: Transport capacity of a flood wave of 14,000 m<sup>3</sup>/s

# Chapter 5

## Discussion & Recommendations

### 5.1 Discussion

#### 5.1.1 Research set-up

##### **Suitability of the paleo-DEM with the coversand ridges**

A coversand ridge in the IJssel floodplain is reconstructed for the representation of a pre-breach paleo-DEM (Figure 2.1). This reconstruction was done by the author using the knowledge about the dimensions and shape of the coversand ridges still present East and West of the eventual breach (Cohen et al., 2009, Makaske et al., 2008, Vermeulen and Haveman, 2008) and expert judgement (Cohen, pers. comm.). The exact dimensions of the coversand ridges and land forms surrounding it are smoothed out. Normally, the coversand ridge would have a shorter crest width (as can be seen West of the reconstructed coversand ridge Figure 2.1), than used in this research. At both locations, equal breach dimensions are used, thus this has no effect on the results.

Together with the width of the crest of the coversand ridge, the upstream and downstream side of the reconstructed coversand ridge have a lower elevation than the surrounding connected coversand ridges. The literature mentions that small streams must have existed at this location (e.g. Vermeulen and Haveman, 2008), which caused for a local lower elevation ('brook valleys', Dutch: 'beekdalen'), but the width of this lower elevated area would be much smaller. The width of the valley in the paleo-DEM partly represents the floodplain (the area between the present banks of the IJssel river, not whole area that can flood during a flood wave) of the present situation of the river IJssel and not the pre-breach situation. The incisional lowering of the floodplain in this part of the IJssel valley, was a problem that Van der Meulen et al. (2020) also encountered during the reconstruction of the paleo-DEM of the Rhine and IJssel floodplain (800 AD). The extent of the IJssel meander belt of the last 1000+ years stayed visible in that reconstruction. For this research only the coversand ridge at Gorssel was added to the paleo-DEM and no other additional eroded coversand ridge edges were restored upstream. Because small streams must have existed at the location of the current river IJssel, a small valley was also present at the pre-breach situation. This has therefore not a large effect on the flood wave propagation and thus not on the results.

Lastly, the crest of the reconstructed coversand ridge has a certain elevation relative to NAP (approximately 9 m+NAP). The elevation of the crest is based on the surrounding coversand ridges and has an equal height along the whole crest of the reconstructed coversand ridge. In reality, the crest would have had local height differences. A certain water level would have overtopped at a certain location, while at another location the water level was not high enough to exceed the threshold. It should be noted that these local height differences could have contributed to the exact breach location. The exact height of the coversand ridge was, like the shape of the coversand ridge, a best guess. On the other hand, the crest height was based on the surrounding coversand ridges, which have the same mean height and deviate approximately 0.5 meters. This would not have had impact on this research, because this research skips the initiation of erosion and thus the exact location of the initiation, because of all the uncertainties in advance. This research starts with a breach with

a depth of 1 meters, and the breach is thus deeper than the crest height deviations. For this reason, the crest height deviations do not affect the results.

### **Assumptions and research constraints breaches**

The case adopted for this modelling research came from geological and archeological/historical research, and it represents a situation of the Rhine and IJssel floodplain of approximately 1300-1700 years ago. Therefore all the input parameters for the reconstruction of the coversand ridges and breach properties are a best guess of the situation of 1300-1700 years ago from geological mapping and dating and thus have their assumptions.

The breaches used in this research are a schematic representation of the reality. Trapezoidal dimensions are used in this research, while other researches consider other shapes like rectangular (Singh & Scarlatos, 1988), triangular (J. N. Fread, 1984) and parabolic shapes (Brown & Rogers, 1981). The hydrodynamic condition like the flow velocity is the most important parameter and mostly dependent on the flood wave and cross-sectional area, so the qualitative analysis using other breach shapes would not be different.

This research only considered the cohesion of loosely packed sediment, which is little, while in reality this sediment locally may have been more cohesive due to the soil formation in the sediment throughout the thousands of years and the vegetation that would have increased the cohesion due to the roots. This again does not have impact on the qualitative analysis that is done in this research, while this research only considered situations in which the vegetation was already washed away at the breach location and only non-cohesive sediment was left. The cohesion increase caused by the vegetation would have had impact on the timing of Stage 1 to Stage 2, but that is outside of the research scope.

## **5.1.2 Sensitivity model**

### **Model set-up**

A lower-fidelity hydrodynamic model was set up in HEC-RAS. In this set-up the 2D grid at the breach locations in the coversand ridges in the floodplain are constructed manually and the 2D grid is aligned with the coversand ridges at the area of interest. The manually refinement resulted in a so-called unstructured grid with various grid cell shapes at the breach location. The output of the breach hydrodynamics of the hydrodynamic model is validated with breach data of other cases. The output was within the boundaries of these observed data, but cannot be validated with in-situ data. Other grid refinements, like a triangular unstructured grid, could lead to a different hydrodynamic output, but it is expected that if both breaches are refined according to the same method, the eventual qualitative analysis would not be different. Besides this, other grid refinements were not possible due to computational time and software limits.

The unstructured grid aligned along a part of the coversand ridge has a major impact on the discharge distribution on the floodplain. The grid is only aligned at the area of interest, but West and East of the 2D grid is a structured 200 x 200 meters grid. These cells overlay a whole coversand ridge and cause that the hydrodynamic model computes water levels on the downstream side of the coversand ridge due to the lower elevation of this side, while in reality no water has overtopped the coversand ridge. In the hydrodynamic model, water is already discharged downstream of the coversand ridges, while in reality the water level still has to increase, before it could overflow the coversand ridge. This research is interested in the interaction between both breaches in the coversand ridges under various circumstances. In reality this means that the water level and thus the pressure caused by the flood wave, would be larger than depicted in this research and the breaches would probably suffer higher flow and erosion velocities. It is expected that with a better aligned grid, the qualitative analysis of the interaction of the developing breaches would not differ significantly.

The modelling approach of the hydrodynamic-erosion model used in this research is a static modelling approach in which a morphodynamic model is not implemented. The development of the breaches in time can only be sketched by extrapolation and interpolation of the results and a qualitative analysis of these results. A sophisticated morphodynamic model can give more insight in the interaction of both breaches during the different stages of the breach development.

Discharge waves scaled on the flood wave of 1925/1926 of Bomers et al. (2019a) are used in this research, because the shape of this flood waves quite accurately represents the average of modelled extreme flood waves

of the Rhine, using the GRADE approach of Hegnauer et al. (2014). A flood wave with a smoother peak discharge cannot dissipate as much as the flood wave used in this research in the downstream direction. The flood wave will cause higher water levels on the floodplain and thus also higher flow and erosion velocities in the breaches due to the higher pressure caused by the flood wave. A flood wave with a smaller peak can, on the other hand, dissipates more in downstream direction and will cause for a lower peak discharge on the IJssel floodplain and at the coversand ridges. This will result in lower erosion velocities and less sediment transport capacity through the breaches. If the peak of the flood wave is smaller or wider, the peak discharge must be respectively higher or lower, to obtain the same results at the coversand ridges.

### Sensitivity of the location of the easterly breach

From geological mapping and dating by Cohen et al. (2009) the breach location of the westerly breach can be determined accurately. The breach location of the easterly breach, the location where the coversand ridge eventually breached, is less accurate. This is caused by the coversand ridge that eroded and expanded in lateral direction and washed away most of the initial breach characteristics. For the computations of the erosion and sediment transport capacity in the previous chapter, only one easterly breach location was considered, located at the 'tail' of the coversand ridge. To validate whether the easterly breach is sensitive to the location along the coversand ridge, one scenario is constructed in which the easterly breach is located at the most easterly location of the reconstructed section of the coversand ridge (Figure 5.1). In this scenario the parameter setting with a breach width of 50 meters and a breach depth of 2 meters is used. The cross-sectional maximal velocity of the easterly breach located at the tail of the coversand ridges and the breach constructed for validation are respectively  $7.34 \text{ m/s}$  and  $7.11 \text{ m/s}$ . This is a deviation of approximately 3%, so it can be concluded that the flow velocities are not that sensitive to the location of the easterly breach along the reconstructed coversand ridge. Besides this, the location of the easterly breach would not have effected the hydrodynamic conditions of the westerly breach.

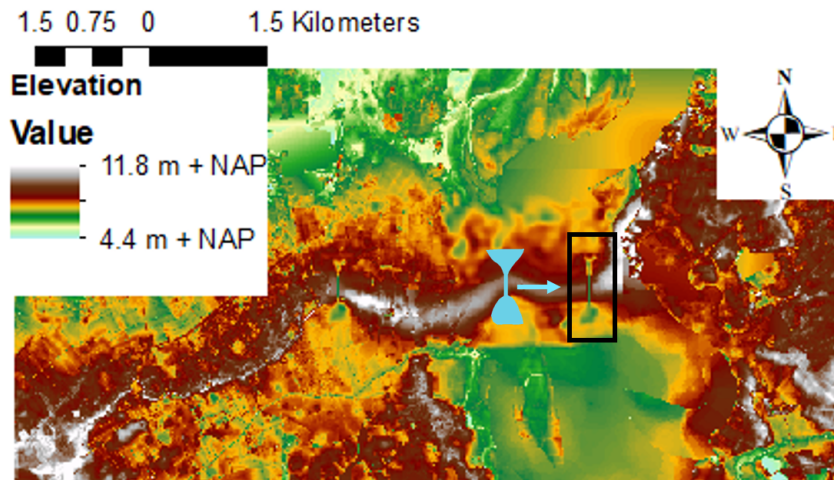


**Figure 5.1:** *Alternatively positioned breach location for the sensitivity analysis of the location of the easterly breach (compared to Figure 2.1)*

### Erosion equation

Oumeraci et al. (2005) stated that it is recommended to use more than one erosion equation to obtain insight into the amount of erosion in the breaches. In this research it is chosen to only use one erosion equation and obtain more insight in the breach development by using a sediment transport capacity equation. Other erosion equations found in the literature, like Chen and Anderson (1984), are also empirical and based on the soil and flow characteristics. In this research we are not interested in the exact amount of erosion, because this is too uncertain on beforehand, but the interaction between both breaches under various circumstances.

Both equations of Chen and Anderson (1984) and van Rhee (2010) are based on the flow velocity, the soil characteristics and a certain calibration factor in the equation. Using the equation of Chen and Anderson (1984) would not have an impact on the differences between the breaches from a qualitative point of view.

In this study a sediment diameter of 210  $\mu\text{m}$  is used for the erosion equations and for the determination of the roughness in the breaches in the hydrodynamic model. It is assumed that this is the median diameter of the sediment and that the sediment is uniformly distributed. If the median grain size of the sediment is, for example, larger than the used median sediment diameter in this research, the Mannings coefficient would be larger. A higher roughness causes lower flow velocities. Both the median grain size as the flow velocity have influence on the erosion velocity and sediment transport capacity. A lower flow velocity and larger grain size, will result in lower erosion velocities and less sediment transport capacity, because the flow has less favourable conditions for picking up the sediment. The sediment distribution is equal along the coversand ridges, so the decrease in erosion velocity and sediment transport capacity will occur in both breaches and will not affect the qualitative analysis.

### 5.1.3 Comparison with the chute cut-off in the river Wabash

Patterns of meandering rivers in their floodplains are complex (Zinger et al., 2013). Little is known about the erosion of natural barriers or river banks and the course change of the meandering river in its floodplain. Even the most advanced models of river migration are quite schematic (Seminara, 2006). This section elaborates on how the results of this coupled static hydrodynamic-erosion modelling study can be related to another case.

In the river Wabash, located at the Illinois-Indiana border, USA, two chute cutoff channels developed in a meander bend during several consecutive large floods on the river Wabash (Zinger et al., 2013). During the first flood, a pre-existing swale eroded into a cutoff channel and it produced a system of gullies east of this channel. Although the first cutoff channel formed rapidly during a single, large flood event, the second cutoff channel was produced by a series of overbank flows into the gullies with recurrence intervals on the order of 1 to 2 years (Zinger et al., 2011). The second chute cutoff channel had a more favourable (shorter) path for the river Wabash to discharge and widened substantially due to the overbank flows. Eventually it had widened such that it captured the largest part of the discharge, while initially the first chute cutoff channel captured the largest part of the discharge.

The river Wabash case can be related to this case study, although the scale differs somewhat. In the river Wabash case, the first chute cutoff channel develops rapidly and the second cutoff channel develops slowly and requires multiple larger floods, but eventually widens substantially. In this research, it is not known which breach developed first, but it is known that the easterly breach eventually expanded the most. The results of this research imply that this breach has the most favourable conditions for a breach to develop, even with the scenarios in which the westerly breach is initially wider. This is also the case in the river Wabash cutoff channels. From relating these studies, it can be concluded that the most favourable path will eventually 'win', although it forms later. Besides this, it teaches that the formation of a breach, the interaction between two breaches and the development of a channel is a dynamic process, which takes several larger floods.

## 5.2 Recommendations

For future research, it is recommended to set up a morphological model of a simple breach or an embankment breach model, with the same dimension as used in this research. The discharge and flow velocity in the breaches are known. A morphological model can give insight in the development of a single breach under various circumstances. The hydrodynamic properties like the flood wave extent, flood pattern, the flow velocities and discharge through the breaches from the simulations in this research, can then be linked to the morphological simulations, resulting in a dynamic morphodynamic model of the breach development. It is recommended to set up a morphological model that is best applicable on the easterly breach, since this breach eventually expanded. With this model a more clear insight can be obtained in the amount of floods that are required for the breach to expand. Besides this, the cumulative time that is required for the breach to expand from a small breach to the dimensions of the current situation can be simulated using a uniform

discharge wave.

A meandering young river formed from the river Rhine to the Zuiderzee flowing through the easterly breach location. On a larger scale this forms the opportunity to set up a long-term morphodynamic model of the evolution of a young meandering river IJssel to a matured river IJssel. In this model also the flow exchange between the channel and floodplain during an extreme flood wave can be implemented.

In this research a maximum breach width of 100 meters is used. From the hydrodynamic model was found that the easterly breach discharged a part of the total discharge on the IJssel floodplain. Increasing the width of the easterly breach will simultaneously increase the discharge through the easterly breach. By increasing the width gradually, insight will be obtained in how wide the easterly breach must have expanded during one flood wave to ensure for the total discharge on the IJssel floodplain.

In this research only non-cohesive sediment is considered to obtain insight in the erosion rates. In reality one flood wave would have caused for the eventual breach of the coversand ridge, but subsequent major floods in the following hundreds of years must have caused for the river IJssel to carve its way in the floodplain. During these years, the breach and the floodplain will become vegetated, because small discharge waves do not reach the coversand ridges. Vegetation on the floodplain and at the easterly breach location causes for an increasing resistance against erosion at the river bed and breach. A next step in obtaining insight in the formation of the river IJssel is to compute erosion using erosion equations established for vegetation covered soil. These erosion equations can then also be applied to the initiation of the erosion (Stage 1) at the crest of the coversand ridges.

# Chapter 6

## Conclusion

The objective of this research is to obtain insight in the erosion processes of two developing breaches in coversand ridges in the IJssel floodplain during flood induced overflows in the early medieval times. This insight is obtained using a static modelling approach. First, a hydrodynamic model is set-up using a paleo pre-breach Digital Elevation Model (DEM) of the Rhine and IJssel floodplain. The output of this hydrodynamic model are the hydrological properties, like the flow velocities, water depths and discharges through the breaches. Erosion rates and sediment transport capacity in the breaches are computed from the output of the hydrological model and a qualitative analysis is then done on the quantified erosion rates and sediment transport capacity of breaches in coversand ridges in the IJssel floodplain. In this section, an answer to each research question is provided. Next, it is described how the research objective is met.

1. *What are the relevant parameters in the breach development process that are used as input of a hydrodynamic model?*

There are various hydrodynamic, geological and physical parameters that are of importance for the computation and simulation of a developing breach. In this case study, there is little detailed information about the breach development during an overflow. Therefore, it is chosen to form a set of parameters that can be varied using literature, geological mapping and dating and expertise knowledge. From these sources the following parameters are found to be the most important: breach depth, breach width and flood wave upstream.

From geological mapping and dating the maximum dimensions of the westerly breach are known. These dimensions are preserved and still present in the current situation of the IJssel floodplain. These dimensions are 100 meters wide and 4 meters deep. For the construction of different scenarios, these dimensions are used as the maximum dimensions. The other dimensions used in this research are a width of 50 meters and depths of 1 and 2 meters.

From the literature and geological mapping and dating is known what flood wave probably caused the coversand ridge to overflow. This is a flood wave with a peak of approximately  $14,000 \text{ m}^3/\text{s}$  at Andernach. This flood wave is used as the most extreme scenario. Next to this extreme flood wave, several smaller flood waves ( $6,000 \text{ m}^3/\text{s}$  and  $10,000 \text{ m}^3/\text{s}$  at Andernach) are used to obtain insight in the breach development under less extreme conditions.

2. *What are the hydrodynamic properties in the breaches under different flood waves, breach depths and breach widths?*

The hydrodynamic model is used for the computation of the flow velocity, water depth and discharge wave for the different parameters settings. By varying breach depth, breach width and the flood wave, insight is obtained in the hydrodynamic properties of the different breaches. From these results can be concluded that the easterly breach, the location where the river IJssel eventually formed, is always subject to higher flow velocities and water levels in the breach and a larger discharge through the breach than the westerly breach (the breach that eventually silted). Because the flood wave reaches the easterly breach as first, before it propagates to the westerly breach, the easterly breach will always be subject to more extreme

hydrodynamic properties than the westerly breach. As the flood wave propagates from the easterly breach to the westerly breach, the flood wave will dissipate, causing the westerly breach to have less extreme hydrodynamic properties. Besides this, smaller flood waves than tested in this research, will only flow through the easterly breach, because the flood wave reaches this breach first, which will cause for an expanding easterly breach, while the westerly breach stays dry.

3. *How does the erosion differ in both breaches for the different parameter settings?*

The erosion in the breaches is quantified using an empirical physically based erosion equation and using an equation for the sediment transport capacity in a breach. From the erosion rates it can be concluded that in each scenario, the erosion velocity in the easterly breach is around 1.5 to 2 times greater than the erosion velocity in the westerly breach. The easterly breach will expand faster under equal circumstances.

From the sediment transport capacity in the breaches the same conclusion can be made as could be concluded from the erosion velocity in both breaches under various circumstances. The easterly breach is able to transport more sediment due to the larger flow velocity in the breach. Thus if erosion occurs in both breaches, the easterly breach will expand faster than the westerly breach, because more erosion occurs in the easterly breach and it is able to transport more sediment.

The hydrological properties of the flood wave are always in the advantage of the easterly breach, but the westerly breach also eroded somewhat. Translating the total eroded volume of the westerly breach to a time that is required to erode this portion of the coversand ridge, results in an erosion time of around half a day that is required for the westerly breach to erode with a peak discharge of  $14,000 \text{ m}^3/\text{s}$  at Andernach. If this event has occurred and the westerly breach started to erode, the same flood event must have washed away the easterly breach to a size large enough to discharge the total flood wave in the same period (half a day). Otherwise the preserved dimensions of the westerly breach would have been larger. The time to wash away the easterly breach also implies that one flood event must have been large enough to fully erode the easterly breach. A flood wave with a peak discharge of  $14,000 \text{ m}^3/\text{s}$  at Andernach reaches the coversand ridges in the IJssel floodplain for around 15 days. This time is significantly larger than the time that the easterly breach must have eroded, thus one flood wave caused for the breaches in the coversand ridges.

The main objective of this research is:

*Obtain quantitative insight in the erosion processes of two developing breaches in a coversand ridge during flood induced overflows in the IJssel floodplain.*

From the hydrodynamic properties, erosion rates and sediment transport capacity for the different parameter settings it can be concluded that the easterly breach has much more favourable conditions to erode, expand and eventually become part of the river IJssel than the westerly breach. Taking the present situation of the river IJssel into consideration, which is also located at the easterly breach, this result can be validated.

Besides this, the hypotheses on a large-magnitude flooding as a mechanism to trigger breaches in the coversand ridges are in line with the results presented in this research. Cohen and Stouthamer (2012) stated that at the westerly location, features like the splay and breach dimensions are more completely preserved, because later floods only used the enlarged and lowered floodplain and the permanent channel that developed at the easterly location, leaving the westerly higher elevated floodplain and breach dry. The results of this research imply the same competition outcome between the westerly and easterly breach locations: the easterly breach eroded that much, that subsequent floods could flow through the easterly breach and did not reach the westerly breach. Cohen (2010) stated that the westerly breach eventually partly filled with sediment and was abandoned as a flood path. The long simulations, which considered Stage 4 (Section 4.2.3), lead to draw the same conclusion. While the easterly breach was still expanding, to eventually become large enough for subsequent floods, the westerly breach silted. After the flood wave that initiated the breach, a flood did not flood that part of the floodplain anymore and the westerly breach has thus not been active since.

# Bibliography

- Allen, J. R. L. (1965). A review of the origin and characteristics of recent alluvial sediments. *Sedimentology*, 5(2), 89–191. <https://doi.org/10.1111/j.1365-3091.1965.tb01561.x>
- Arcement, G. J., & Schneider, V. R. (1989). Guide for selecting Manning's roughness coefficients for natural channels and flood plains. *United States Geological Survey Water-Supply*, (2339). <https://doi.org/10.3133/wsp2339>
- Bisschop, R., Visser, P. J., Rhee, C. V., & Verhagen, H. J. (2010). Erosion due to high flow velocities : A description of relevant processes. *Coastal Engineering Proceedings*, (July). <https://doi.org/10.9753/icce.v32.sediment.24>
- Blanton, J. (1977). Flood plain inundation caused by dam failure. proceedings of the dam-breack flood routing workshop. *Water Resources Council*, 47–64.
- Boggs, S. (2014). *Principles of sedimentology and stratigraphy*. <https://lib.hpu.edu.vn/handle/123456789/28988>
- Bomers, A., Schielen, R. M. J., & Hulscher, S. J. M. H. (2019a). Application of a lower-fidelity surrogate hydraulic model for historic flood reconstruction. *Environmental Modelling and Software*, 117, 223–236. <https://doi.org/10.1016/j.envsoft.2019.03.019>
- Bomers, A., Schielen, R. M. J., & Hulscher, S. J. M. H. (2019b). Decreasing uncertainty in flood frequency analyses by including historic flood events in an efficient bootstrap approach. *Natural Hazards and Earth System Sciences*, 19(8), 1895–1908. <https://doi.org/10.5194/nhess-19-1895-2019>
- Brown, R. J., & Rogers, D. C. (1981). BRDAM Users Manual. *Water and Power Resources Services, U.S. Department of Interior*.
- Brunner, G. W. (2016). *Hydraulic Reference Manual Version 5.0*.
- Casulli, V. (2008). A high-resolution wetting and drying algorithm for free-surface hydrodynamics. *International Journal for Numerical Methods in Fluids*, 60, 391–408. <https://doi.org/10.1002/fld.1896>
- Chen, Y., & Anderson, B. A. (1984). Methodology for Estimating Embankment Damage Caused by Flood Overtopping. *Transportation Research Record*, (1151).
- Chow, V. (1959). *Open-channel hydraulics*. McGraw-Hill.
- Cohen, K. M. (2010). Holocene Rhine reoccupation of the IJssel valley by divide dissection North of Zutphen, (April).
- Cohen, K. M., & Lodder, Q. J. (2007). *Paleogeografie en veiligheid tegen overstromen*.
- Cohen, K. M., & Stouthamer, E. (2012). Digitaal basisbestand paleogeografie van de rijn-maas delta. <https://doi.org/10.17026/dans-x7g-sjtw>
- Cohen, K. M., Stouthamer, E., Hoek, W. Z., Berendsen, H. J. a., & Kempen, H. F. J. (2009). *Zand in Banen. Gemeente Deventer*.
- Cohen, K. M., Toonen, W. H. J., & Weerts, H. J. T. (2016). *Overstromingen van de Rijn gedurende het Holoceen: Relevantie van de grootste overstromingen voor archeologie van het Nederlandse rivierengebied*.
- Coleman, S. E., Andrews, D. P., & Webby, M. G. (2002). Overtopping Breaching of Noncohesive Homogeneous Embankments. *Journal of Hydraulic Engineering*, 128, 829–838. [https://doi.org/10.1061/\(ASCE\)0733-9429\(2002\)128:9\(829\)](https://doi.org/10.1061/(ASCE)0733-9429(2002)128:9(829))
- Engelund, F., & Hansen, E. (1967). A monograph on sediment transport in alluvial streams.
- Fread, D. L. (1988). BREACH: An erosion model for earthen dam failures. *Geology*, (July).

- Fread, J. N., D. L. Wetmore. (1984). DAMBRK: The NWS dam break flood forecasting model. *National Oceanic and Atmospheric Administration*.
- Gary Nichols. (2009). *Sedimentology and Stratigraphy* (2nd Edition). Wiley-Blackwell.
- Groothedde, M. (2010). De 'nieuwe' IJssel. Wat vertellen de geschreven bronnen en archeologische vondsten? *Historisch Jaarboek voor Gelderland*, 101, 7–26.
- Hajek, E. A., & Wolinsky, M. A. (2012). Simplified process modeling of river avulsion and alluvial architecture: Connecting models and field data. <https://doi.org/10.1016/j.sedgeo.2011.09.005>
- Hegnauer, M. (2017). Analysis GRADE results for different locations in the Rhine Basin. *Deltares*, (11200540-000).
- Hegnauer, M., Beersma, J., van den Boogaard, H., Buishand, T., & Passchier, R. (2014). Generator of Rainfall And Discharge Extremes (GRADE) for the Rhine and Meuse basins. *Deltares*, (1209424-004).
- Kleinmans, M. G., Ferguson, R. I., Lane, S. N., & Hardy, R. J. (2013). Splitting rivers at their seams: bifurcations and avulsion. *Earth Surface Processes and Landforms*, 38(1), 47–61. <https://doi.org/10.1002/esp.3268>
- Lee, K., & Duncan, J. (1975). Landslide of april 25, 1974 on the mantaro river, peru. *National Academy of Sciences, Washington, DC*.
- Makaske, B., Maas, G. J., & van Smeerdijk, D. G. (2008). The age and origin of the Gelderse IJssel. *Netherlands Journal of Geosciences*, (87), 323–337.
- Meyer-Peter, E., & Müller, R. (1948). Formulas for bed-load transport. *International Association for Hydraulic Structures Research*, (2), 39–64.
- Mohrig, D., Heller, P. L., & Paola, C. (2000). Interpreting avulsion process from ancient alluvial sequences : Guadalupe- Matarranya system (Northern Spain) and Wasatch formation (Western Colorado). *Geological Society of America Bulletin*, (December). [https://doi.org/10.1130/0016-7606\(2000\)112<1787](https://doi.org/10.1130/0016-7606(2000)112<1787)
- North, C. P., & Davidson, S. K. (2012). Unconfined alluvial flow processes: Recognition and interpretation of their deposits, and the significance for palaeogeographic reconstruction. *Earth-Science Reviews*, 111(1-2), 199–223. <https://doi.org/10.1016/J.EARSCIREV.2011.11.008>
- Oumeraci, H., D'ELISO, C., & Kortenhaus, A. (2005). Breaching of coastal dikes: state of the art. *LWI Report*, (910). <http://repository.tudelft.nl/view/hydro/uuid:e569363f-587a-4378-99dc-72fb35098fbc/>
- Polanco-Boulevard, L., & Rice, J. (2016). reliability-based three-dimensional assessment of internal erosion potential due to crevasse splays. *Journal of Geotechnical and Geoenvironmental Engineering*, 143. [https://doi.org/10.1061/\(ASCE\)GT.1943-5606.0001596](https://doi.org/10.1061/(ASCE)GT.1943-5606.0001596)
- Razavi, S., Tolson, B. A., & Burn, D. H. (2012). Review of surrogate modeling in water resources. *Water Resources Research*, 48(7). <https://doi.org/10.1029/2011WR011527>
- Robert, D., & Jarrett, M. (1985). Hydraulics of high-gradient streams. *Journal of Hydraulic Engineering*, 110(11), 1519–1539.
- Seminara, G. (2006). Meanders. *Journal of Fluid Mechanics*, 554, 271–297. <https://doi.org/10.1017/S0022112006008925>
- Shields, A. (1936). Anwendung der Aehnlichkeitsmechanik und der Turbulenzforschung auf die Geschiebebewegung.
- Singh, V. P. (1996). Dam breach modeling technology.
- Singh, V. P., & Scarlatos, C. A. (1988). Analysis of gradual earth-dam failure. *Journal of Hydraulic Engineering*, 114(1), 21–42.
- Smith, N. D., Cross, T. A., Dufficy, J. P., & Clough, S. R. (1989). Anatomy of an avulsion. *Sedimentology*, 36(1), 1–23. <https://doi.org/10.1111/j.1365-3091.1989.tb00817.x>
- Southard, J. B., & Boguchwal, L. A. (1990). Bed configuration in steady unidirectional water flows; Part 2, Synthesis of flume data. *Journal of Sedimentary Research*, 60(5), 658–679. <https://doi.org/10.1306/212F9241-2B24-11D7-8648000102C1865D>
- Stouthamer, E. (2001). Sedimentary products of avulsions in the Holocene Rhine–Meuse Delta. *Sedimentary Geology*, 145(1), 73–92. [https://doi.org/10.1016/S0037-0738\(01\)00117-8](https://doi.org/10.1016/S0037-0738(01)00117-8)
- Van der Meulen, B., Cohen, K., Pierik, H., Zinsmeister, J., & Middelkoop, H. (2020). LiDAR derived high resolution palaeo DEM construction workflow and application to the early medieval Lower Rhine valley and upper delta. *Geomorphology*. <https://doi.org/10.1016/j.geomorph.2020.107370>

- van der Meulen, B., Bomers, A., Cohen, K., & Middelkoop, H. (In Prep). Late holocene flood dynamics and magnitudes in the lower rhine river valley and upper delta resolved by two-dimensional hydraulic modelling. *Earth Surface Processes and Landforms*.
- Van Lottum, H. (2020). *Hoogwater in de ijssel*. <https://luuk1945.wordpress.com/2020/02/08/hoog-water/>
- van Rhee, C. (2010). Sediment Entrainment at High Flow Velocity. *Journal of Hydraulic Engineering*, 136(September), 572–582. [https://doi.org/10.1061/\(ASCE\)HY.1943-7900.0000214](https://doi.org/10.1061/(ASCE)HY.1943-7900.0000214)
- van Rijn, L. C. (1984a). Sediment Pick-Up functions. *Journal of Hydraulic Engineering*, 110.
- van Rijn, L. C. (1984b). Sediment Transport, Suspended Load Transport. *Journal of Hydraulic Engineering*, 110.
- van Rijn, L. C. (1993). *Principles of sediment transport in rivers, estuaries and coastal seas*. Aqua Publications.
- Verheij, H. (2002). Time-dependent breach development in cohesive material. *Delft Hydraulics*.
- Vermeulen, B., & Haveman, E. (2008). *Bureauonderzoek, geofysisch en geomorfologie in het plangebied Bolwerksplas, Worp en Ossenwaard. Ruimte voor de Rivier, fase document archeologie, Fase 2. Rapportages Archeologie Deventer*.
- Visser, P. J. (1998). *Breach growth in sand-dikes*. Faculty of Civil Engineering and Geosciences, Report Nr. 98-1.
- Wahl, T. (2004). Uncertainty of Predictions of Embankment Dam Breach Parameters. *Journal of Hydraulic Engineering*, 130, 389–397. [https://doi.org/10.1061/\(ASCE\)0733-9429\(2004\)130](https://doi.org/10.1061/(ASCE)0733-9429(2004)130)
- Wang, L., Chen, Z., Wang, N., Sun, P., Yu, S., Li, S., & Du, X. (2016). Modeling lateral enlargement in dam breaches using slope stability analysis based on circular slip mode. *Engineering Geology*, 209, 70–81. <https://doi.org/10.1016/j.enggeo.2016.04.027>
- Wu, W., Marsooli, R., & He, Z. (2012). Depth-Averaged Two-Dimensional Model of Unsteady Flow and Sediment Transport due to Noncohesive Embankment Breaching. *Journal of Hydraulic Engineering*, 138, 503–516. [https://doi.org/10.1061/\(ASCE\)HY.1943-7900.0000546](https://doi.org/10.1061/(ASCE)HY.1943-7900.0000546)
- Yuill, B., Khadka, A., Pereira, J., Allison, M., & Meselhe, E. (2016). Morphodynamics of the erosional phase of crevasse-splay evolution and implications for river sediment diversion function. *Geomorphology*, 259, 12–29. <https://doi.org/10.1016/j.geomorph.2016.02.005>
- Zinger, J. A., Rhoads, B. L., & Best, J. L. (2011). Extreme sediment pulse generated by bend cutoffs along a large meandering river. *Nature Geoscience*, 4, 675–678. <https://doi.org/10.1038/ngeo1260>
- Zinger, J. A., Rhoads, B. L., Best, J. L., & Johnson, K. K. (2013). Flow structure and channel morphodynamics of meander bend chute cutoffs : A case study of the Wabash River , USA. *Journal of Geophysical Research. Earth Surface*, 118, 2468–2487. <https://doi.org/10.1002/jgrf.20155>

# Appendix A

## Study area

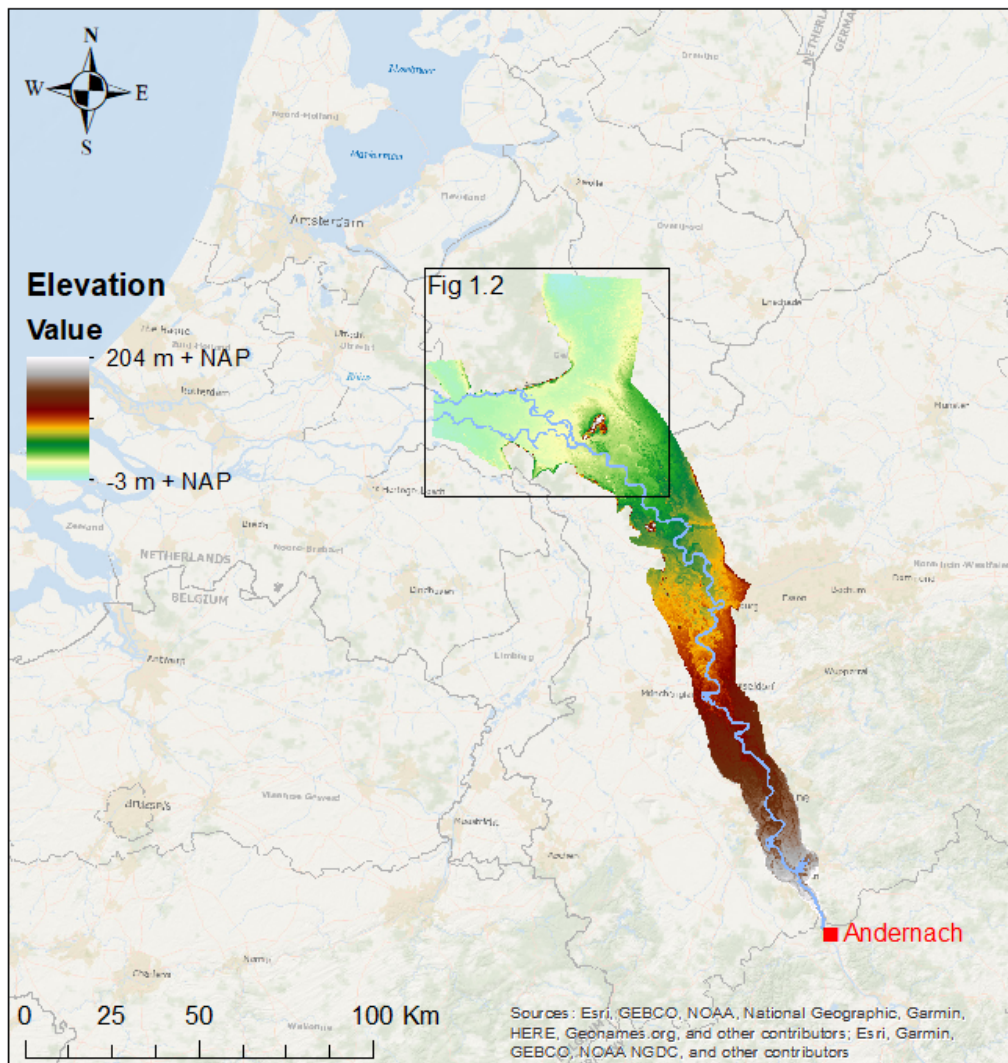


Figure A.1: Study area of the river Rhine and its distributaries around 600 AD from Andernach upstream to the Betuwe region and Deventer downstream

# Appendix B

## Hydrodynamic model equations

The equations in the following sections are used for the computations in the 1D-2D coupled hydrodynamic model. The variables used in these equations are not necessarily the same as the variables as stated in the List of Symbols. The explanation of the variables is elaborated on below the equations.

### B.1 1D Unsteady flow equations

The continuity equation and the momentum equation are used to compute the flow in the 1D profiles (Brunner, 2016). The continuity equation can be written as:

$$\frac{\partial A}{\partial t} + \frac{\partial S}{\partial t} + \frac{\partial Q}{\partial x} - q_l = 0 \quad (\text{B.1})$$

Where:

- $x$  = Distance along the channel,
- $t$  = Time,
- $Q$  = Flow,
- $A$  = Cross-sectional area
- $S$  = Storage from non conveying portions of cross section,
- $q_l$  = Lateral inflow per unit distance.

The Momentum equation for a single channel can be written as:

$$\frac{\partial Q}{\partial t} + \frac{\partial(VQ)}{\partial x} + gA \left( \frac{\partial H}{\partial x} + S_f \right) = 0 \quad (\text{B.2})$$

Where:

- $x$  = Distance along the channel,
- $Q$  = Flow,
- $t$  = Time,
- $g$  = Acceleration of gravity,
- $S_f$  = friction slope,
- $V$  = Velocity,

- $A$  = Cross-sectional area,  
 $H$  = Elevation of the water surface.

## B.2 2D Full momentum equations

The continuity equation and the momentum equation are used to compute the flow in the 2D grid (Brunner, 2016). The continuity equation can be written as:

$$\frac{\partial H}{\partial t} + \frac{\partial(hu)}{\partial x} + \frac{\partial(hv)}{\partial y} + q = 0 \quad (\text{B.3})$$

Where:

- $t$  = Time,  
 $H$  = Elevation of the water surface,  
 $h$  = Water depth,  
 $u$  = Velocity in x-direction,  
 $v$  = Velocity in y-direction,  
 $q$  = Flux term.

The conservation of momentum equation (Shallow Water equations):

$$\frac{\partial u}{\partial t} + u \frac{\partial u}{\partial x} + v \frac{\partial u}{\partial y} = -g \frac{\partial H}{\partial x} + v_t \left( \frac{\partial^2 u}{\partial x^2} + \frac{\partial^2 u}{\partial y^2} \right) - c_f u + f v \quad (\text{B.4})$$

$$\frac{\partial v}{\partial t} + u \frac{\partial v}{\partial x} + v \frac{\partial v}{\partial y} = -g \frac{\partial H}{\partial y} + v_t \left( \frac{\partial^2 v}{\partial x^2} + \frac{\partial^2 v}{\partial y^2} \right) - c_f v + f u \quad (\text{B.5})$$

Where:

- $t$  = Time,  
 $u$  = Velocity in x-direction,  
 $v$  = Velocity in y-direction,  
 $g$  = Acceleration of gravity,  
 $H$  = Elevation of the water surface,  
 $v_t$  = Horizontal eddy viscosity coefficient,  
 $c_f$  = Bottom friction coefficient,  
 $f$  = Coriolis parameter.

## B.3 Weir flow coefficient

The Weir equation is used to couple the 1D profiles to the 2D grid and can be written as:

$$Q = CLH^{3/2} \quad (\text{B.6})$$

Where:

- $Q$  = Flow rate,  $C$  = Weir flow coefficient,  $L$  = Weir length,  $H$  = Weir energy head.

# Appendix C

## Overview of results

In the table on the next page, an overview is shown of all the different parameter settings and the hydrodynamic and erosional results.

Westerly breach									Easterly breach							
Discharge	Width	Depth	Water depth	Flow velocity	% of total discharge	Erosion velocity	Sediment transport capacity		Width	Depth	Water depth	Flow velocity	% of total discharge	Erosion velocity	Sediment transport capacity	
[ $m^3/s$ ]	[ $m$ ]	[ $m$ ]	[ $m$ ]	[ $m/s$ ]	[%]	[ $mm/s$ ]	[ $m^2/s$ ]	[ $m^3/s$ ]	[ $m$ ]	[ $m$ ]	[ $m$ ]	[ $m/s$ ]	[%]	[ $mm/s$ ]	[ $m^2/s$ ]	[ $m^3/s$ ]
<i>Equal dimensions</i>																
10000	50	1	1.2	3.2	5	8.2	0.004	0.2	50	1	1.3	4.8	8	12.4	0.01	0.5
14000	50	1	1.4	3.8	5	9.7	0.01	0.4	50	1	1.5	5.5	7	13.8	0.02	1
10000	50	2	2.1	4.4	12	10.3	0.02	0.7	50	2	2.2	6.8	16	16.0	0.04	2.1
14000	50	2	2.3	5.0	10	11.7	0.03	1.3	50	2	2.4	7.3	13	17.0	0.07	3.2
10000	50	4	4.2	3.3	17	6.7	0.004	0.2	50	4	4.3	6.5	27	13.7	0.03	1.2
14000	50	4	4.3	4.1	14	8.6	0.01	0.4	50	4	4.5	7.1	21	15.0	0.05	2.3
10000	100	4	4.3	2.1	20	3.6	0.0002	0.02	100	4	4.4	4.0	32	8.4	0.003	0.3
14000	100	4	4.3	2.7	17	5.5	0.0007	0.07	100	4	4.5	4.7	26	9.8	0.006	0.6
<i>Shallow shoulders</i>																
10000	100	4	4.3	2.9	19	5.8	0.0008	0.08	100	4	4.4	5.1	31	10.8	0.006	0.6
14000	100	4	4.4	3.5	16	7.3	0.002	0.2	100	4	4.6	5.9	25	12.3	0.01	1.3
<i>Different widths</i>																
6000	50	4	3.8	2.0	21	3.0	0.002	0.01	100	4	3.9	2.6	44	5.5	0.003	0.03
10000	50	4	4.1	3.3	17	6.7	0.004	0.15	100	4	4.2	4.0	32	8.4	0.003	0.3
14000	50	4	4.3	4.1	14	8.5	0.01	0.43	100	4	4.4	4.7	26	9.7	0.006	0.6
10000	100	4	4.1	2.5	20	5.0	0.0003	0.03	50	4	4.3	6.3	28	13.2	0.04	1.6
14000	100	4	4.3	3.1	17	6.4	0.001	0.11	50	4	4.5	7.0	23	14.7	0.07	3

Table C.1: Overview of results per parameter setting

## Appendix D

# Manning Coefficient determination

Bed material	Median size of bed material (in millimeters)	Base $n$ value	
		Straight uniform channel <sup>1</sup>	Smooth channel <sup>2</sup>
Sand channels			
Sand <sup>3</sup> .....	0.2	0.012	—
	.3	.017	—
	.4	.020	—
	.5	.022	—
	.6	.023	—
	.8	.025	—
	1.0	.026	—
Stable channels and flood plains			
Concrete .....	—	0.012–0.018	0.011
Rock cut .....	—	—	.025
Firm soil .....	—	0.025–0.032	.020
Coarse sand .....	1–2	0.026–0.035	—
Fine gravel .....	—	—	.024
Gravel .....	2–64	0.028–0.035	—
Coarse gravel .....	—	—	.026
Cobble .....	64–256	0.030–0.050	—
Boulder .....	>256	0.040–0.070	—

<sup>1</sup> Benson and Dalrymple (1967).

<sup>2</sup> For indicated material; Chow (1959).

<sup>3</sup> Only for upper regime flow where grain roughness is predominant.

Figure D.1: Mannings coefficient according to the table of Arcement and Schneider (1989)

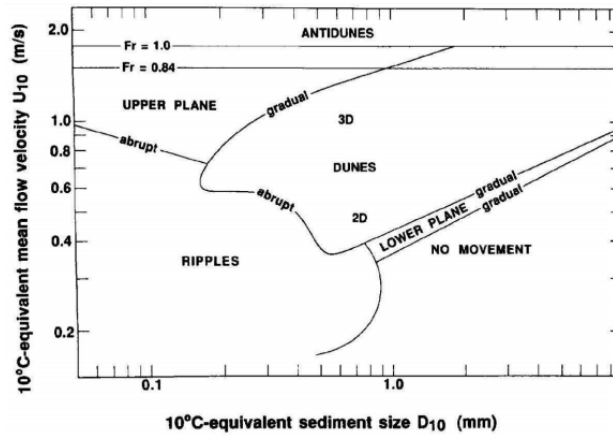


Figure D.2: *Stability diagram of Southard and Boguchwal (1990)*

# Appendix E

## Figures

### E.1 Erosion velocity

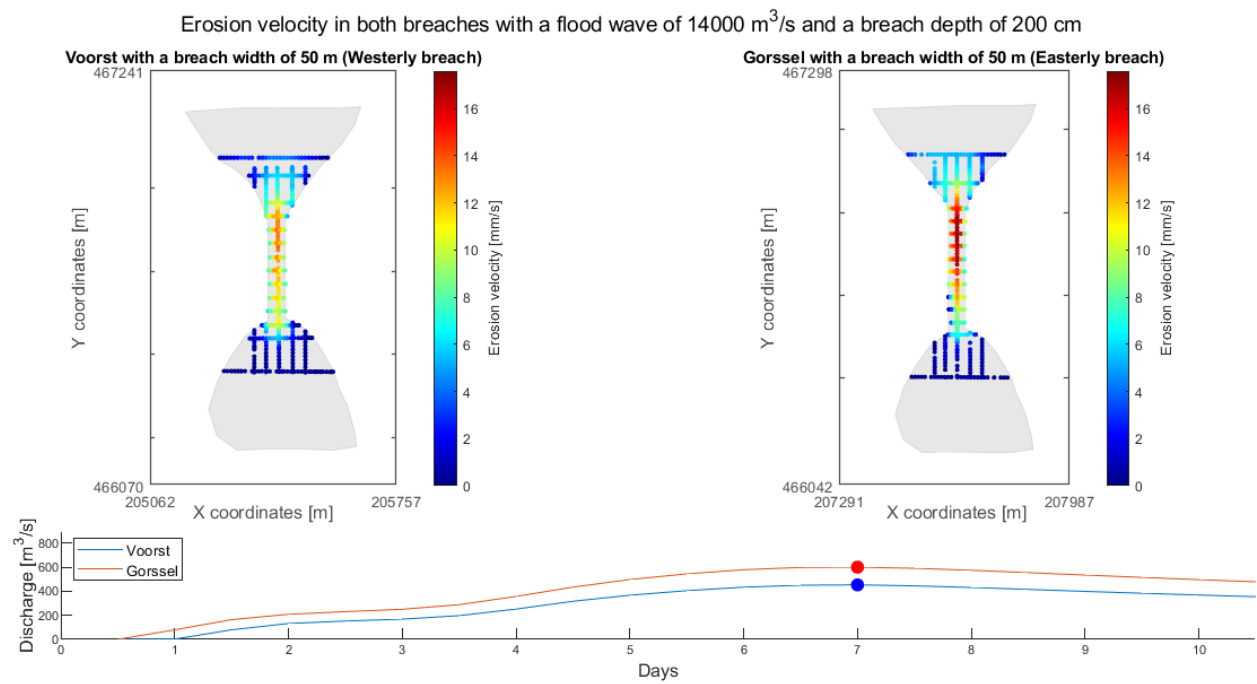


Figure E.1

## E.2 Sediment transport capacity

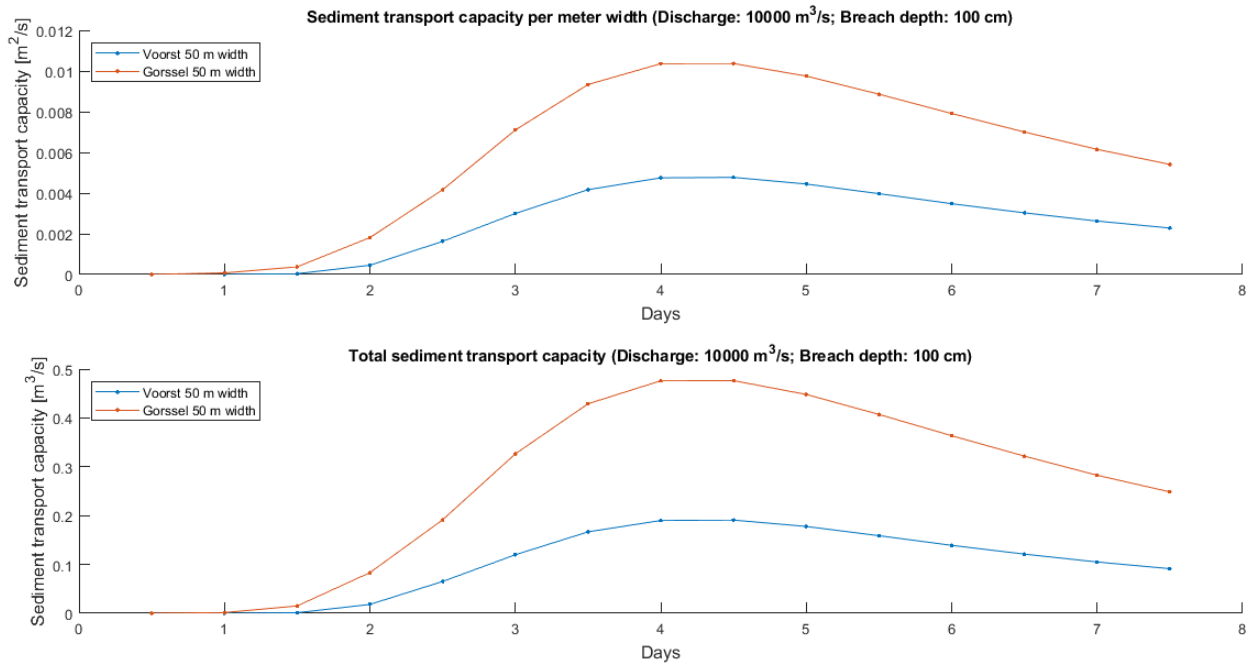


Figure E.2

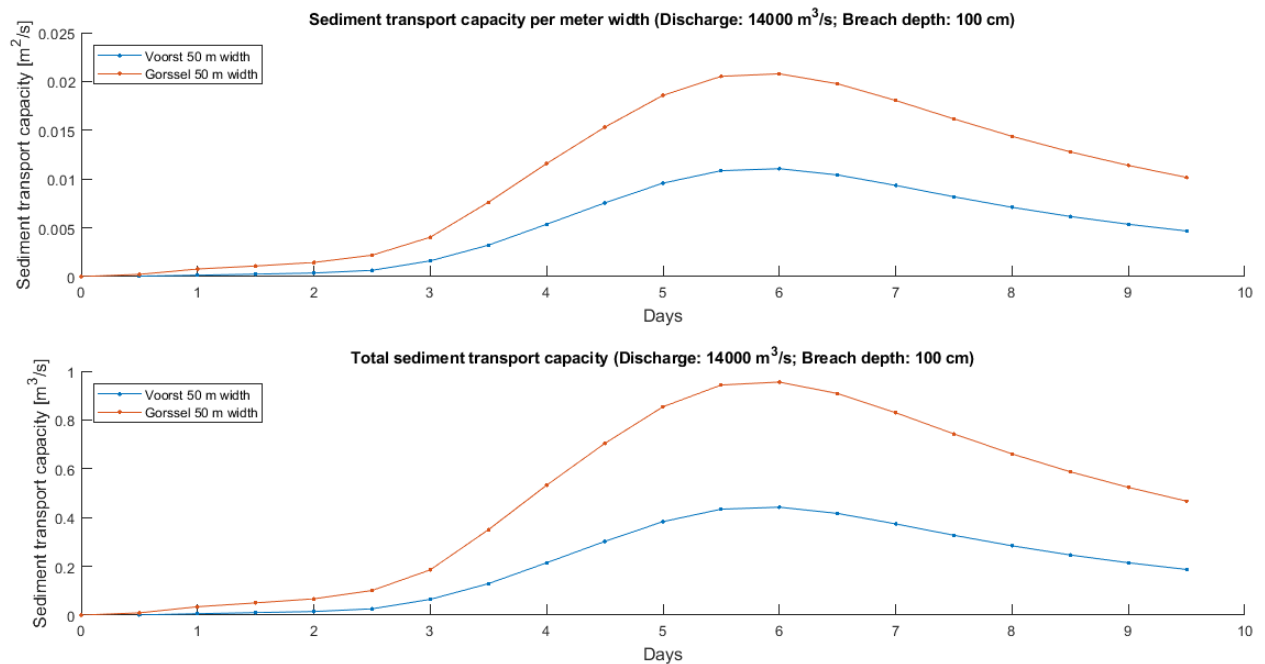


Figure E.3

APPENDIX E. FIGURES

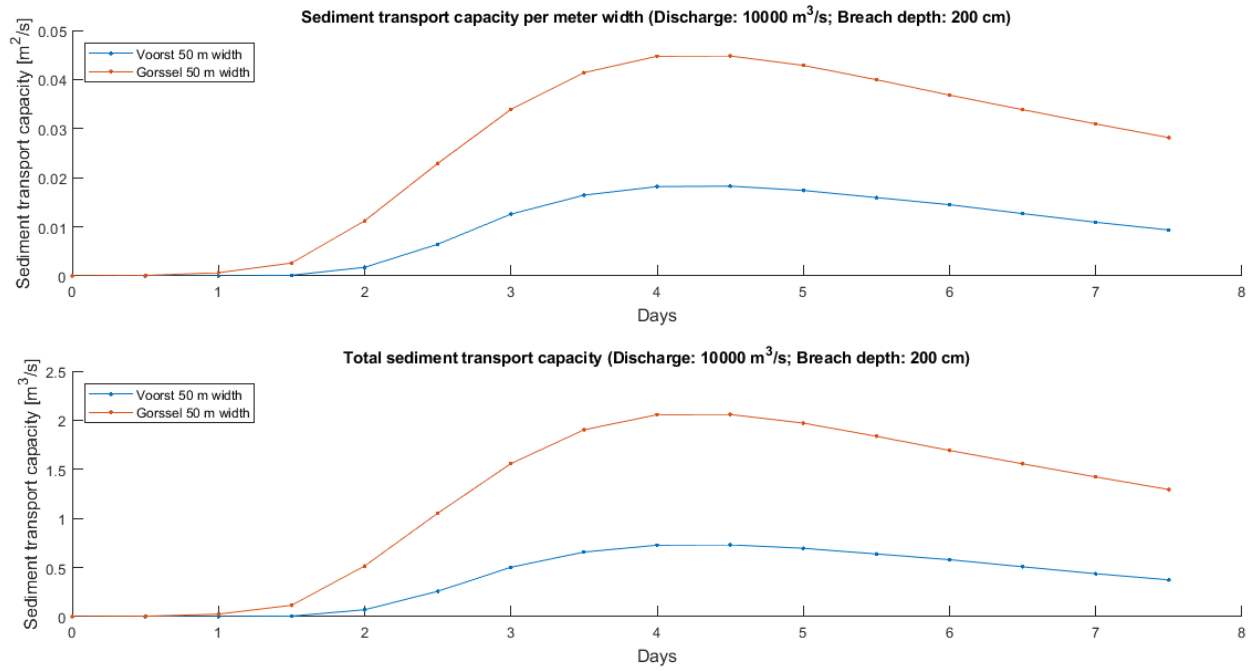


Figure E.4

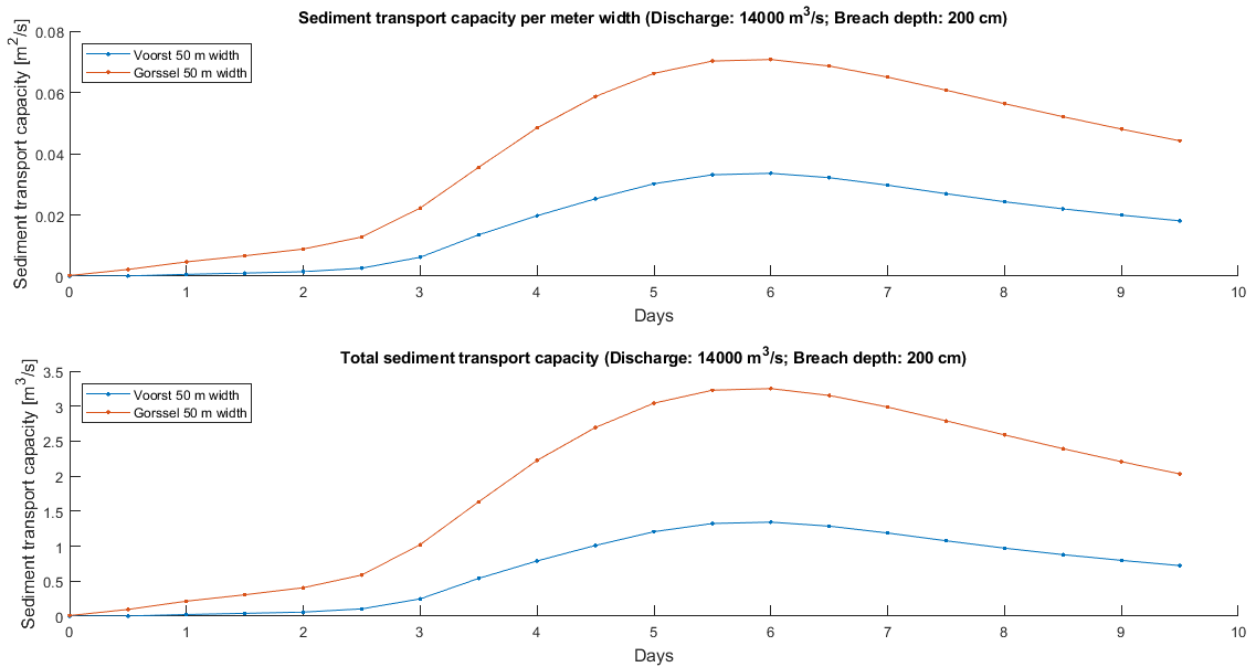


Figure E.5

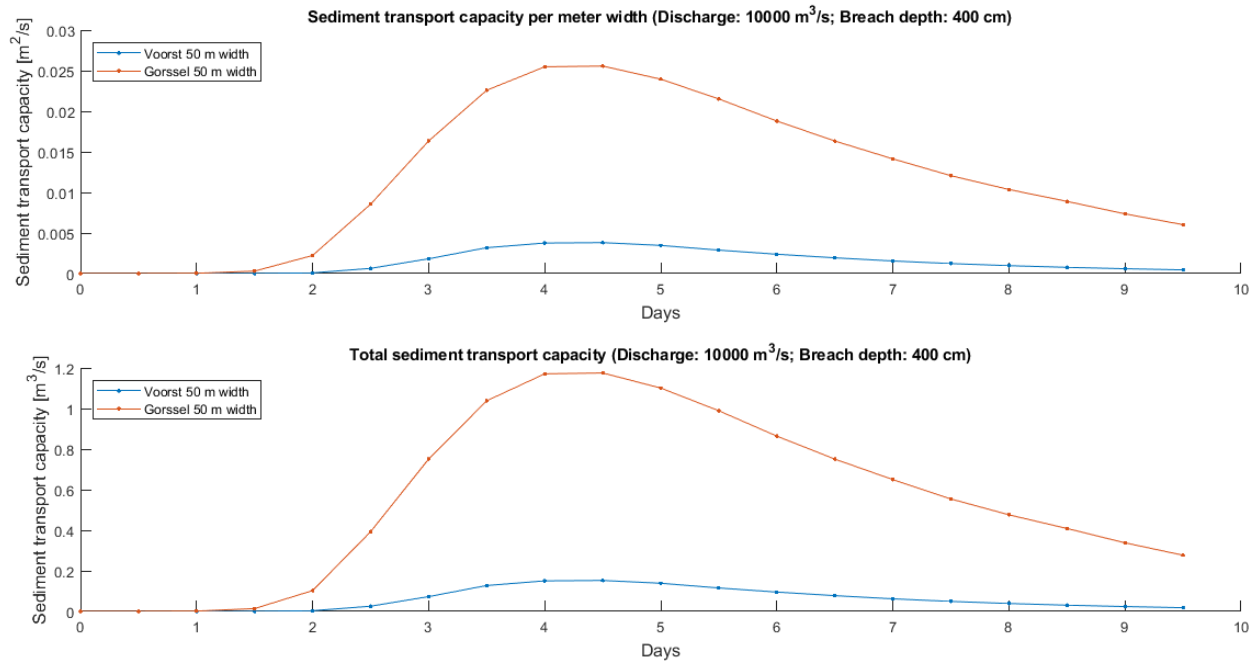


Figure E.6

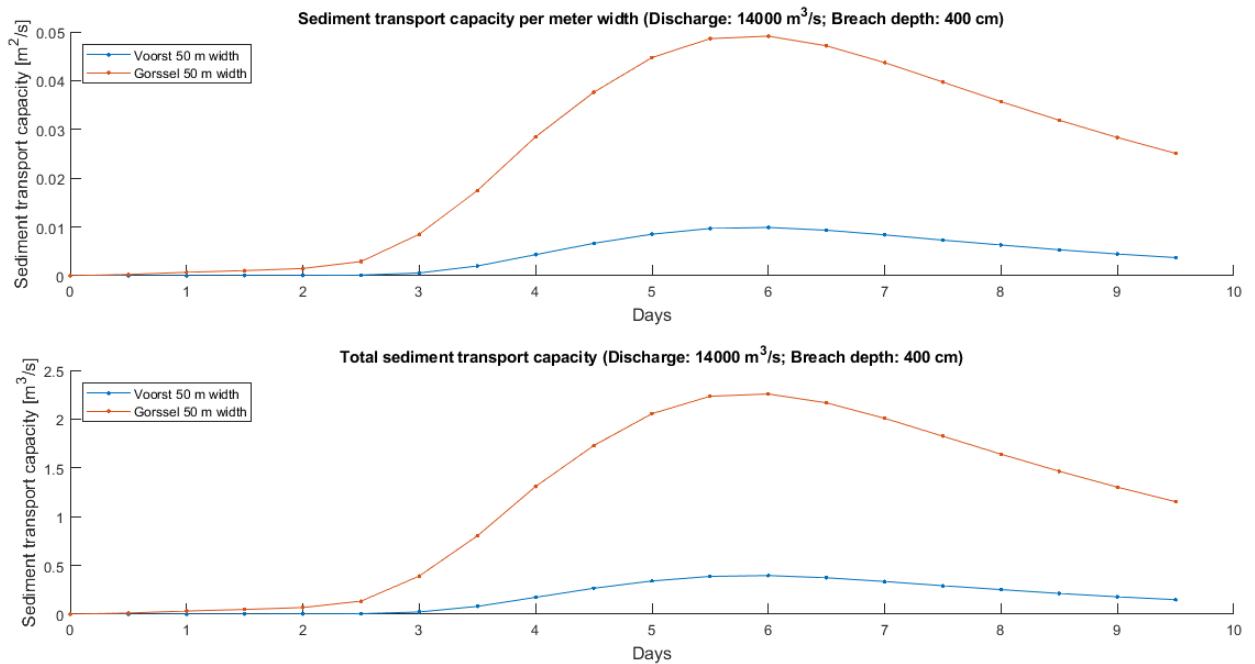


Figure E.7

APPENDIX E. FIGURES

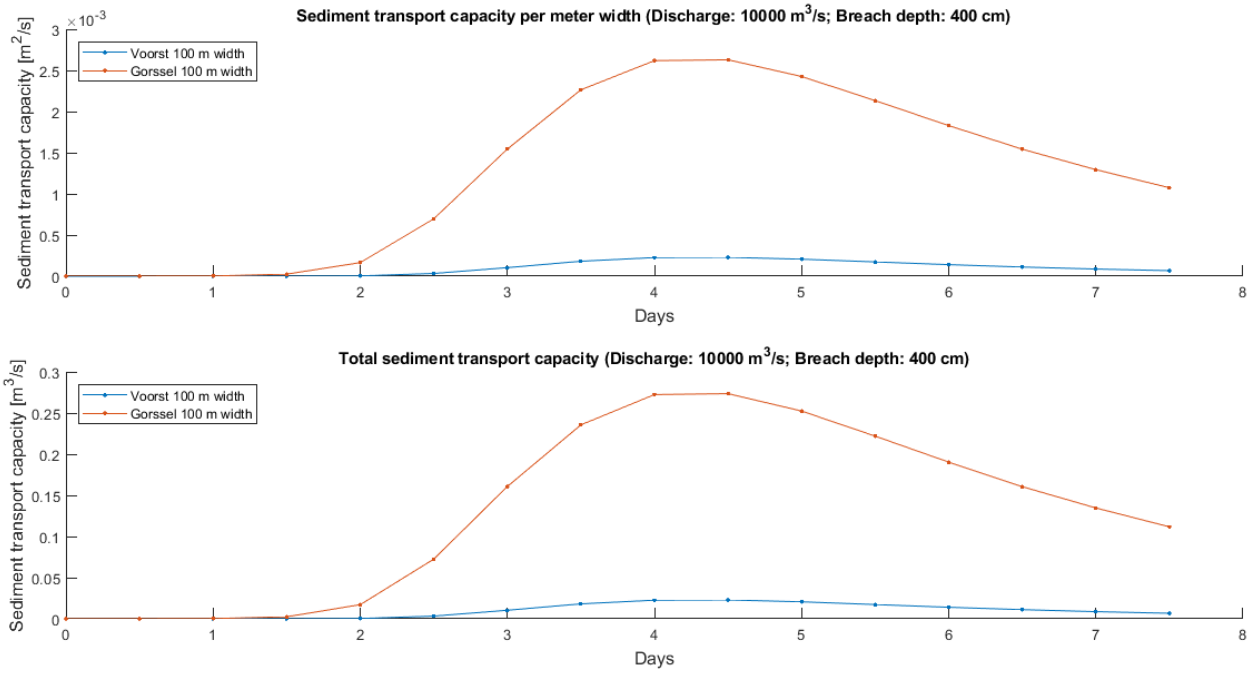


Figure E.8

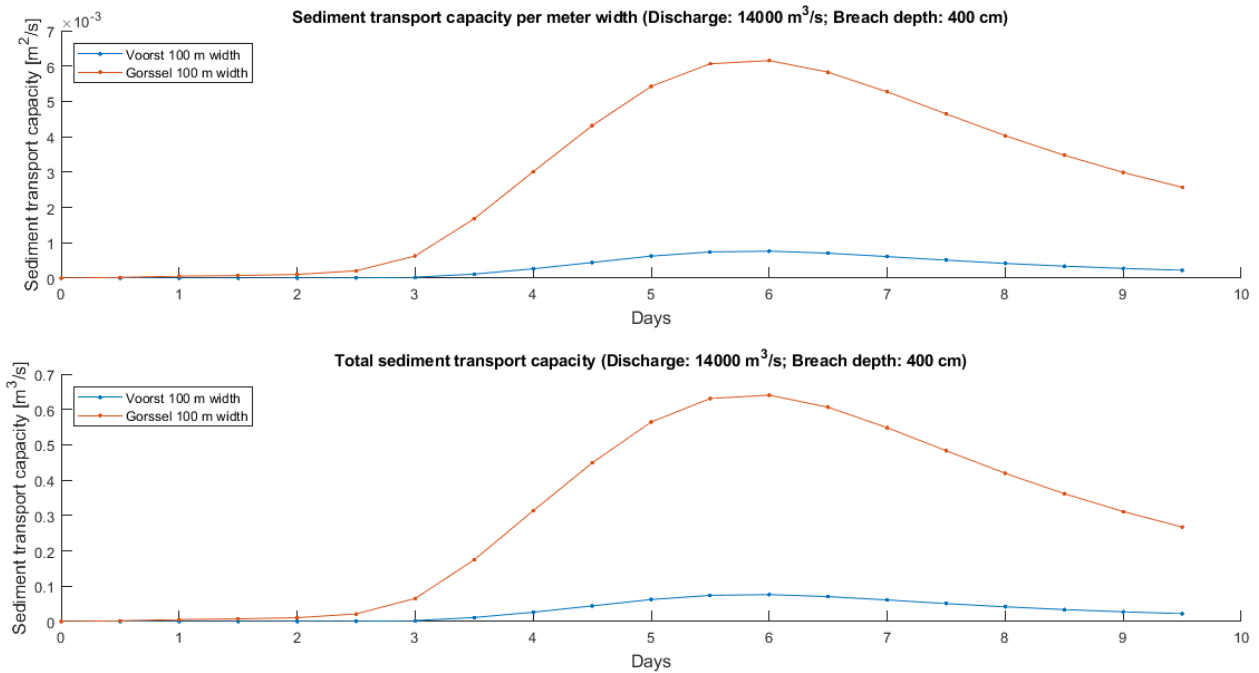


Figure E.9

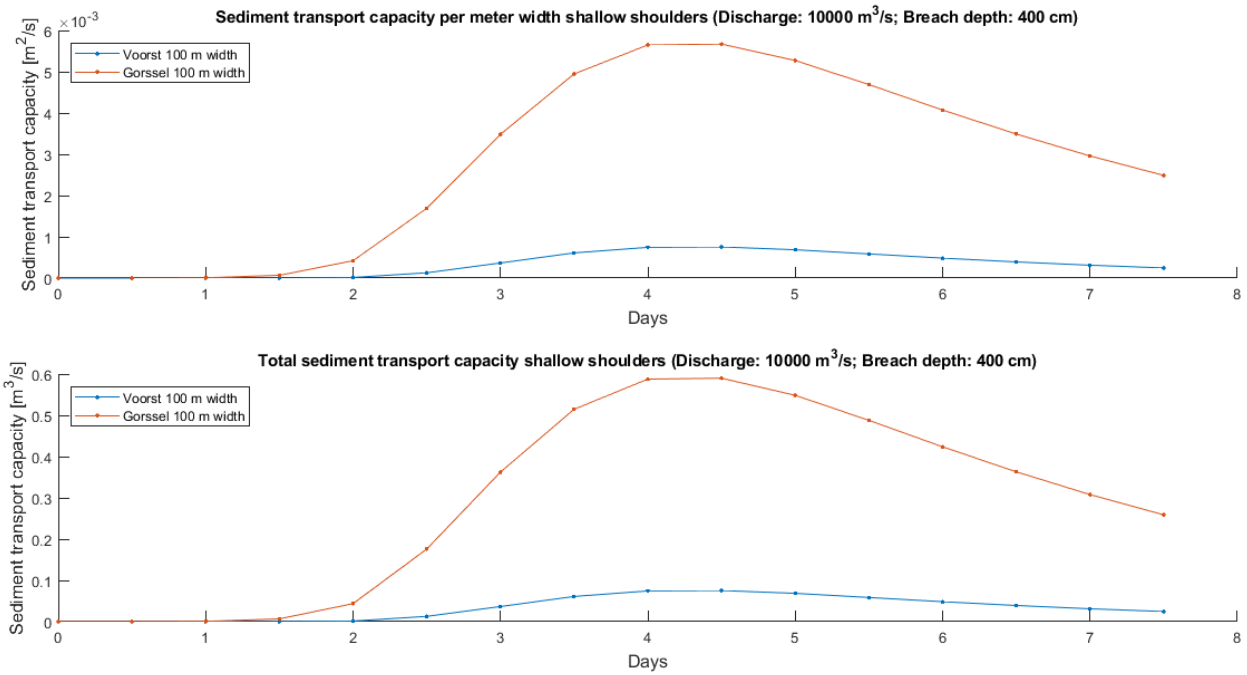


Figure E.10

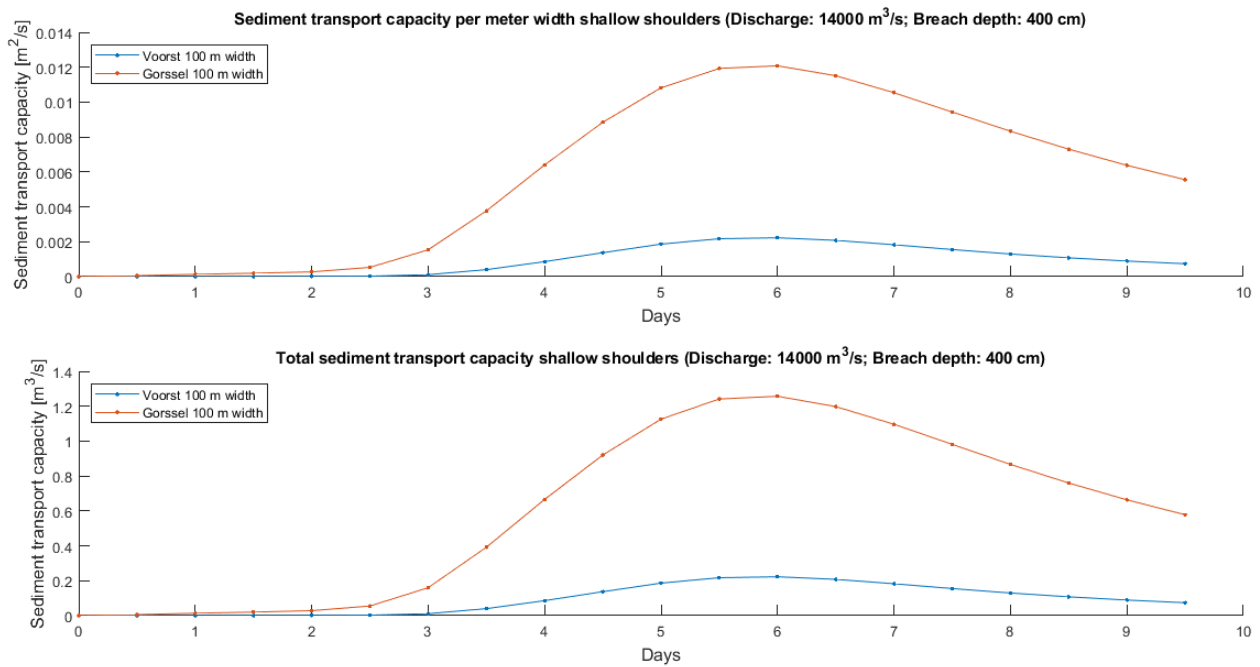


Figure E.11

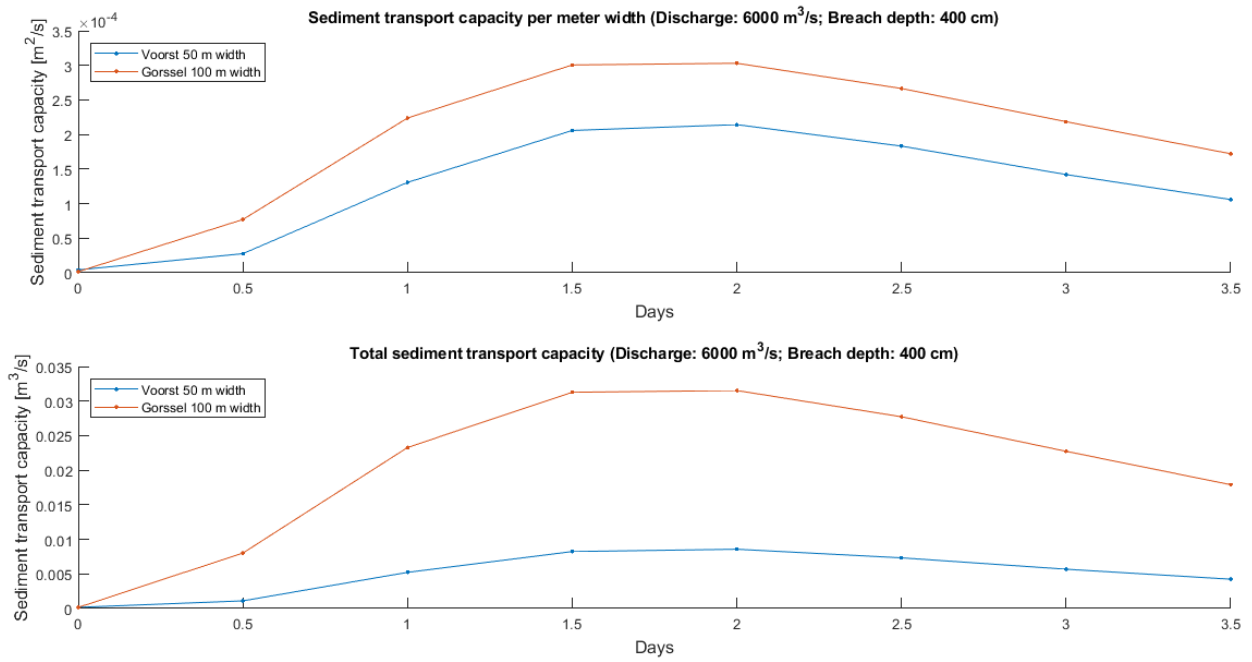


Figure E.12

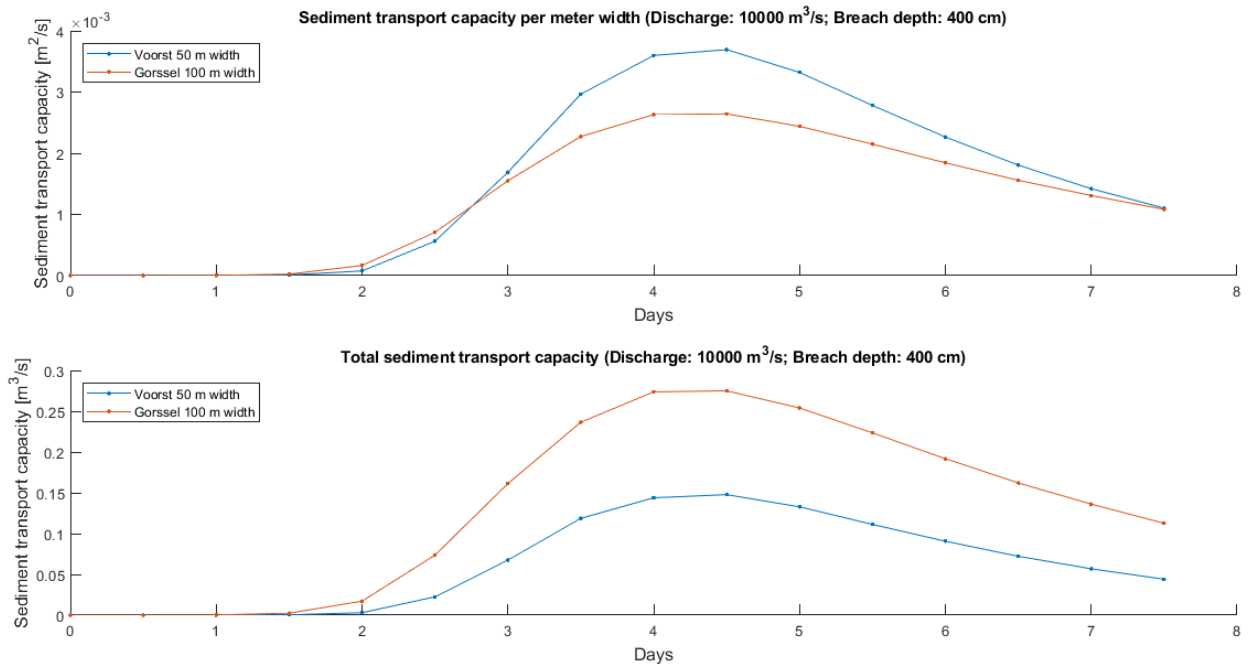


Figure E.13

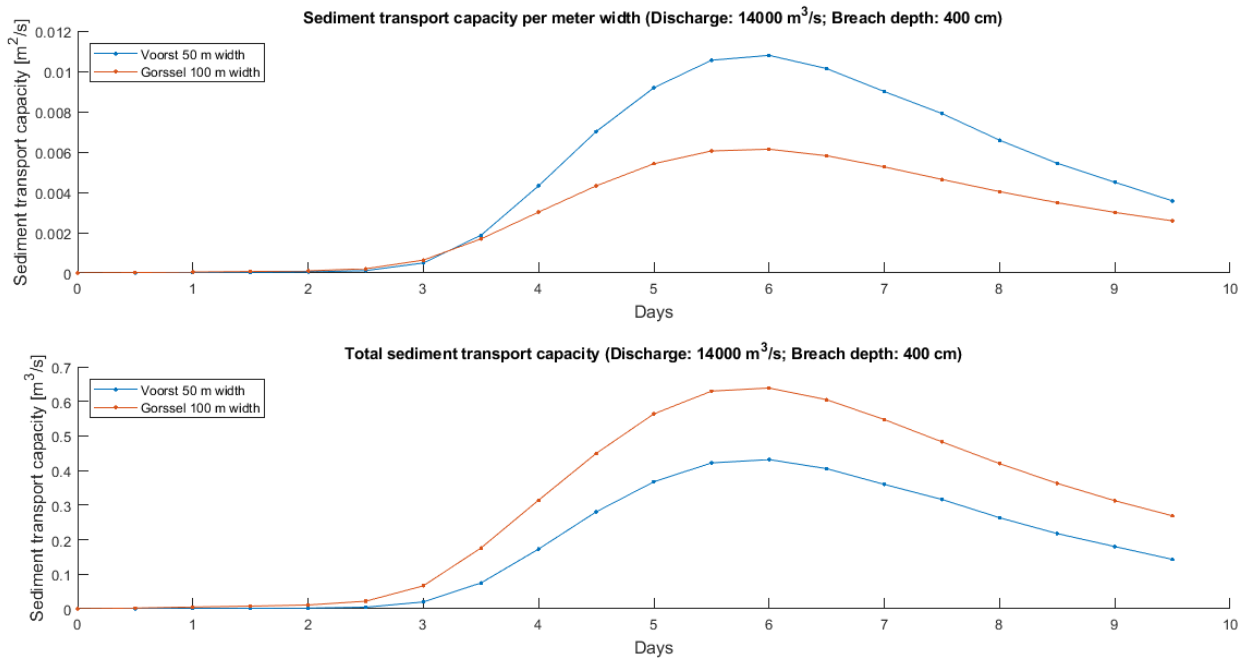


Figure E.14

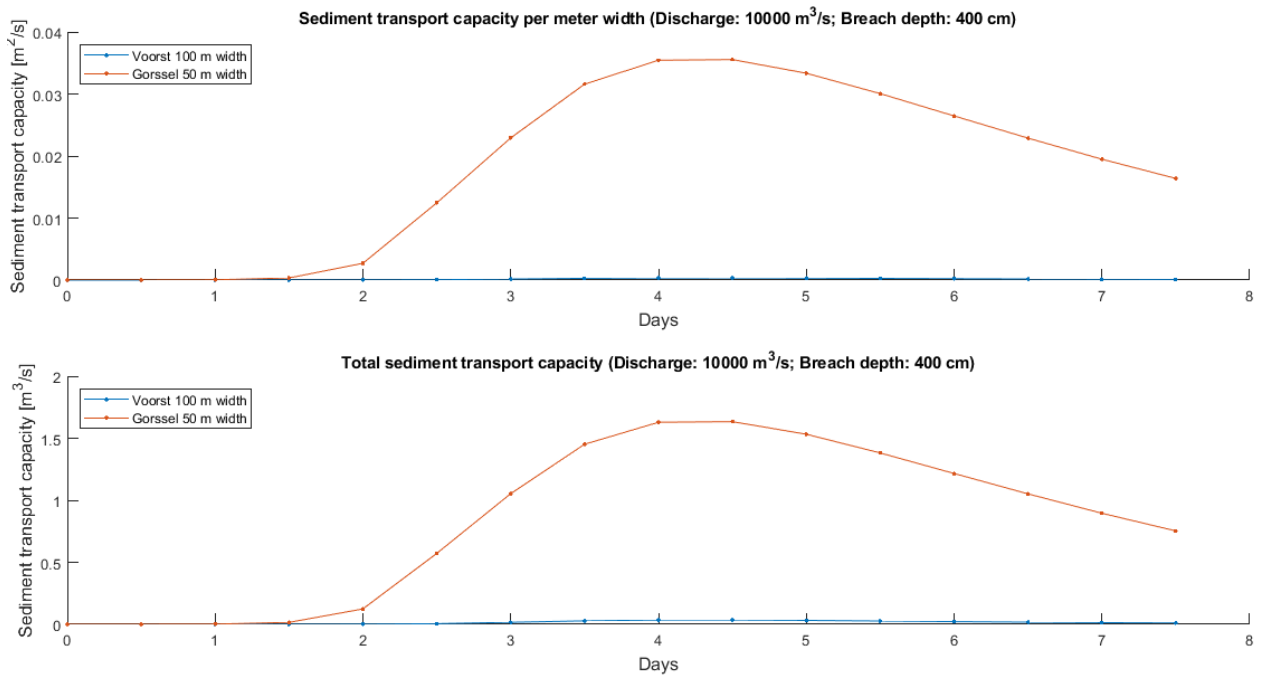


Figure E.15

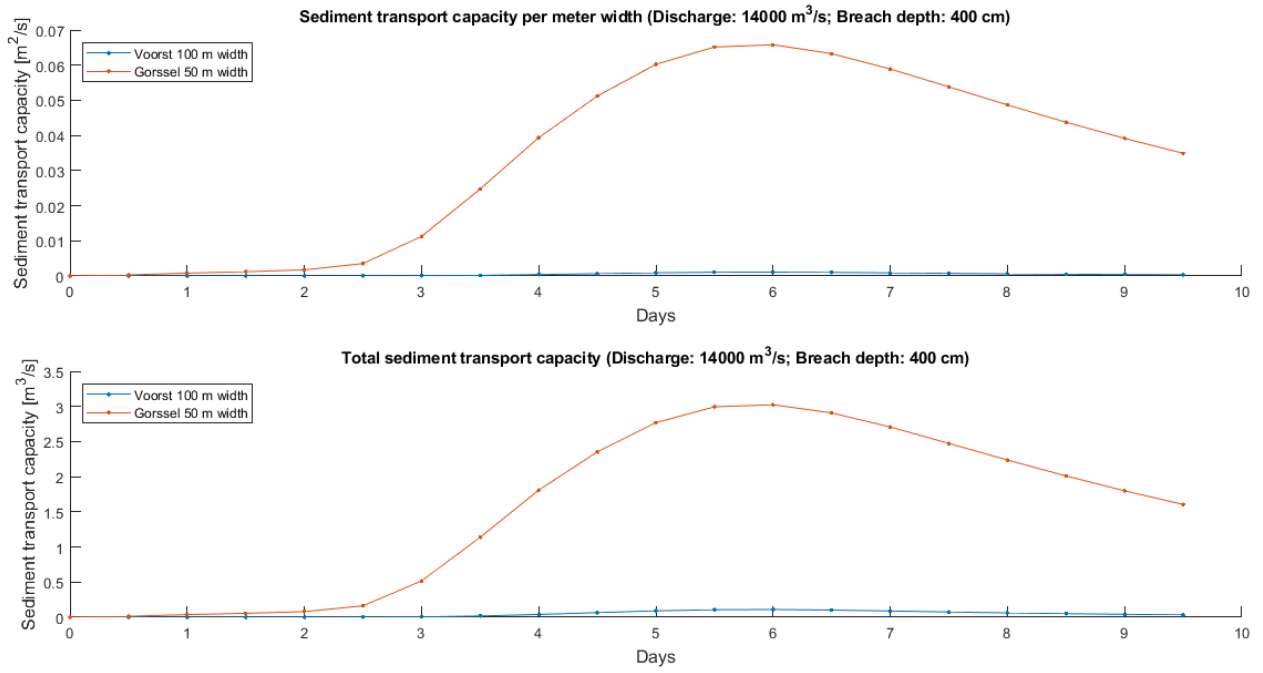


Figure E.16